SUPPORTING INFORMATION

Triple Resonance Experiments for Rapid Detection of ^{103}Rh NMR Shifts. A Combined Experimental and Theoretical Study into Dirhodium- and Bismuth-Rhodium Paddlewheel Complexes

Fabio P. Caló, Giovanni Bistoni, Alexander A. Auer, Markus Leutzsch,* and Alois Fürstner*

Max-Planck-Institut für Kohlenforschung, 45470 Mülheim/Ruhr, Germany

fuerstner@kofo.mpg.de

leutzsch@kofo.mpg.de

Table of Contents

1. General

Unless stated otherwise, all reactions were carried out under argon atmosphere in flame dried Schlenk glassware, ensuring inert conditions. The solvents were purified by distillation over the indicated drying agents under argon: THF, Et_2O (Mg/anthracene), pentane, toluene (Na/K), CH_2Cl_2, chlorobenzene (CaH_2); MeCN was dried by an absorption solvent purification system based on molecular sieves. Flash chromatography: Merck Geduran silica gel 60 (40 – 63 µm).

NMR spectra were recorded on Bruker AVIII 400, AVIII 500 or AVNeo 600 spectrometers in the solvents indicated at 298 K unless indicated otherwise; chemical shifts (δ) are given in ppm relative to TMS, coupling constants (*J*) in Hz. The solvent signals were used as internal references and the chemical shifts converted to the TMS scale ($CDCl_3$: δ_C = 77.16 ppm; residual $CHCl_3$: δ_H = 7.26 ppm; CD_2Cl_2: δ_C = 54.0 ppm; residual $CHDCl_2$: δ_H = 5.32 ppm; C_6D_6: δ_C = 128.1 ppm; residual C_6HD_5: δ_H = 7.16 ppm; CD_3CN: δ_C = 1.32, 118.3 ppm; residual CD_2HCN: δ_H = 1.94 ppm).[1] Signal assignments were established using ^{1}H-^{13}C-*edited*-HSQC and ^{1}H-^{13}C-HMBC experiments. ^{19}F and ^{103}Rh NMR shifts were referenced indirectly to the ^{1}H NMR frequency of the sample with the '*xiref*'-macro in Bruker TOPSPIN 3.6.2 (for ^{103}Rh)/TOPSPIN 4.0.6.[2] ^{19}F shifts are reported relative to $\delta(CFCl_3)$ = 0 ppm ($\Xi(^{19}F)$= 94.094011 %). ^{103}Rh NMR shifts are referenced to $\Xi(^{103}Rh)$ = 3.16% unless indicated otherwise.

1D ^{103}Rh NMR (pulse sequence: zg) and 2D ^{1}H-^{103}Rh-HMBC spectra (pulse sequence: hmbcgpqfnd) were acquired on a AVIII 500 MHz NMR spectrometer equipped with a 5 mm BBFO probe (^{1}H, ^{19}F & ^{31}P-^{109}Ag) with z-gradient which could be tuned on the X-channel to ^{103}Rh beyond the specifications. The typical $\pi/2$ ^{103}Rh pulse length was 40 µs when a pulse power of 180 W was used.

For the 1D ^{103}Rh NMR measurements, saturated samples in 5 mm NMR tubes were used. After excitation with a 70° pulse, 32k complex data points were acquired. The total acquisition time per scan was approximately 4s. To obtain an acceptable SNR 15000 scans were averaged (17 h measurement time).

The 1D ^{13}C{^{1}H, ^{103}Rh} (pulse sequence: zgigf2igf3), 2D ^{13}C{^{1}H}-^{103}Rh-HMBC and 2D H(C)Rh spectra were acquired on a AVIII 500 MHz NMR spectrometer equipped with a 5 mm TBI probe (^{1}H, ^{31}P-^{109}Ag, ^{13}C) with z-gradient coil which could be tuned on the broadband X-channel to ^{103}Rh beyond the specifications. The typical $\pi/2$ ^{103}Rh pulse length was 90 µs when a pulse power of 180 W was used.

Spectra with ^{103}Rh in the indirect dimension (X-^{103}Rh-HMBC, H(C)Rh) were generally sparsely sampled (10% - 15% NUS), which reduced the measurement time significantly.

IR: Alpha Platinum ATR (Bruker), wavenumbers ($\tilde{\nu}$) in cm^{-1} Most medium and weak resonances were omitted.

MS (EI): Finnigan MAT 8200 (70 eV), ESI-MS: ESQ 3000 (Bruker) or Thermo Scientific LTQ-FT or Thermo Scientific Exactive Spectrometer. HRMS: Bruker APEX III FT-MS (7 T magnet), MAT 95 (Finnigan), Thermo Scientific LTQ-FT or Thermo Scientific Exactive Spectrometer. GC-MS spectra were measured on a Shimadzu GCMS-QP2010 Ultra instrument.

Unless stated othewise, all commercially available compounds including the complexes $Rh(acac)_3$, $Rh_2(OAc)_4$ (**1**), $Rh_2(TPA)_4$ (**13**), $Rh_2(esp)_2$ (**14**) and Rh_2(*S*-PTTL)$_4$ (**15**) (abcr, Acros, Aldrich, Alfa Aesar, Fluoro Chem, Strem, TCI) were used as received.
$Rh_2(OTfa)_4$ (**6**),[3] $Rh_2(MHP)_4$ (**17**)[4] and BiRh(OTfa)$_4$ (**19**)[5] were prepared according to literature procedures.

2. Dirhodium Complexes

The heteroleptic dirhodium acetate/trifluoroacetate complexes (**2**, **3** and **5**) were prepared according to a modified literature protocol, originally reported for the synthesis of **3**.[6] A flame dried two-neck flask with attached reflux condenser was charged with $[Rh_2(OAc)_4]2H_2O$ (200 mg, 0.42 mmol) under Ar atmosphere. Trifluoroacetic acid (20 mL, 261.17 mmol) was added and the resulting suspension was stirred at the indicated temperature. After the allocated reaction time had passed, the mixture was allowed to cool to ambient temperature and all volatile materials were removed under reduced pressure. The resulting green residue contained a mixture of heteroleptic complexes which were separated by flash chromatography (silica, gradient of CH_3CN/toluene: 2 : 98 – 1 : 1).
Variation of temperature and reaction time strongly influenced the composition of the obtained mixture. When the reaction mixture was stirred for **150 min at ambient temperature**, the following composition was obtained: $Rh_2(OAc)_3$(OTfa): 2mg, 0.01 mmol, 1%; *cis*-$Rh_2(OAc)_2(OTfa)_2$: 143 mg, 0.26 mmol, 62%; $Rh_2(OAc)(OTfa)_3$: 67 mg, 0.11 mmol, 27%; $Rh_2(OTfa)_4$: 10 mg, 0.02 mmol, 4%.
After **15 min at 72°C**, the composition was as follows (starting with 150 mg $[Rh_2(OAc)_4]2H_2O$ (0.36 mmol)): *cis*-$Rh_2(OAc)_2(OTfa)_2$: 36 mg, 0.07 mmol 18%; $Rh_2(OAc)(OTfa)_3$: 69 mg, 0.16 mmol, 46%; $Rh_2(OTfa)_4$: 78 mg, 0.12 mmol 33%.

Dirhodium(II)tris(acetate)trifluoroacetate [$Rh_2(OAc)_3(OTfa)$] (2): Green solid material; 1H NMR (500 MHz, CD_3CN) δ 1.82 (s, 6H), 1.8 (s, 3H) ppm; ^{13}C-NMR (151 MHz, CD_3CN): δ = 194.0, 193.2, 174.1 (q, $J_{C\text{-}F}$ = 38.4 Hz), 23.7, 23.6 ppm (CF_3 not detected); ^{19}F-NMR (565 MHz, $CDCl_3$): δ = −70.5 ppm; HRMS (ESI+): m/z calcd. for $C_8H_9F_3O_8Rh_2Na$ [M+Na]: 518.8252; found: 518.8255.

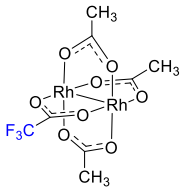

***cis*-Dirhodium(II)bis(acetate)bis(trifluoroacetate) [*cis*-$Rh_2(OAc)_2(OTfa)_2$] (3):** Analytical data is in agreement with the reported data.[6] Blue-green solid material; ^{1}H-NMR (600 MHz, CD_3CN): δ = 1.85 ppm; ^{13}C{^{1}H}-NMR (151 MHz, CD_3CN): δ = 195.3, 175.1 (q, $J_{C\text{-}F}$ = 38.9 Hz), 111.8 (q, $J_{C\text{-}F}$ = 285.0 Hz), 23.8 (d, $J_{C\text{-}Rh}$ = 1.8 Hz) ppm; ^{19}F-NMR (565 MHz, CD_3CN): δ = −70.5 ppm; HRMS (ESI+): m/z calcd. for $C_8H_6F_6O_8Rh_2Na$ [M+Na]: 572.7969; found: 572.7960.

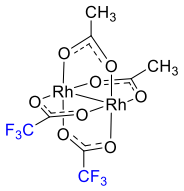

***trans*-Dirhodium(II) bis(acetate)bis(trifluoroacetate) [*trans*-$Rh_2(OAc)_2(OTfa)_2$] (4):** Prepared according to a reported literature protocol.[6] ^{1}H-NMR (600 MHz, CD_3CN): δ = 1.86 ppm; ^{13}C{^{1}H}-NMR (151 MHz, CD_3CN): δ = 194.5, 175.7 (q, $J_{C\text{-}F}$ = 39.1 Hz), 111.3 (q, $J_{C\text{-}F}$ = 284.4 Hz), 23.9 (d, $^3J_{C\text{-}Rh}$ = 1.4 Hz) ppm; ^{19}F-NMR (565 MHz, CD_3CN): δ = −75.7 ppm; HRMS (ESI-): m/z calcd. for $C_8H_7F_6O_9Rh_2$ [M+OH]: 566.8110; found: 566.8114.

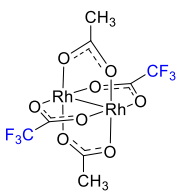

Dirhodium(II)acetatetris(trifluoroacetate) [$Rh_2(OAc)(OTfa)_3$] (5): Blue solid material; ^{1}H-NMR (500 MHz, CD_3CN): δ = 1.96 (s, CH_3CN), 1.90 (s, 3H) ppm; $^{13}C\{^1H\}$-NMR (151 MHz, CD_3CN): δ = 196.7, 176.8 (q, $^2J_{C\text{-}F}$ = 39.6 Hz), 176.0 (q, $^2J_{C\text{-}F}$ = 39.4 Hz), 111.4 (m, $2CF_3$) 24.0 (d, $^3J_{C\text{-}Rh}$ = 1.6 Hz) ppm; ^{19}F-NMR (565 MHz, CD_3CN): δ = -70.4, -70.5 ppm; HRMS (DP-EI): m/z calcd. for $C_8H_3F_9O_8Rh_2$ [M+]: 603.77888; found: 603.7798.

Dirhodium(II) (acetamidate)tris(pivalate) [$Rh_2(ACAM)(OPiv)_3$] (16): A flame dried two-neck flask with an attached reflux condenser was charged under Ar with dirhodium(II) tetrakis(acetamidate) dihydrat [$Rh_2(ACAM)$]·$2H_2O$ (80 mg, 0.17 mmol)[7] and pivalic acid (53 mg, 0.51 mmol). Chlorobenzene (20 mL) was added and the purple suspension was first degassed by bubbling Ar through it for 15 min before it was stirred at 132°C for 18 h, during which the color changed from purple to green. The mixture was allowed to cool to ambient temperature and the volatile materials were removed under reduced pressure. The resulting green-blue residue was purified by flash chromatography (silica, acetonitrile:toluene 1:9) to give the title compound as a green solid material (15 mg, 16%). ^{1}H-NMR (600 MHz, CD_3CN): δ = 4.86 (s, 1H), 1.78 (s, 3H), 0.93 (s, 9H), 0.89 (s, 18H) ppm; $^{13}C\{^1H\}$-NMR (151 MHz, CD_3CN): δ = 198.5, 196.8, 187.0, 40.7, 40.5, 28.3, 28.0, 24.2 ppm; ^{15}N-NMR (^{1}H-^{15}N-HMBC, CD_3CN): δ = 296.0 ppm. HRMS (ESI-): m/z calcd. for $C_{17}H_{30}O_7NRh$ [M-H]: 566.0138; found: 566.0142.

Dirhodium(II) tetrakis(pivalate) [$Rh_2(OPiv)_4$] (7). Isolated as a second fraction from the crude product; green solid material (21 mg, 20%); Analytical data matches the literature.[8] ^{1}H-NMR (400 MHz, CD_3CN): δ = 0.91 (s, 36H) ppm; HRMS (ESI+): m/z calcd. for $C_{20}H_{36}O_8Rh_2Na$ [M+Na]: 633.0407; found: 633.0407.

Dirhodium tetraformiat [$Rh_2(HCO_2)_4$] (8): Prepared according to a literature procedure.[9] ^{1}H-NMR (400 MHz, CD_3CN): δ = 6.89 (t, $^3J_{H\text{-}Rh}$ = 4.7 Hz, 4H) ppm; $^{13}C\{^1H\}$-NMR (101 MHz, CD_3CN): δ = 183.2 ppm.

Representative Procedure for Ligand Exchange on [$Rh_2(OTfa)_4$] or [$BiRh(OTfa)_4$]. Dirhodium(II) tetra(acetate-2-^{13}C) ($Rh_2(OAc\text{-}2\text{-}^{13}C)_4$): A flame dried Schlenk flask was charged under Ar with dirhodium(II) tetrakis(trifluoroacetate) [$Rh_2(OTfa)_4$] (35 mg, 0.05 mmol) and acetonitrile (0.1 mL). Acetic acid-2-^{13}C (44 μL, 0.32 mmol) and triethylamine (19 μL, 0.33 mmol) were added to the red suspension, which was stirred at 60°C for 30 min. The mixture was allowed to cool to ambient temperature before all volatile materials were removed under reduced pressure. The resulting purple residue was purified by flash chromatography (silica, acetonitrile) to give the title compound with axially coordinated acetonitrile as a purple solid compound (24 mg, 97%). ^{1}H-NMR (400 MHz, CD_3CN): δ = 1.77 (d, $^1J_{CH}$ = 128.7 Hz, 12H) ppm; $^{13}C\{^1H\}$-NMR (101 MHz, CD_3CN): δ = 191.7, 23.5 (t, $^3J_{C\text{-}Rh}$ = 1.8 Hz) ppm; HRMS (ESI+): m/z calcd. for $^{13}C_4C_4H_{12}O_8Rh_2Na$ [M+Na]: 468.8669; found: 468.8674.

Dirhodium(II) tetra(acetate-1-^{13}C) [Rh_2(OAc-2-^{13}C)$_4$]. Prepared analogously from [Rh_2(OTfa)$_4$] (35 mg, 0.05 mmol), acetic acid-1-^{13}C (44 μL, 0.32 mmol) and triethylamine (19 μL, 0.33 mmol) as a purple solid material (21 mg, 82%). ^{1}H-NMR (400 MHz, CD_3CN): δ = 1.77 (d, $^2J_{C\text{-}H}$ = 6.4 Hz, 1H) ppm; ^{13}C{^{1}H}-NMR (101 MHz, CD_3CN): δ = 191.9, 23.5 (d, $^2J_{C\text{-}C}$ = 56.7 Hz) ppm; HRMS (ESI+): m/z calcd. for $^{13}C_4C_4H_{12}O_8Rh_2Na$ [M+Na]: 468.8669; found: 468.8671.

Dirhodium(II) tetra(benzoate) [Rh_2(OBz)$_4$] (9): Prepared analogously from (Rh_2(OTfa)$_4$) (30 mg, 0.05 mmol), benzoic acid (35 mg, 0.29 mmol) and triethylamine (40 μL, 0.29 mmol) as a green solid material (33 mg, 94%). ^{1}H-NMR (400 MHz, CD_3CN): δ = 7.88 – 7.78 (m, 8H), 7.43 (m, 4H), 7.35 – 7.26 (m, 8H) ppm; ^{13}C{^{1}H}-NMR (101 MHz, CD_3CN): δ = 186.2, 133.1, 132.3, 129.2, 129.0 ppm; HRMS (ESI+): m/z calcd. for $C_{28}H_{20}O_8Rh_2Na$ [M+Na]: 712.9161; found: 712.9157.

Dirhodium(II) tetrakis(*p*-fluorobenzoate) [Rh_2(*p*-F-C_6H_4COO)$_4$] (10): Prepared analogously from [Rh_2(OTfa)$_4$] (30 mg, 0.05 mmol), *p*-fluorobenzoic acid (39 mg, 0.28 mmol) and triethylamine (40 μL, 0.29 mmol) as a blue-green solid material (30 mg, 86%). Analytical data matches the literature.[10] ^{1}H-NMR (400 MHz, THF-d_8): δ = 7.95 – 7.83 (m, 8H), 6.96 (t, *J* = 8.7 Hz, 8H) ppm; HRMS (ESI+): m/z calcd. for $C_{28}H_{16}O_8F_4Rh_2Na$ [M+Na]: 784.8784; found: 784.8772.

Dirhodium(II) tetrakis(*p*-trifluoromethylbenzoate) [Rh_2(*p*-F_3C-C_6H_4COO)$_4$] (11): Prepared analogously from [Rh_2(OTfa)$_4$] (30 mg, 0.05 mmol), *p*-trifluoromethylbenzoic acid (39 mg, 0.28 mmol) and triethylamine (40 μL, 0.29 mmol) as a green solid material (35 mg, 80%). Analytical data matches the literature.[10] ^{1}H-NMR (400 MHz, THF-d_8): δ = 8.02 (d, *J* = 8.1 Hz, 8H), 7.59 (d, *J* = 8.2 Hz, 8H) ppm; HRMS (APPI+): m/z calcd. for $C_{32}H_{17}O_8F_{12}Rh_2$ [M+H]: 962.8836; found: 962.8834.

Dirhodium(II) tetrakis(chloroacetate) (12): Prepared analogously from [Rh_2(OTfa)$_4$] (30 mg, 0.05 mmol), chloroacetic acid (16 mg, 0.28 mmol) and triethylamine (40 μL, 0.29 mmol) as a green solid material (35 mg, 80%). ^{1}H-NMR (600 MHz, CD_3CN): δ = 3.92 (s, 8H) ppm; ^{13}C{^{1}H}-NMR (151 MHz, CD_3CN): δ = 187.8, 42.4 ppm; HRMS (ESI+): m/z calcd. for $C_8H_8O_8Cl_4Rh_2Na$ [M+Na]: 600.6976; found: 600.6973.

[Rh_2(*S*-BNAZ)$_4$] (18): Prepared according to a literature procedure.[11] The crude material was purified by HPLC (150 mm x 30 mm, YMC-Triart C18, 5 μm, 4.6 mm i.D., 10 % methanol in water, 42.5 mL·min^{-1}, 7 min, UV 220 nm; retention time of product: 3.5 min).

^{1}H-NMR (400 MHz, CD_3CN): δ = 7.48 – 7.27 (m, 20H), 5.22 – 5.05 (m, 8H), 3.79 – 3.72 (m, 4H), 3.23 (dd, *J* = 13.4, 4.6 Hz, 2H), 3.03 (m, 4H), 2.85 (dd, *J* = 13.4, 4.6 Hz, 2H) ppm; ^{13}C{^{1}H}-NMR (101 MHz, CD_3CN): δ = 189.6, 189.3, 174.7, 173.9,

137.6, 137.2, 129.7, 129.4, 129.3, 129.2, 129.1, 128.9, 67.5, 67.0, 53.4, 52.9, 44.0, 43.1 ppm. HRMS (ESI+): m/z calcd. for $C_{44}H_{40}O_{12}Rh_2Na$ [M+Na]: 1045.0645; found: 1045.0649.

3. Bismuth-Rhodium Complexes

Bismuth-rhodium tetra(acetate-2-^{13}C) (20-2-^{13}C): Prepared analogously from [BiRh(OTfa)$_4$] (25 mg, 0.03 mmol), acetic acid-2-^{13}C (30 μL, 0.22 mmol) and triethylamine (13 μL, 0.22 mmol) as a yellow solid material, which precipitated during the reaction and was isolated by filtering the reaction mixture and washing the yellow solid compound with cold acetonitrile (11 mg, 69%). NMR samples were prepared by heating a suspension of the title compound in CD_3CN to reflux for 1 min, until the compound had partially dissolved. ^{1}H-NMR (400 MHz, CD_3CN): δ = 1.93 (d, $^1J_{C\text{-}H}$ = 129.9 Hz, 12H) ppm; ^{13}C{^{1}H}-NMR (101 MHz, CD_3CN): δ =22.4 (d, $^3J_{C\text{-}Rh}$= 0.9 Hz) ppm (Carboxylate-C not detected); HRMS (ESI+): m/z calcd. for $^{13}C_4C_4H_{12}O_8BiRhNa$ [M+Na]: 574.9417; found: 574.9420.

Bismuth-rhodium tetra(acetate) [BiRh(OAc)$_4$] (20): Prepared analogously from [BiRh(OTfa)$_4$] (50 mg, 0.07 mmol), acetic acid (55 μL, 0.39 mmol) and triethylamine (23 μL, 0.40 mmol) as a yellow solid material, which precipitated during the reaction and was isolated by filtering the mixture and washing the yellow solid material with cold acetonitrile (28mg, 78%). NMR samples were prepared by heating a suspension of the title compound in CD_3CN to reflux for 1 min, until the compound had partially dissolved. Analytical data matches the literature.[12] ^{1}H-NMR (400 MHz, CD_3CN): δ = 1.91 (s, 12H) ppm; ^{13}C{^{1}H}-NMR (151 MHz, CD_3CN): δ = 187.2, 22.4 ppm; HRMS (ESI+): m/z calcd. for $C_8H_{12}O_8BiRhNa$ [M+Na]: 570.928; found: 570.9282.

Bismuth-rhodium tetraformiat [BiRh(HCO$_2$)$_4$] (21): Prepared analogously from [BiRh(OTfa)$_4$] (15 mg, 0.02 mmol), formic acid (5 μL, 0.12 mmol) and triethylamine (17 μL, 0.12 mmol) and purified by flash chromatography (silica, CH_3CN : toluene 1:9) to give the title compound as a yellow solid (6 mg, 66%). ^{1}H-NMR (400 MHz, CD_3CN): δ = 8.44 (d, ^3J = 3.0 Hz, 4H) ppm; ^{13}C{^{1}H}-NMR (101 MHz, CD_3CN): δ = 177.4 ppm; HRMS (ESI+): m/z calcd. for $C_4H_5O_8BiRh$ [M+H]: 492.8838; found: 492.8836.

[BiRh(esp)$_2$] (22): Prepared analogously from [BiRh(OTfa)$_4$] (8 mg, 0.01 mmol), α,α,α',α'-tetramethyl-1,3-benzodipropionic acid (9 mg, 0.06 mmol) and triethylamine (9 μL, 0.6 mmol); purification by flash chromatography (silica, CH_3CN) gave the title compound as a yellow solid material (9 mg, 93%). Analytical data matched the literature.[12] ^{1}H-NMR (400 MHz, CD_3CN): δ = 7.08 (t, J = 7.5 Hz, 2H), 6.89 (dd, J = 7.6, 1.8 Hz, 4H), 6.72 (m, 2H), 2.79 (d, $^2J_{H\text{-}H}$ = 12.5 Hz, 4H), 2.55 (d, $^2J_{H\text{-}H}$ = 12.6 Hz, 4H), 1.07 (s, 12H), 0.98 (s, 12H) ppm; HRMS (ESI+): m/z calcd. for $C_{32}H_{40}O_8BiRhNa$ [M+Na]: 887.1472; found: 887.1472.

Table S1. Overview of ^{103}Rh NMR shifts of different rhodium paddlewheel complexes. All shifts were measured at 298K and are referenced to Ξ(^{103}Rh) = 3.16 MHz.

#	Compound	pKa ligand	solvent	δ ^{103}Rh [ppm]	NMR-experiment
1	$Rh_2(OAc)_4$	4.76 [13]	CD_3CN	7301	H(C)Rh
			[D_8]-THF	7427	H(C)Rh
			[D_6]-acetone	7495	H(C)Rh
			CD_2Cl_2 / PPh_3	7005	H(C)Rh
2	$Rh_2(OAc)_3(OTfa)$	3.51[c]	CD_3CN	7382	H(C)Rh
3	*cis*-$Rh_2(OAc)_2(OTfa)_2$	2.26[c]	CD_3CN	7466	H(C)Rh
4	*trans*-$Rh_2(OAc)_2(OTfa)_2$	2.26 [c]	CD_3CN	7489	H(C)Rh
5	$Rh_2(OAc)(OTfa)_3$	1.00[c]	CD_3CN	7574	H(C)Rh
6	$Rh_2(OTfa)_4$	-0.25[b]	CD_3CN	7686	1D-^{103}Rh
7	$Rh_2(OPiv)_4$	5.05[13]	CD_3CN	7306	H(C)Rh
8	$Rh_2(HCO_2)_4$	3.77[b]	CD_3CN	7422	^{1}H-^{103}Rh-HMBC
9	$Rh_2(OBz)_4$	4.20[b]	CD_3CN	7339	H(C)Rh
			[D_8]-THF	7411	H(C)Rh
10	$Rh_2(p\text{-}FC_6H_4COO)_4$	4.14[d]	[D_8]-THF	7437	H(C)Rh
11	$Rh_2(p\text{-}F_3CC_6H_4COO)_4$	3.69[d]	[D_8]-THF	7444	H(C)Rh
12	$Rh_2(ClCH_2CO_2)_4$	2.86[13]	CD_3CN	7456	H(C)Rh
13	$Rh_2(TPA)_4$	4.03[d]	[D_8]-THF	7479	H(C)Rh
14	$Rh_2(esp)_2$	4.45[d]	CD_3CN	7327	H(C)Rh
15	$Rh_2(PTTL)_4$	3.66	CD_3CN	7382	H(C)Rh
16	$Rh_2(ACAM)(OPiv)_4$		CD_3CN	7333/6288	H(C)Rh
17	$Rh_2(mhp)_4$	12.12[d]	CD_2Cl_2/CD_3CN (50/50 *v/v*)	5725	H(C)Rh
				5726	^{1}H-^{103}Rh-HMBC
18	$Rh_2(BNAZ)_4$	13.75[d]	CD_3CN	5709	^{1}H-^{103}Rh-HMBC
19	$BiRh(TFA)_4$	-0.25[b]	CD_3CN	6858	1D-^{103}Rh
20	$BiRh(OAc)_4$	4.76 [13]	CD_3CN	6423	H(C)Rh
21	$BiRh(HCO_2)_4$	3.77[b]	CD_3CN	6445	HMBC
22	$BiRh(esp)_2$	4.45[d]	[D_8]-THF	6323	H(C)Rh

[a] M. B. Smith, March's Advanced Organic Chemistry: Reactions, Mechanisms, and Structure 7th Edition, Wiley, New York, 2001. [b] D.H. Ripin, D.A. Evans, pKa's of Inorganic and Oxo-Acids, available at http://ccc.chem.pitt.edu/wipf/MechOMs/evans_pKa_table.pdf [c] The arithmetic mean of the pKa values of the ligands were used [d] Predicted pKa values from Scifinder; Calculated using Advanced Chemistry Development (ACD/Labs) Software V11.02 (© 1994-2021 ACD/Labs)

4. Supporting NMR Spectroscopic Data

Comments on the H(C)Rh sequence

Example parameters are shown in the following Table:

Table S2. Typical H(C)Rh acquisition parameters (example: $Rh_2(OAc)_4$ in CD_3CN)

	Channel				
	^{1}H	**^{13}C**	**^{103}Rh**	NS	8
	f1		f2	GPNAM	SMSQ10.100
pulse program	H(C)Rh			GPZ(1)	80%
Offset (ppm)	5	22.565	-1000*	GPZ(2)	80%
SW (ppm)	20	x	500	GPZ(3)	5.06%
TD	2048		128	gradient pulse	1 ms
P90 (µs)	8.8	23.3	90	Δ_1	1.95 ms
PL (W)	13	240	180	Δ_2	52 ms
CPD		waltz16 (1120.00 µs, 0.157W)		NUS	10%

** Ξ(^{103}Rh)= 3.186447%*

Generally, a second H(C)Rh with the same Rh offset O3, but different SW (normally 700 ppm) in the indirect dimension was acquired to make sure that the observed peak is not folded. For highly concentrated samples (e.g. sat. $Rh(acac)_3$ in $CDCl_3$), a significant t_1 noise from ^{1}H attached to ^{12}C was observed in the spectra. *Mobley*[14] suggested a modified gradient scheme in his work, which is aimed to suppress artefacts from direct ^{1}H-X couplings due to a better coherence pathway selection at a cost of losing half of the signal. Although there was no residual ^{1}H-^{103}Rh coupling present in the systems, the t_1 noise was also significantly reduced. The alternative gradient ratios for the H(C)Rh sequence are the following: G1:G2:G3=75:42:14.2.

HMQC Magnetisation Transfer – The Importance of Δ_2

During the initial measurements, $\Delta_2 = 1/(4\times J_{CRh})$ was used in the H(C)Rh sequence for the $Rh_2(OAc)_4$ sample in CD_3CN. None of the two proposed magnetisation transfer pathways resulted in an observable NMR signal; only t_1 noise was observed. When taking a closer look at the magnetization transfer, a difference to mononuclear rhodium complexes becomes visible. In the latter case the magnetization is only transferred to a single ^{103}Rh, similar to analogue classic ^{1}H,^{13}C measurements at natural abundance. In dirhodium paddlewheel systems, the magnetization is transferred from one carbon to two chemically equivalent ^{103}Rh nuclei. The magnetization transfer efficiency in the HMQC step of generic IS_n spin systems has been investigated by *Xiang* et al.[15] Adapted for the H(C)Rh sequence, the cross peak intensity *I* can be described as following:

$$I \sim [\sin(\pi J_{CRh} 2\Delta_2) \cos^{n-1}(\pi J_{CRh} 2\Delta_2)]^2 \quad \text{(I)}$$

whereby $2\Delta_2$ is the delay for the ^{13}C-^{103}Rh transfer in the pulse sequence, J_{CRh} the ^{13}C-^{103}Rh coupling constant and *n* the chemically equivalent ^{103}Rh atoms coupled to ^{13}C.

The theoretically optimal magnetization transfer delay for the IS_2 spin system in $Rh_2(OAc)_4$ is at $\Delta_2 = 1/(8\times J_{CRh})$. To verify this experimentally, $Rh_2(^{13}CH_3COO)_4$ and $Rh_2(CH_3{}^{13}COO)_4$ were used as model substrates. Different H(C)Rh spectra with different delays Δ_2 were acquired and compared to the theoretical prediction (Figure S1). Experimentally it was found that an good cross peak intensity for both transfer pathways is obtained at a delay of $\Delta_2 = 1/(12\times J_{CRh})$, which does not match the theoretical prediction. As J_{CRh} is small in the Rh(II) systems of interest (<1.7 Hz), the transverse multiple quantum relaxation, simplified denoted as T_2^*, has a significant contribution to the transfer efficiency. When adding a relaxation term to equation (I):

$$I_{\text{exp}} \sim I * e^{\frac{-4\Delta_2}{T_2^*}} \qquad \text{(II)}$$

the experimentally observed values can be described by the theoretical equation. The value Δ_2 is multiplied by factor 4 as is present 4 times in the H(C)Rh pulse sequence. These results also show limitations of the general determination of ^{103}Rh shifts with the current H(C)Rh sequence. If J_{CRh} becomes smaller or T_2^* decreases further, the expected ^{103}Rh cross peak intensity becomes smaller and the detection of the peak more challenging.

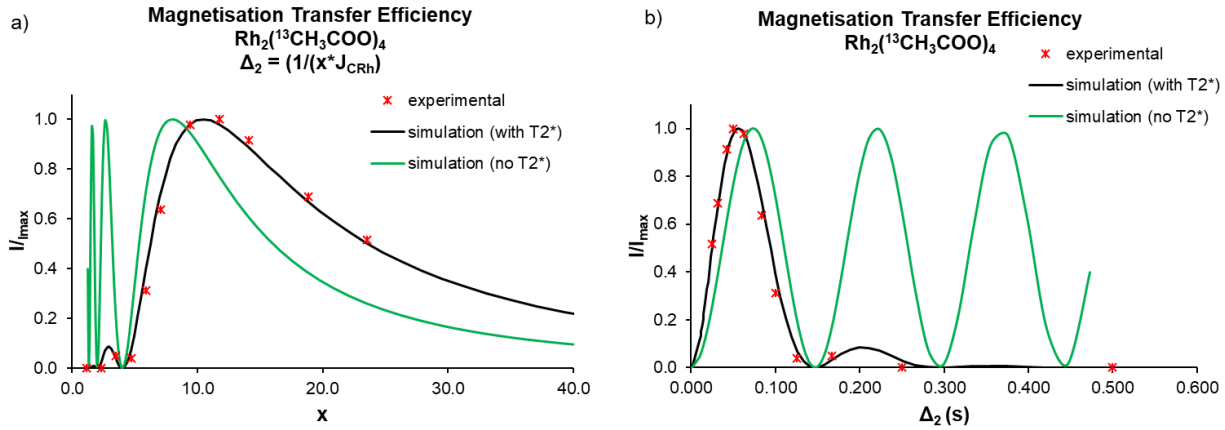

Figure S1. Analysis of the magnetization transfer efficiency from ^{13}C to ^{103}Rh. Relative cross peak intensity I/I_{max} plotted against a) x for $\Delta_2 = 1/(x \times J_{CRh})$ and b) against Δ_2. Red crosses show the experimentally measured values, the green line the theoretical expectation for equation (I) and the black line the theoretical values for equation (II). Values used for the simulations: $n_{Rh} = 2$; $J_{CRh} = 1.7$ Hz, $T_2^* = 0.24$. Sample: 15 mM $Rh_2(^{13}CH_3COO)_4$ in CD_3CN

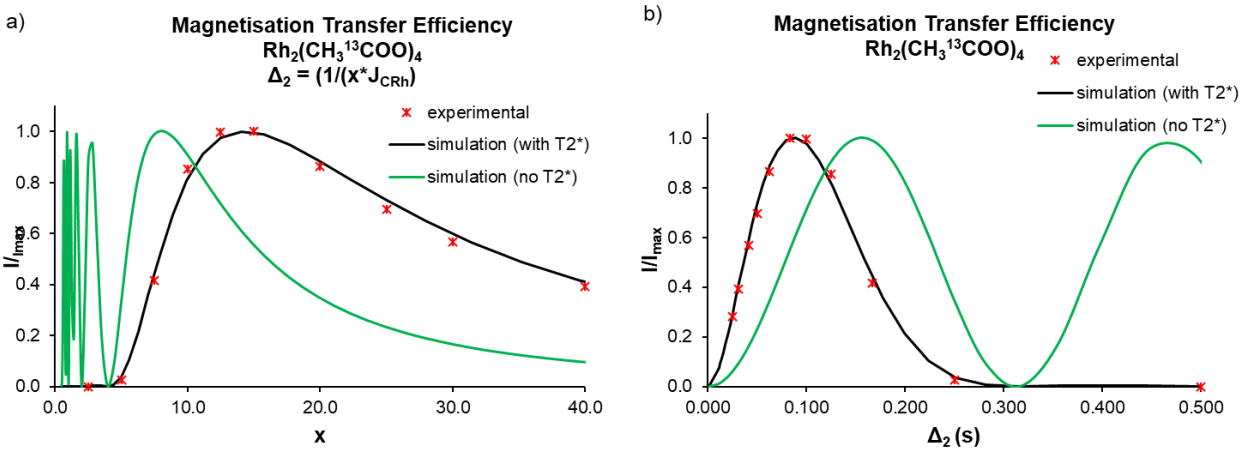

Figure S2. Analysis of the magnetization transfer efficiency from ^{13}C to ^{103}Rh. Relative cross peak intensity I/I_{max} plotted against a) x for $\Delta_2 = 1/(x \times J_{CRh})$ and b) against Δ_2. Red crosses show the experimentally measured values, the green line the theoretical expectation for equation (I) and the black line the theoretical values for equation (II). Values used for the simulations: $n_{Rh} = 2$; $J_{CRh} = 0.8$ Hz, $T_2^* = 0.24$ s. Sample: 15 mM $Rh_2(CH_3{}^{13}COO)_4$ in CD_3CN

The detailed analysis and optimization of the delay Δ_2 helped to significantly improve the cross peak signal intensity (factor >20) for $Rh_2(^{13}CH_3COO)_4$ from the H(C)Rh sequence. Using the optimized parameters ($\Delta_2 = 1/(12*J_{CRh})$), it was possible to determine the ^{103}Rh chemical shieldings of a non-enriched sample of $Rh_2(OAc)_4$ sample as well as all other complexes shown in this manuscript.

5. Computational Study

The systems considered in this study are shown in Figure S3.

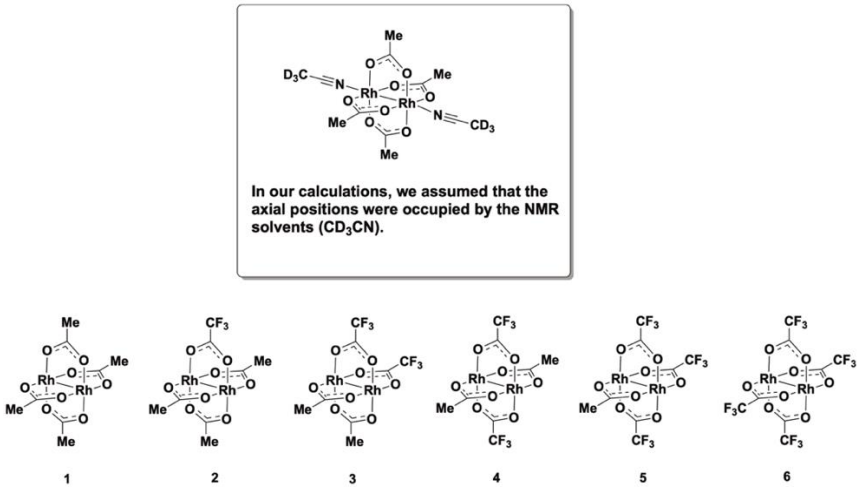

Figure S3. Systems studied in the present work

Note that the values of chemical shifts we compute using electronic structure theory which will be compared with experiment need to be referenced to a standard. For this purpose, we used the shielding of compound **1**, hence providing some compensation of systematic errors and ensuring optimal comparability. This is also done because of the special type of reference used for ^{103}Rh chemical shifts (see Experimental Section). Furthermore, due to numerical influences in the optimization and the property calculations, one might observe small asymmetries in the shieldings for nuclei that should be equivalent by symmetry. While these are typically small, in the following we report the arithmetic averages throughout the main manuscript. Further details can be found in the computational section below.

Choice of Basis Set and Influence of the DFT Integration Grid

The NMR chemical shift is a property that stresses the electron density close to the nucleus and has basis set requirements which are quite different from energies or geometry optimizations.[16] Hence, we have chosen to apply large triple-zeta quality basis sets, which were fully decontracted to allow for maximum flexibility in the core region.

Another important parameter besides the basis set is the integration grid used for computing numerical integrals. In order to assess the quality of the integration grid used in DFT, especially in conjunction with the ZORA approximation, we have computed the ^{103}Rh NMR chemical shifts using the standard grid available in ORCA 5.0 (“defgrid 2”) in comparison to a tight integration grid that should provide results close to convergence. The results at the TPSS/unc-def2-TZVPP level of theory in conjunction with the geometry optimized using CPCM and CPCM for the GIAO-NMR calculation are shown in Table S2.

Table S2 Comparison of results obtained with standard "defgrid2" and tight "defgrid3" DFT integration grid settings. Geometries obtained using CPCM, NMR shifts calculated at the TPSSh/unc-def2-TZVPP (incl. CPCM, "defgrid3" settings).

	defgrid2 settings				*defgrid3 settings*			
Comp.	σ_{iso} Rh_1	σ_{iso} Rh_2	σ_{iso} avg	δ_{iso}	σ_{iso} Rh_1	σ_{iso} Rh_2	σ_{iso} avg	δ_{iso}
1	-6841.63	-6994.49	-6918.06	0.00	-6856.62	-6863.74	-6860.18	0.00
2	-6975.99	-6895.05	-6935.52	17.46	-6936.29	-6943.07	-6939.68	79.50
3	-7004.31	-7051.59	-7027.95	109.89	-7009.53	-7014.65	-7012.09	151.91
4	-7010.67	-7127.20	-7068.93	150.88	-7037.21	-7021.84	-7029.53	169.35
5	-7325.22	-6976.30	-7150.76	232.70	-7129.95	-7139.39	-7134.67	274.49
6	-7257.47	-7195.02	-7226.25	308.19	-7207.44	-7204.24	-7205.84	345.66

Overall, the effect of a tighter integration is substantial in the absolute shieldings and still amounts to 50 ppm for the relative shifts with regard to compound **1**. As the computational effort is not drastically increased if the "defgrid 3" settings are employed, these will be used in the following, assuming that grid size effects are by far smaller when going to even tighter integration grids. Note that applying less dense grids for the evaluation of NMR chemical shifts in this case also leads to stronger asymmetry in the equivalent ^{103}Rh shifts for species such as compound **1**, which is also why standard grids are not recommended in this case.

Effect of Relativistic Contributions to the ^{103}Rh NMR Chemical Shifts

In order to assess the importance of relativistic effects, we have applied the Zeroth Order Regular Approximation (ZORA) developed by van Lenthe et al.[17,18,19] and extended to NMR Chemical shifts using the GIAO formalism as described by Wolff, Ziegler, van Lenthe and Baerends.[20,21] As we have used a new re-implementation of the scheme described in the ORCA 5.0 package, we will give some details of this implementation here. In principle, our implementation strictly follows the GIAO formalism outlined in the literature,[22,23] applying the ZORA Hamiltonian in the SCF for the calculation of the density. The ZORA Hamiltonian is defined as follows :

$$h^{ZORA}(\pi) = \boldsymbol{\sigma} \cdot \boldsymbol{\pi} \frac{K}{2} \boldsymbol{\sigma} \boldsymbol{\pi} + V \tag{1}$$

$$K = \left(1 - \frac{V}{2c^2}\right)^{-1} \tag{2}$$

with the typical scaling factor K which goes to 1 in the non-relativistic limit. For the analytical evaluation of the GIAO NMR chemical shifts, in addition to including the ZORA Hamiltonian terms in the CPSCF,

this leads to modified operators required for the computation of the para- and diamagnetic contributions of the shielding tensor. Equations 3-8 illustrate this difference in the operators.

$$\sigma^d = \sum_{\mu\nu} P_{\mu\nu} \langle\mu| \frac{\partial^2 h^{11}}{\partial \mathbf{B_i} \partial \mathbf{m_K}} |\nu\rangle \tag{3}$$

$$\left(\frac{\partial^2 h^{11}_{\mu\nu}}{\partial \mathbf{B} \partial \mathbf{m_k}} \right)_{nrel} = \frac{\alpha^2}{2} \langle\mu| \frac{(\mathbf{r}_k \cdot \mathbf{r}_N)\mathbf{1} - \mathbf{r}_k \tilde{\mathbf{r}}_N + i\mathbf{Q}_{MN} \mathbf{r} \tilde{\mathbf{L}}_K}{r_K^3} |\nu\rangle \tag{4}$$

$$\left(\frac{\partial^2 h^{11}_{\mu\nu}}{\partial \mathbf{B} \partial \mathbf{m_k}} \right)_{ZORA} = \frac{\alpha^2}{2} \langle\mu| \frac{K[(\mathbf{r}_k \cdot \mathbf{r}_N)\mathbf{1} - \mathbf{r}_k \tilde{\mathbf{r}}_N] + iK\mathbf{Q}_{MN} \mathbf{r} \tilde{\mathbf{L}}_K}{r_K^3} |\nu\rangle \tag{5}$$

$$\sigma^p = \sum_{\mu\nu} \tilde{P}_{\mu\nu} \langle\mu| \frac{\partial h^{01}}{\partial \mathbf{m_K}} |\nu\rangle \tag{6}$$

$$\left(\frac{\partial h^{01}_{\mu\nu}}{\partial \mathbf{m_K}} \right)_{nrel} = \alpha^2 \langle\mu| \frac{\mathbf{r_N} \times \mathbf{p}}{r_N^3} |\nu\rangle \tag{7}$$

$$\left(\frac{\partial h^{01}_{\mu\nu}}{\partial \mathbf{m_K}} \right)_{ZORA} = \alpha^2 \langle\mu| \frac{iK}{4} \frac{\mathbf{r_N} \times \mathbf{p}}{r_N^3} |\nu\rangle \tag{8}$$

The dia- and paramagnetic contributions to the shielding constants are evaluated as the corresponding derivatives of the density and operators, including the density and the perturbed density evaluated in the CPSCF equations with the magnetic field components as perturbation (eq. 3 and 6). The property integrals required for the evaluation of the contributions are given in equations 4,5 and 7,8 for the dia- and paramagnetic contributions (using Gauge Including Atomic Orbitals). Here one can see that the basic difference in the operator derivatives arise from the scaling with K.

Due to this feature, the corresponding property integrals are typically not evaluated analytically, and our new implementation is based on a numerical integration for the evaluation of the operators from equations 5 and 8. However, as these property integrals exhibit an extremely steep dependence with 1/r, the numerical integration for ZORA requires special care. In order to avoid problems with numerical integration of singular functions, the ORCA 5.0 implementation is built around the "subtraction of singularity" strategy, subtracting the analytical non-ZORA integrals from the ZORA counterpart, such that effectively only the numerical integration of the additional ZORA contribution enters the resulting integral, hence making to solution robust and accurate for the standard grids used in the ORCA program package.[24]

Table S3. Comparison of results obtained with and without the ZORA relativistic approximation. Geometries obtained using CPCM, NMR shifts calculated at the TPSSh/unc-def2-TZVPP (incl. CPCM, "defgrid3" settings)

	non-relativistic				ZORA			
Comp.	σ_{iso} Rh_1	σ_{iso} Rh_2	σ_{iso} avg	δ_{iso}	σ_{iso} Rh_1	σ_{iso} Rh_2	σ_{iso} avg	δ_{iso}
1	-6829.88	-6829.77	-6829.82	0.00	-6856.62	-6863.74	-6860.18	0.00
2	-6899.32	-6907.50	-6903.41	73.59	-6936.29	-6943.07	-6939.68	79.50
3	-6977.74	-6981.48	-6979.61	149.79	-7009.53	-7014.65	-7012.09	151.91
4	-7009.36	-6991.39	-7000.37	170.55	-7037.21	-7021.84	-7029.53	169.35
5	-7094.62	-7111.26	-7102.94	273.12	-7129.95	-7139.39	-7134.67	274.49
6	-7181.85	-7181.79	-7181.82	352.00	-7207.44	-7204.24	-7205.84	345.66

While this conceptually simple scalar relativistic approach does not contain higher-order or spin-orbit-coupling effects, the results in Table S4 show that relativistic effects should be small in general, as the ZORA correction only amounts to changes of less than 7 ppm and typically 2-3 ppm for the shifts. Hence, we assume that relativistic effects are small and captured sufficiently well by using the ZORA approximation in our case.

Influence of Reference Geometry and CPCM in the Computed NMR Shieldings

In order to assess the importance of solvent effects for the computation of the NMR shieldings, three schemes are compared in the following: (1) Optimizing the molecular geometry without any solvent correction and computing the NMR chemical shifts at a given level of theory, (2) optimizing the geometry including an implicit solvent correction and then computing the NMR chemical shifts at the same level of theory, and (3) optimizing the geometry with implicit solvation and including the implicit solvation also in the calculation of the NMR chemicals shifts.

Table S4. Comparison of the TPSSh results using geometries and NMR chemical shifts computed with and witout using an implicit solvation model. Right column: experimental reference values. Level of theory: TPSSh/unc-def2-TZVPP (inc. ZORA, "defgrid3" settings)

	Geometry and shieldings without implicit solvation				Geometry obtained using CPCM				Geometry obtained using CPCM, shieldings computed incl. CPCM				
Comp.	σ_{iso} Rh_1	σ_{iso} Rh_2	σ_{iso} avg	δ_{iso}	σ_{iso} Rh_1	σ_{iso} Rh_2	σ_{iso} avg	δ_{iso}	σ_{iso} Rh_1	σ_{iso} Rh_2	σ_{iso} avg	δ_{iso}	δ_{iso} exp.
1	-6811.49	-6816.69	-6814.09	0.00	-6928.49	-6933.55	-6931.02	0.00	-6856.62	-6863.74	-6860.182	0	0.0
2	-6877.52	-6889.10	-6883.31	69.22	-6982.18	-6990.68	-6986.43	55.41	-6936.29	-6943.07	-6939.682	79.5	77.8
3	-7033.37	-7039.11	-7036.24	222.15	-7033.37	-7039.11	-7036.24	105.22	-7009.53	-7014.65	-7012.090	151.91	161.2
4	-6959.61	-6944.89	-6952.25	138.16	-7054.54	-7033.55	-7044.04	113.02	-7037.21	-7021.84	-7029.529	169.35	184.3
5	-7039.34	-7045.30	-7042.32	228.23	-7118.08	-7129.08	-7123.58	192.56	-7129.95	-7139.39	-7134.672	274.49	269.4
6	-7115.47	-7110.21	-7112.84	298.75	-7161.16	-7156.37	-7158.76	227.74	-7207.44	-7204.24	-7205.842	345.66	381.7

The results are displayed in Table S4 together with the experimental shifts. It becomes obvious, that a critical ingredient for good agreement between theory and experiment are well-converged geometries that include the most important contributions for the effective effects of the solvent including implicit solvent corrections for the computation of the actual shieldings.

Influence of the Functional

In recent studies performed in our group, the TPSS and TPSSh functional have been found to offer very good accuracy at low computational cost for the calculation of a broad range of NMR chemical shifts, including several elements besides Carbon and Hydrogen.[25] For this reason, we have chosen to use these functionals. Table S5 displays the results for the TPSS and TPSSH functional in comparison to experiment. While the difference is noticable but not large, the TPSSH results show better agreement with experiment. This indicates that the obtained trends are fairly robust with choice of functional, while the functional which is considered as "higher rung" functional also delivers more accurate results.[26]

Table S5. Comparison between computed and experimental ^{103}Rh NMR chemical shifts at the TPSS and TPSSh level of theory ("defgrid3" settings, geometry and shieldings obtained using CPCM, shieldings calculated using the unc-def2-TZVPP basis and ZORA approximation).

	TPSS				TPSSh				
Comp.	σ_{iso} Rh$_1$	σ_{iso} Rh$_2$	σ_{iso} avg	δ_{iso}	σ_{iso} Rh$_1$	σ_{iso} Rh$_2$	σ_{iso} avg	δ_{iso}	δ_{iso} exp.
1	-6240.09	-6247.56	-6243.82	0.00	-6856.62	-6863.74	-6860.18	0.00	0.0
2	-6315.27	-6320.12	-6317.69	73.87	-6936.29	-6943.07	-6939.68	79.50	77.8
3	-6381.42	-6386.36	-6383.89	140.07	-7009.53	-7014.65	-7012.09	151.91	161.2
4	-6404.25	-6392.81	-6398.53	154.71	-7037.21	-7021.84	-7029.53	169.35	184.3
5	-6492.35	-6497.53	-6494.94	251.11	-7129.95	-7139.39	-7134.67	274.49	269.4
6	-6559.74	-6556.81	-6558.28	314.46	-7207.44	-7204.24	-7205.84	345.66	381.7

Analysis of the NMR Shielding Tensors using Ramsey's Expression

To gain a deeper insight into the relationship between the NMR chemical shifts and the electronic structure of these complexes, it is useful to analyze the principal components of the shielding tensor (Table S7). A graphical representation of the data is shown in Figure S4. For the sake of simplicity, only the paramagnetic contributions of the shielding tensor are discussed (the diamagnetic component is small and roughly constant for all the systems investigated here, as shown in Table S7).

Table S6. Decomposition of the paramagnetic ^{103}Rh NMR $\delta_{para,\ calc}$ shift into its principal tensor components, panel on the right displays the anisotropy of the ^{103}Rh shielding tensor using compound **1** as example.

Compound	$\delta_{para,\ calc}$	$\delta_{dia,\ calc}$	$\delta_{xx,\ calc}$	$\delta_{yy,\ calc}$	$\delta_{zz,\ calc}$
1	0	0	0	0	0
2	80	0	117	-2	112
3	153	1	110	111	196
4	171	2	263	-15	237
5	277	3	307	146	367
6	349	3	306	310	487

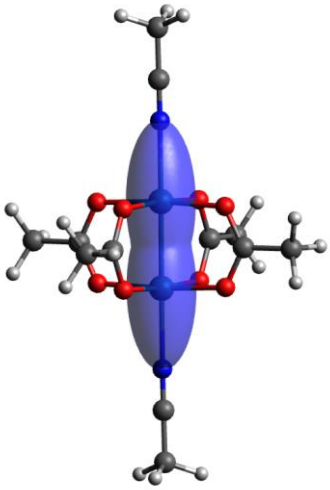

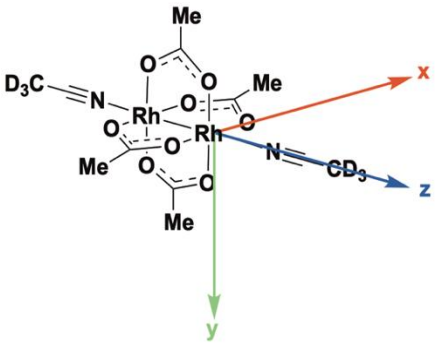

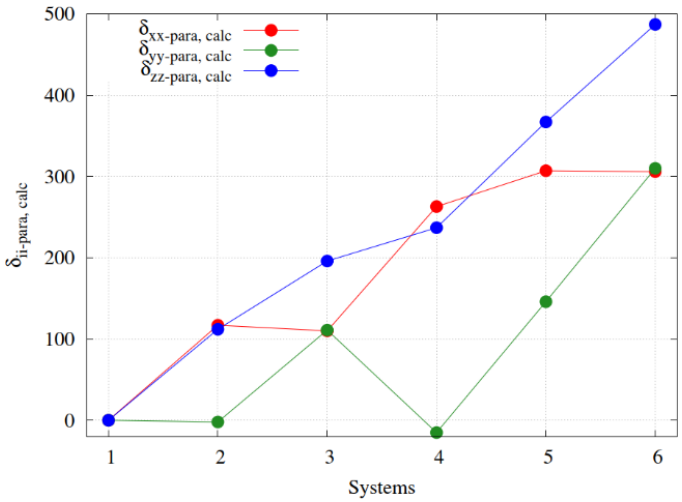

Figure S4. Left: The principal axis of the shielding tensor of Rh; right: the paramagnetic contribution to each principal component of the shielding tensor for the systems investigated here.

It is important to emphasize that the individual principal components of different systems can be safely compared because the principal axes coincide in all cases. The orientation of the principal axes is dictated by the local symmetry at the Rh center, and all the systems investigated here are classified by the lowest common point group, which is C_{2v}.

The individual components of the shielding tensor show non-intuitive variations along the series:

I. $\delta_{zz,calc}$ is the only component that shows a qualitative linear correlation with the total chemical shift. It increases with increasing the fluorination.

II. $\delta_{yy,\ calc}$ is roughly constant for complexes **1, 2** and **4,** which are not fluorinated along the x-axis

III. $\delta_{xx,\ calc}$ is roughly constant for complexes **4**,**5**,**6**, which are all fully fluorinated along the y-axis.

These variations can be interpreted in a simple orbital picture using the Ramsey formula:[27]

$$\sigma_{ii-para} = \sum_{virt}\sum_{occ} \frac{\langle \varphi_{occ}|\hat{L}_i|\varphi_{vir}\rangle\langle \varphi_{vir}|\hat{L}_i/r^3|\varphi_{occ}\rangle}{E_{vir-}E_{occ}}$$

In which Ψ_{occ} and Ψ_{vir} denote occupied and virtual orbitals, respectively; E_{occ} and E_{vir} represent the corresponding orbital energies and $\hat{L}_i$ is the angular momentum operator. Thus, deshielding in the direction $\sigma_{ii,para}$ depends on which $\Psi_{occ}$and Ψ_{vir} orbitals can be coupled by the corresponding $\hat{L}_i$ operator and by the relative energy between the orbitals.

For the complexes studied here, the three occupied molecular orbitals of highest energy correlate with the d_{xy}, d_{xz} and d_{yz} orbitals of Rh, whilst the virtual orbitals correlate with the d_{x2-y2} and d_{z2} (Figure S5).

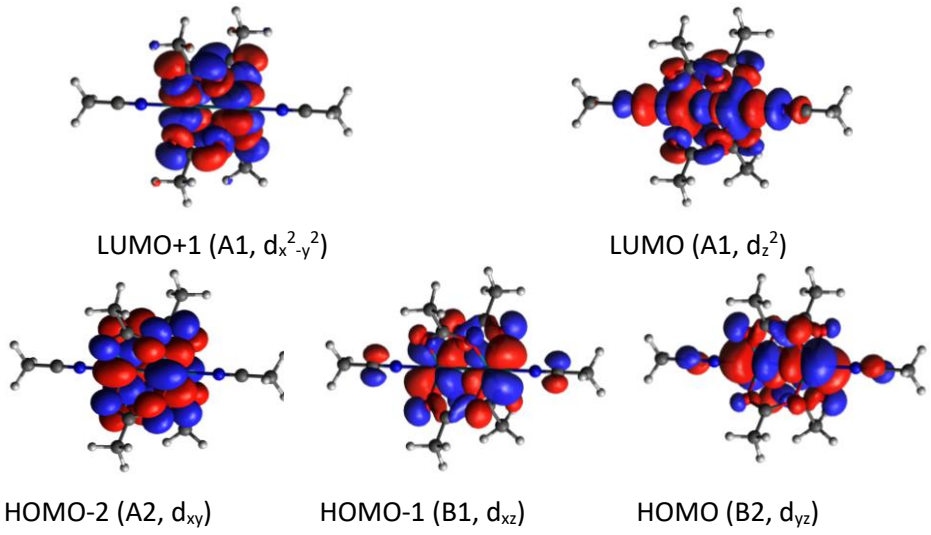

Figure S5. Key frontier orbitals for compound **1**. The associated irreducible representation in the C_{2v} molecular point group is reported in brackets. The Rh d orbital associated with each molecular orbital is also shown in brackets.

As all complexes studied here are classified as C_{2v} symmetry, these orbitals transform like the irreducible representations of this molecular point group. Thus, the d_{xy}, d_{xz}, d_{yz}, d_{x2-y2} and d_{z2} orbitals of Rh feature A2, B1, B2, A1 and A1 symmetry, respectively. The angular momentum operator belongs to the same irreducible representation of the corresponding rotation operator,[28] i.e., B2, B1 and A2 for L_X, $L_Y$and L_Z, respectively. By evaluating which products of irreducible representations of orbtials and operator yield the totally symmetric representation, it is found that the only non-zero contributions from the orbitals to the $\sigma_{xx,para}$, $\sigma_{yy,para}$ and $\sigma_{zz,para}$ components of the shielding tensor stem from the virtual orbitals with the occupied d_{yz} and d_{xz} and d_{xy} orbitals, respectively.

Thus, a detailed analysis of shielding tensor can provide unique information into the nature of the bond between the Rh and the ligands. In fact, for symmetry reasons, the d_{xy} orbital of Rh can mix with the ligands on both axis, whilst the d_{xz} and d_{yz} orbitals only mix with the orbitals of the ligands on the x- and y-axis, respectively. As a consequence, fluorination will always affect $\delta_{zz,}$ irrespective of the position of the substitution, whilst $\sigma_{xx,para}$ and $\sigma_{yy,para}$ mainly respond to fluorination on the

perpendicular y- and x-axis, respectively. These results demonstrate the connection between the experimentally observed shifts and the nature of the Rh-ligand bond for these complexes.

Note that this applies to all compounds that were analyzed (**1**-**6**). For comparison, the frontier orbitals for all computed compounds are displayed in below:

Compound 1

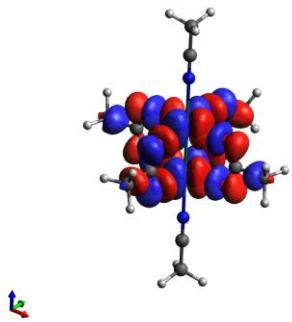

$d_{x^2-y^2}$ LUMO+2

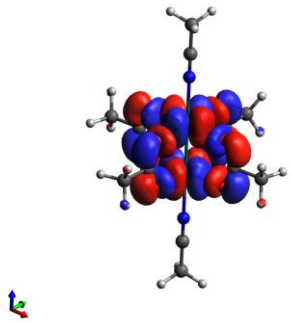

$d_{x^2-y^2}$ LUMO+1

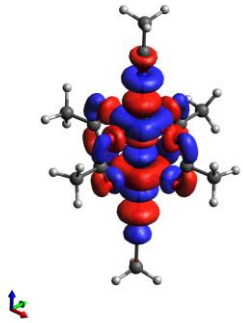

d_{z^2} LUMO

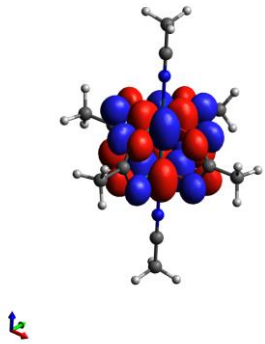

d_{xy} HOMO-2

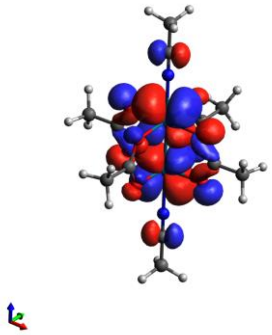

d_{xz} HOMO-1

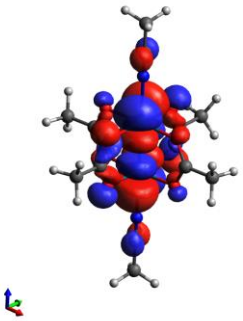

d_{yz} HOMO

Compound 2

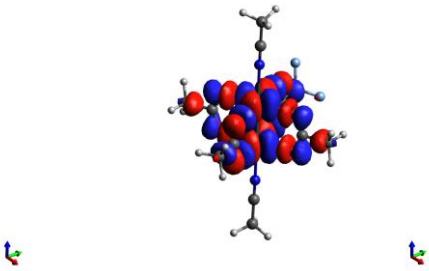

$d_{x^2-y^2}$ LUMO+2

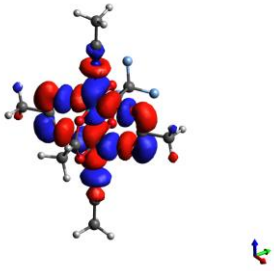

$d_{x^2-y^2}$ LUMO+1

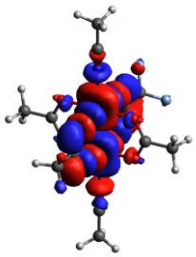

d_{z^2} LUMO

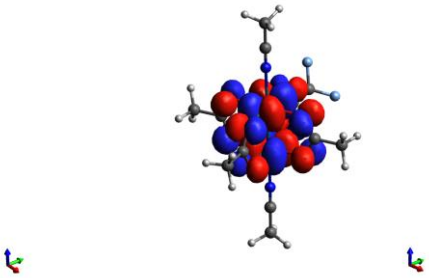

d_{xy} HOMO-2

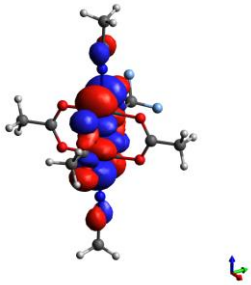

d_{yz} HOMO-1

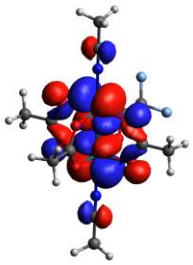

d_{xz} HOMO

Compound 3

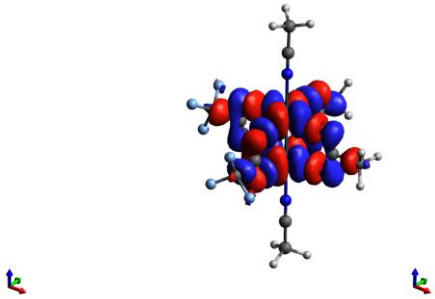

$d_{x^2-y^2}$ LUMO+2

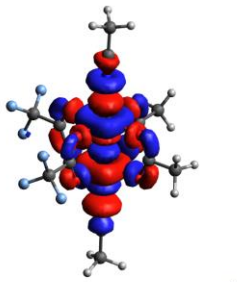

d_{z^2} LUMO+1

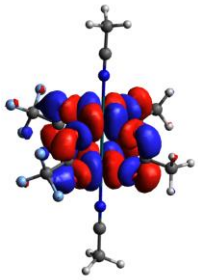

$d_{x^2-y^2}$ LUMO

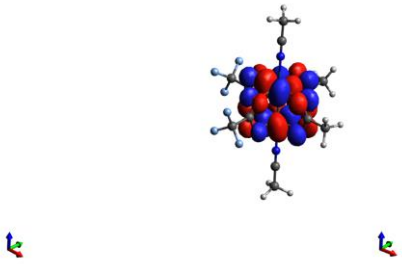

d_{xy} HOMO-2

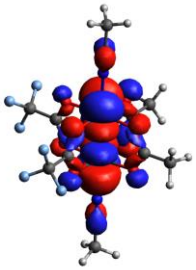

d_{yz} HOMO-1

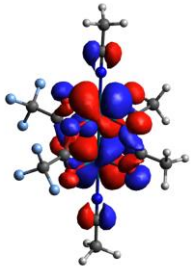

d_{xz} HOMO

Compound 4

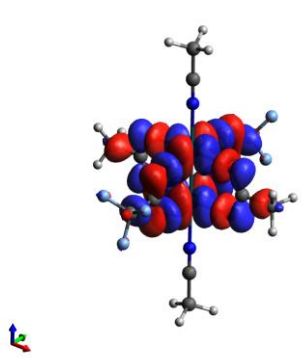

$d_{x^2-y^2}$ LUMO+2

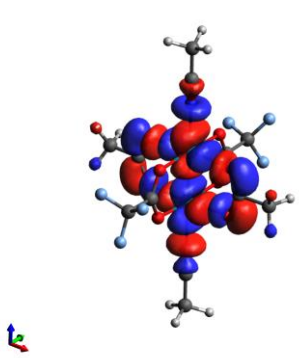

$d_{x^2-y^2}$ LUMO+1

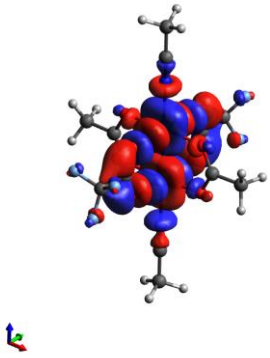

d_{x^2} LUMO

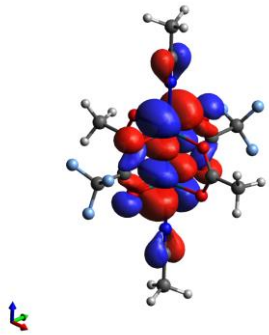

d_{yz} HOMO-2

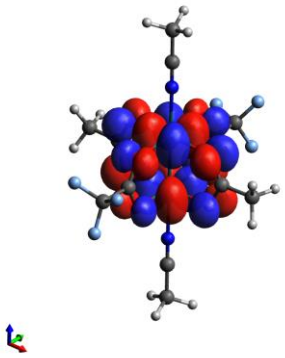

d_{xy} HOMO-1

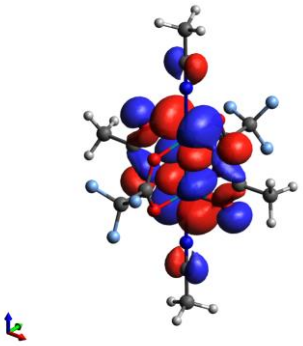

d_{xz} HOMO

Compound 5

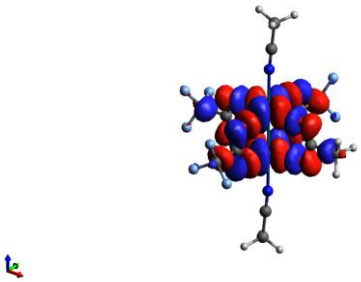

$d_{x^2-y^2}$ LUMO+2

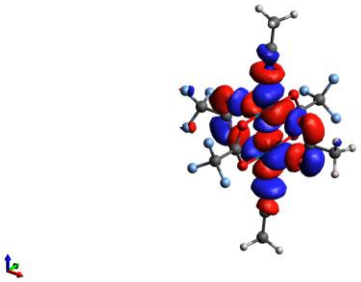

$d_{x^2-y^2}$ LUMO+1

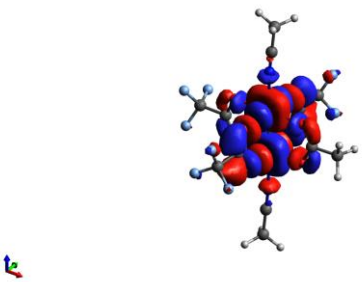

d_{x^2} LUMO

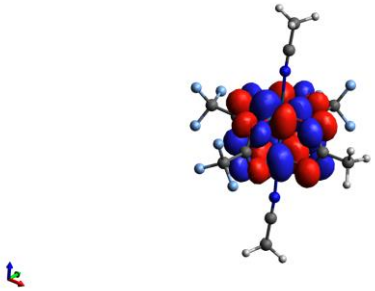

d_{xy} HOMO-2

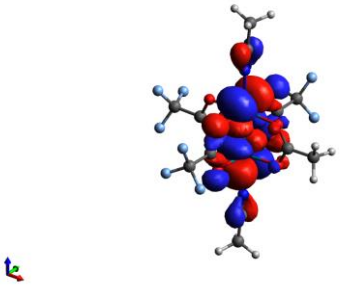

d_{yz} HOMO-1

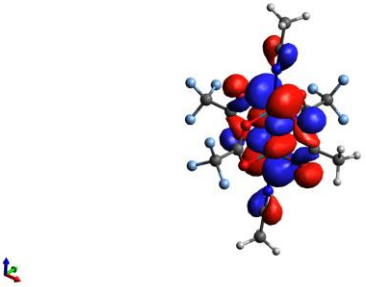

d_{xz} HOMO

Compound 6

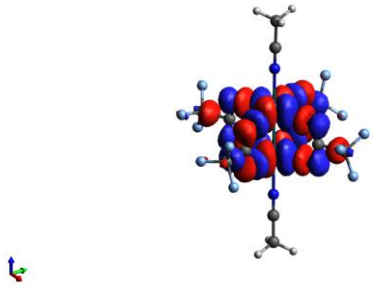

$d_{x^2-y^2}$ LUMO+2

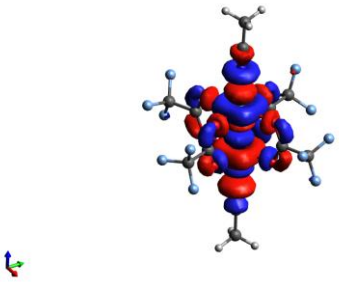

d_{z^2} LUMO+1

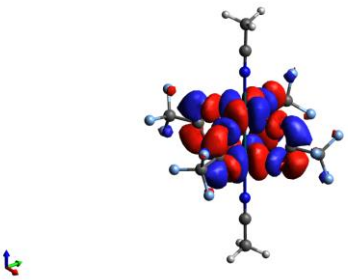

$d_{x^2-y^2}$ LUMO

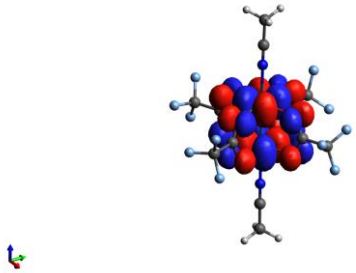

d_{xy} HOMO-2

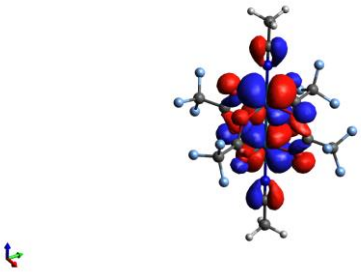

d_{xz} HOMO-1

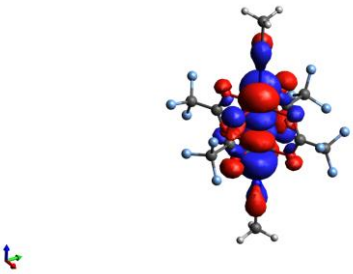

d_{yz} HOMO

Computational Details

The computational study has been carried out using a local development version of the ORCA 5.0 program package. All geometries have been optimized at the B3LYP-D3/def2-tzvp level of theory[29,30,31,32,33] employing very tight convergence criteria for SCF and structure optimization and very conservative DFT grids. In order to account for the effect of solvation, the CPCM model (acetonitrile)[34] has been applied. All minima have been confirmed by normal mode analysis.

GIAO NMR chemical shift calculations[35,36,37,38,39] have been carried out using the TPSS and TPSSH functional[40,41,42] employing the RI and RIJCOSX approximations as previous benchmarks have demonstrated good performance of this family of functionals.[25] In order to provide a sufficiently flexible basis set for the description of the 103Rh NMR chemical shifts, the SARC-ZORA-TZVPP basis set[43] has been used for Rh, while the def2-TZVPP basis set[32,33] has been chosen for all other nuclei and all basis set have been decontracted and complemented with the Autoaux auxiliary basis sets[44] available in ORCA. In order to assess whether scalar relativistic effects have a considerable effect on the relative chemical shifts, the ZORA approximation has been employed. This includes a new local implementation of the computation of NMR chemical shieldings following the scheme of Barends et al. (see above).[45] For all NMR calculations very tight SCF convergence and tight integration grid settings have been employed in conjunction with the CPCM model (Acetonitrile), see above.

Geometries and complete set of NMR chemcial shifts

1

42

C	6.21271631411349	0.45591405129841	3.13115275989291
C	7.13565441100939	1.54891553538627	3.59504547055573
O	6.99648580944699	1.95973526327767	4.78532550666839
Rh	8.26582457587901	3.40645381622545	5.51760407127364
O	9.60971942897008	4.85159877707754	6.10492526302135
C	10.47812593188086	5.26884080108469	5.28222388264636
C	11.40068458354789	6.36209359243894	5.74618322969183
Rh	9.34785751243447	3.41084542035957	3.35947627034676
O	10.61736101551509	4.85781007738536	4.09200015565479
O	8.00403890920208	1.96600352215534	2.77225059109897
O	8.01309512634564	4.86825957183082	2.78294118308944
C	7.14677374803361	5.28434130374059	3.60842367716209
C	6.23022138356561	6.38581899011324	3.15205435861836
O	10.60880103883995	1.95157996177410	4.08106083933558
C	10.47935589216711	1.54669375544230	5.27445752448014
C	11.46686836787327	0.52570483560406	5.76838519687862
O	7.00539128210615	4.86610766739902	4.79586310266079
O	9.60125848264930	1.94953129059200	6.09407698404827
H	6.08413572652533	0.49570369977689	2.05150742890686
H	6.66196235131068	-0.50609713916576	3.39061398918534
H	5.25061531861972	0.53055720690888	3.63420401914898
H	11.01599277079829	-0.10239178715463	6.53415106260568
H	11.83492969667629	-0.08101247374357	4.94361238152137
H	12.31400039915283	1.05452829087162	6.21262344092124
H	12.36160307288117	6.29014532320341	5.24053265908971
H	10.94918372091912	7.32401267611750	5.49030845673235
H	11.53200767433862	6.31996893395958	6.82542581394581
H	5.26865534937833	6.31523794708989	3.65666454465100
H	6.68669193820047	7.34337470609975	3.41540852304300
H	6.09930070157134	6.35249853354603	2.07246237548519
N	7.25078774156462	3.40203120713788	7.52124236640498
C	6.71474791675285	3.39631652598117	8.53626346220451
C	6.03698725282983	3.38936019499697	9.81703691492973
H	6.32360656934793	4.27237357658375	10.38917510188215
H	4.95776637258754	3.39651016416145	9.66049420692786
H	6.31398607364154	2.49391100720482	10.37440725507174
N	10.36290346243928	3.41511562335444	1.35588600153984
C	10.89805744386133	3.41933698561603	0.34039365039007
C	11.57472499625445	3.42431161621144	-0.94095972803321
H	11.28751382369458	2.54045605231228	-1.51150070248712
H	11.29733161146080	4.31894016523127	-1.49944648632726
H	12.65407620161112	3.41728473051288	-0.78531980486479

Nucleus	Element	Isotropic	Anisotropy
0	C	161.281	49.169
1	C	-9.519	-78.215
2	O	128.544	354.120
3	Rh	-6856.621	-6449.175
4	O	135.103	373.065
5	C	-9.356	-82.514
6	C	161.885	48.055
7	Rh	-6863.742	-6415.878
8	O	138.106	372.801
9	O	129.007	354.358
10	O	128.446	362.825
11	C	-9.371	-79.801

12	C	161.534	49.070
13	O	136.529	364.327
14	C	-9.546	-77.027
15	C	161.658	48.349
16	O	129.620	361.773
17	O	135.952	366.432
18	H	29.896	6.445
19	H	29.596	5.562
20	H	29.855	6.427
21	H	29.950	6.449
22	H	29.961	6.414
23	H	29.752	5.761
24	H	29.998	6.212
25	H	29.843	6.106
26	H	29.997	6.317
27	H	29.926	6.427
28	H	29.697	5.471
29	H	29.969	6.478
30	N	33.220	404.643
31	C	66.434	328.934
32	C	185.801	26.384
33	H	29.316	9.892
34	H	29.291	9.871
35	H	29.310	9.943
36	N	33.095	405.299
37	C	66.536	329.065
38	C	185.736	26.516
39	H	29.312	9.924
40	H	29.319	9.871
41	H	29.319	9.902

2

42

Coordinates from ORCA-job opt

C	6.23637459599114	0.44581084346502	3.09604602972484
C	7.18279765912262	1.57629295336362	3.57544515177191
O	8.02868657996944	1.97242826331893	2.74502099699637
Rh	9.36708813047956	3.44116859978985	3.36369033363655
N	10.39409544113958	3.46811201070728	1.37409447457554
C	10.94023259748188	3.46935361955494	0.36478617192769
C	11.63102432794518	3.47016402493052	-0.90861926507162
O	7.00213861193787	1.93817059516663	4.75956023376335
Rh	8.26827115880829	3.40555958883064	5.52055110801448
N	7.25153700320530	3.38556250992207	7.51442974889142
C	6.72889522621999	3.39798403242903	8.53600911138546
C	6.07002822237310	3.41512186937593	9.82608573376822
O	9.58812697944779	4.84356263130188	6.12214471812586
C	10.45606182107827	5.28021003407642	5.30849758615841
O	10.60346436842026	4.88376608888646	4.11382553877290
O	7.00253889159473	4.85964371309625	4.80219095911045
C	7.14800103009664	5.29151746911562	3.61959438322145
C	6.22728764636670	6.39038207578320	3.16885849314888
O	9.61070093396840	1.95484787288203	6.08802427801682
C	10.48873875661129	1.55681336666299	5.26523834457737
C	11.41224523676343	0.46059357006873	5.71677511820940
C	11.36487224535842	6.37577297556412	5.78763684153975
O	8.02189956752225	4.88877063362724	2.79459423929986
O	10.63500532458410	1.98970107937825	4.08306833636438
F	6.24030482316062	0.31287705237025	1.76573827368905
F	6.62791530274919	-0.72856536180373	3.62955569117795
F	4.97298046997593	0.67059334438965	3.48659796752185
H	11.53280891621390	0.48303303807796	6.79777560087071
H	10.96768161364621	-0.49815023835885	5.43789489683380
H	12.37711979816674	0.54750658366108	5.22124933941679
H	12.33544247609789	6.30381693145875	5.30076064179024
H	10.91607581614400	7.33526911261458	5.51844615316304
H	11.47425532139985	6.33634310723320	6.86921146677122
H	5.26397760694203	6.30909467575481	3.66830975655473
H	6.67727846847866	7.34784586701575	3.44342777092291
H	6.10255238012221	6.36576299856289	2.08837591150228
H	6.00583680330389	4.44082258822872	10.19094120081794
H	5.06486932009791	3.00324146288850	9.73020527358439
H	6.63959432040576	2.81475304627512	10.53622615875970
H	11.35910109460565	2.57815071259645	-1.47394887610932
H	11.35057929391091	4.35696207613564	-1.47792221180824
H	12.70848281809130	3.47567458160120	-0.74026568138931

Nucleus	Element	Isotropic	Anisotropy
0	C	59.435	30.460
1	C	9.773	-124.086
2	O	114.009	407.151
3	Rh	-6936.292	-6450.394
4	N	34.797	402.346
5	C	65.878	329.565
6	C	185.774	26.633
7	O	120.555	392.002
8	Rh	-6943.071	-6476.891
9	N	34.927	401.682
10	C	65.754	329.473
11	C	185.823	26.715
12	O	147.149	370.649
13	C	-10.808	-78.704

14	O	150.391	371.063
15	O	132.778	358.566
16	C	-10.407	-76.170
17	C	161.316	49.323
18	O	140.250	361.755
19	C	-10.334	-81.325
20	C	161.478	48.386
21	C	161.790	48.113
22	O	131.770	358.907
23	O	141.049	361.159
24	F	265.902	115.324
25	F	254.426	137.035
26	F	260.514	128.369
27	H	29.905	6.337
28	H	29.746	6.134
29	H	29.913	6.251
30	H	29.947	6.248
31	H	29.826	6.274
32	H	29.973	6.302
33	H	29.872	6.397
34	H	29.642	5.590
35	H	29.911	6.423
36	H	29.284	9.936
37	H	29.267	9.861
38	H	29.291	9.936
39	H	29.299	9.843
40	H	29.301	9.924
41	H	29.303	9.947

3

42

Coordinates from ORCA-job opt

C	6.21311535699713	0.49150706437989	3.07736392833844
F	4.94929498795931	0.94684631994461	3.13821016003176
C	7.19941996192897	1.58026701717868	3.57262653922046
O	7.01458062758213	1.93924725787831	4.75781869958122
Rh	8.27169363796692	3.40661421730663	5.52929997736494
O	9.62751533726001	1.94399308479864	6.11538775649576
C	10.49079626898363	1.58993294191471	5.28389383176310
O	10.66897323400175	1.98149241973383	4.10806955333875
Rh	9.38469067544945	3.44378523974890	3.37174010192053
O	8.04578156450362	4.87478753945799	2.80364296221695
C	7.15527377477847	5.26424357252465	3.61786807842894
C	6.16479779545686	6.27771632913730	3.12359799908728
F	6.45782669057406	0.12071083265449	1.81775147748396
F	6.29351865901197	-0.60137438011059	3.85570886433424
O	8.05316406898603	1.97364720049177	2.74901982985286
N	10.40734089033846	3.47919560662909	1.38857126700983
C	10.93081046142117	3.49630417499845	0.36777087223524
C	11.59015012352058	3.51791982597631	-0.92162115063795
O	10.60982829626047	4.88877318132797	4.12862096693017
C	10.45600131387503	5.28563860817123	5.32289208349455
C	11.35775580823869	6.38425962188850	5.80502373786680
N	7.24795173491807	3.38789555482656	7.51164113504656
C	6.72080100457128	3.40301464158371	8.53055159571002
C	6.05496852060640	3.42398989951843	9.81658354568629
O	9.58705556996772	4.84435709950321	6.13394668338004
O	7.01942347005361	4.84699928385765	4.80730109857630
C	11.49789087520104	0.50869093721757	5.75307488193350
F	11.28046227770126	0.12608995456972	7.01421497750135
F	11.41307433180561	-0.57948843157277	4.96800103517209
F	12.75557381739463	0.97646500714986	5.67199993534804
H	12.32801109781935	6.32016336871702	5.31662453682108
H	10.90154457087441	7.34135863159952	5.53968572464581
H	11.46773410962313	6.34113470110024	6.88635178863962
H	5.78170537618714	6.87120511351830	3.95088637549202
H	6.61919274250711	6.91691276617310	2.36941260210860
H	5.32948329093112	5.74277004057666	2.66462637192407
H	6.34597095079684	4.32084254136959	10.36457627749967
H	4.97449366927403	3.42584805583954	9.66890223420484
H	6.33935370922805	2.54189802750137	10.39121538658855
H	10.89043369094721	3.20035706942364	-1.69546514096817
H	11.93457802805880	4.52941579794059	-1.13961382240047
H	12.44493762643797	2.84091126355497	-0.90765775926789

Nucleus	Element	Isotropic	Anisotropy
0	C	59.365	29.954
1	F	256.068	134.898
2	C	9.078	-121.509
3	O	124.591	384.692
4	Rh	-7009.530	-6504.688
5	O	122.212	417.996
6	C	8.865	-124.189
7	O	133.864	399.052
8	Rh	-7014.649	-6502.319
9	O	143.183	350.728
10	C	-12.050	-78.596
11	C	161.046	49.574
12	F	266.911	113.051
13	F	257.345	132.474

14	O	114.109	406.929
15	N	36.657	399.109
16	C	65.194	330.130
17	C	185.847	26.836
18	O	154.280	367.955
19	C	-11.749	-66.007
20	C	161.568	48.211
21	N	36.787	398.601
22	C	65.126	329.998
23	C	185.810	26.678
24	O	151.309	366.309
25	O	141.403	352.216
26	C	59.328	29.241
27	F	264.770	113.259
28	F	255.346	135.959
29	F	256.047	134.748
30	H	29.905	6.126
31	H	29.792	6.516
32	H	29.929	6.187
33	H	29.809	6.348
34	H	29.795	6.355
35	H	29.596	5.958
36	H	29.260	9.997
37	H	29.247	9.866
38	H	29.266	9.892
39	H	29.261	9.891
40	H	29.283	10.012
41	H	29.287	9.896

4

42

Coordinates from ORCA-job opt

C	6.19946128968192	0.49276879181924	3.08545570397375
F	4.93809143679272	0.95339896511011	3.14981375716530
C	7.19058926887217	1.57898272809698	3.57558965194280
O	7.01849429407795	1.93409945788812	4.76373156142821
Rh	8.27030796406387	3.39093510733262	5.52074100724221
O	9.61729548329561	1.94355756141984	6.07777660962535
C	10.50180532097493	1.55713931885994	5.25548291269168
O	10.63306024340911	1.98067313741081	4.06755665476272
Rh	9.36568541446140	3.43231739306224	3.35449344411350
O	8.01869192508805	4.87992144720387	2.79740340881813
C	7.14358935600667	5.27715939939499	3.62474832985605
C	6.21954673335342	6.37369427680475	3.17875518474412
F	6.43992202301838	0.12038059896205	1.82584862490243
F	6.27886558686158	-0.59857302380187	3.86523003664816
O	8.03520751282137	1.97788066499101	2.74514197431263
N	10.37244124670656	3.44833846298229	1.36253992373623
C	10.89192336119160	3.40684137122110	0.34041946285586
C	11.54751463609808	3.35122476987223	-0.94983697314554
O	10.61886248886474	4.88922191293522	4.10905885000332
C	10.44267465882288	5.25056895533303	5.29336086911832
C	11.36535608789424	6.39059336712828	5.79521392150705
N	7.26076140478892	3.36295384166938	7.50913815043861
C	6.73428039627232	3.36555813174794	8.52849499913740
C	6.06909231672141	3.37037163510742	9.81501319068295
O	9.60080164040153	4.84761290981041	6.12678559148384
O	7.00148476249762	4.84105735306818	4.80679553187316
C	11.49146425628919	0.53584001478069	5.73798979993295
H	11.03599584726002	-0.11205192056767	6.48417883950944
H	11.87477892376061	-0.04832951668544	4.90421233527547
H	12.32700337499063	1.06376280284970	6.20465397254968
F	12.49749237506533	6.46489437439585	5.08855387766070
F	10.72424579456340	7.56994526223605	5.67567291718040
F	11.68795686467315	6.22770140172898	7.08458051992201
H	5.26093971539996	6.29396426487099	3.68717632647282
H	6.67304382075010	7.33156137148401	3.44609601810680
H	6.08608521670910	6.34502369623056	2.09944833514679
H	6.36852581687048	4.25482269834178	10.37837879842771
H	4.98864239165268	3.38484407341535	9.66780851570797
H	6.34548178278375	2.47582210500658	10.37409195635193
H	11.23413647891477	2.45114740296813	-1.48001520123778
H	11.27656540560944	4.22891511395127	-1.53748979546813
H	12.62880708166787	3.32979231956276	-0.80997259545722

Nucleus	Element	Isotropic	Anisotropy
0	C	59.475	30.182
1	F	255.857	134.672
2	C	8.608	-122.484
3	O	130.946	385.146
4	Rh	-7037.213	-6552.894
5	O	144.762	359.118
6	C	-11.320	-69.051
7	O	144.647	356.667
8	Rh	-7021.844	-6515.008
9	O	134.703	355.751
10	C	-11.345	-69.238
11	C	161.127	49.586
12	F	266.922	112.904
13	F	257.210	131.998

14	O	120.975	406.706
15	N	36.641	399.240
16	C	65.144	330.163
17	C	185.802	26.884
18	O	134.540	420.675
19	C	8.404	-123.955
20	C	59.332	29.502
21	N	36.822	398.260
22	C	65.077	330.022
23	C	185.801	26.665
24	O	136.678	412.702
25	O	135.069	355.574
26	C	161.276	48.679
27	H	29.860	6.461
28	H	29.884	6.435
29	H	29.687	5.788
30	F	263.519	117.737
31	F	251.908	139.985
32	F	260.916	124.205
33	H	29.807	6.501
34	H	29.571	5.377
35	H	29.843	6.510
36	H	29.259	9.929
37	H	29.239	9.869
38	H	29.259	9.937
39	H	29.266	9.876
40	H	29.280	9.946
41	H	29.289	9.936

5

42

Coordinates from ORCA-job opt

C	6.07259848051764	0.55272955744823	3.18048053532478
C	7.13233878762312	1.58263535686151	3.64887450044337
O	7.96686218355761	1.95115059979106	2.79380572956546
Rh	9.34141137116104	3.38892391327849	3.33881050077651
N	10.32354763714809	3.40310882598550	1.34227147043749
C	10.91565666348624	3.42782211597545	0.36015246784391
C	11.66729954863829	3.46097022557912	-0.87709989642356
O	7.01185943285725	1.93832439151798	4.84407701231980
Rh	8.30860126768112	3.38127373502854	5.54665494083411
N	7.33178880590099	3.37461565138477	7.54224355339896
C	6.74663753122907	3.37161116929510	8.52877579823483
C	6.00496885539027	3.36853329911875	9.77235963406133
O	9.67923533794870	4.82304546568788	6.08682664428209
C	10.51178750352861	5.19588943508004	5.22983738331050
O	10.64126465242349	4.82988145066969	4.04004855802638
O	6.99474337037250	4.83574995738420	4.84864673539670
C	7.12368789672151	5.20636933445121	3.66030310668951
C	6.13539289050234	6.30243193862054	3.18422482714581
O	9.66442042835993	1.95226483393702	6.06828706895765
C	10.52749824983731	1.55579782206367	5.22712621400456
C	11.53928145724893	0.55605717460584	5.70255103599779
C	11.48956546284342	6.30081058964306	5.70522616777836
O	7.95939020105562	4.84316006972331	2.80205064278212
O	10.61867058551595	1.95626791708831	4.02676476573676
F	6.25719039932303	0.17999903559292	1.91211431805983
F	6.11313051693170	-0.54619617173744	3.95081175942133
F	4.84221910420298	1.08397760280086	3.28508315771123
H	11.09686650239859	-0.10593153975273	6.44432636615864
H	11.93679425677030	-0.01333476641924	4.86562292706346
H	12.35944050899975	1.10221231587094	6.17547603815635
F	12.62722588111399	6.29495121753521	5.00325801351319
F	10.90850031590254	7.50514051162208	5.54580223962816
F	11.79579408958325	6.15870090527989	7.00007969205100
F	5.00123200602676	6.29431567609548	3.89216151340283
F	6.70825201419784	7.51272864898291	3.33177305802066
F	5.82184752843805	6.15011071782130	1.89169043989894
H	5.94563101674682	4.38401828595326	10.16541468655870
H	4.99731558492180	2.99095625334433	9.59449129041813
H	6.50825197327398	2.72851386579963	10.49769963387716
H	11.61645837113823	2.48650510952911	-1.36373181570466
H	11.24855650222053	4.21879326545441	-1.54011728564656
H	12.70892482625957	3.70383823600740	-0.66362942951423

Nucleus	Element	Isotropic	Anisotropy
0	C	59.451	29.775
1	C	7.717	-121.226
2	O	125.062	406.081
3	Rh	-7129.952	-6541.728
4	N	38.432	396.357
5	C	64.413	330.527
6	C	185.900	27.045
7	O	134.987	382.541
8	Rh	-7139.391	-6584.411
9	N	38.606	394.966
10	C	64.273	330.432
11	C	185.762	26.960
12	O	139.073	412.381
13	C	7.504	-121.798

14	O	137.738	411.984
15	O	122.205	401.633
16	C	8.303	-121.243
17	C	59.446	30.389
18	O	156.838	356.524
19	C	-13.060	-68.126
20	C	160.878	49.088
21	C	59.298	29.708
22	O	125.719	399.901
23	O	155.104	351.174
24	F	266.998	112.350
25	F	257.446	131.303
26	F	254.848	134.267
27	H	29.775	6.529
28	H	29.826	6.479
29	H	29.664	5.754
30	F	263.157	119.155
31	F	251.680	137.676
32	F	260.798	123.786
33	F	264.405	119.191
34	F	254.190	136.395
35	F	261.897	122.907
36	H	29.231	9.822
37	H	29.208	9.828
38	H	29.237	10.039
39	H	29.268	10.040
40	H	29.259	9.908
41	H	29.261	9.866

6

42

Coordinates from ORCA-job opt

C	6.20925956545915	0.48651951931657	3.09720387864367
C	7.19466118682694	1.57973842432852	3.58490428032045
O	8.04490852275780	1.97414003367083	2.75676732165051
Rh	9.37132203912246	3.43047774114679	3.35651178968425
N	10.38036209255456	3.44097597922758	1.38389782985822
C	10.89909335469220	3.42063453668310	0.36139056845445
C	11.55372821561503	3.39360039572169	-0.92938746471185
O	7.01534286330366	1.94514166885201	4.76987821597610
Rh	8.25560276028155	3.40543504171350	5.52878243654040
N	7.24758747585667	3.38113043081654	7.50158068948624
C	6.73143154452879	3.36278349034332	8.52541660425509
C	6.08008108470511	3.33928227752154	9.81790824949714
O	9.58236320824984	4.86405072922680	6.12452944320588
C	10.43019245193934	5.26196289023099	5.29323768922751
O	10.61346071849625	4.89020909574000	4.11235811103940
O	6.98944541481240	4.85553327610633	4.79361316341059
C	7.16749983435459	5.24843300527407	3.61895256431865
C	6.23049908866826	6.38422637365160	3.13299464422384
O	9.60406747518222	1.96072002731259	6.10738798656332
C	10.46221445825145	1.59428412282512	5.27454648742898
C	11.46565772919785	0.51073250952792	5.74665387876953
C	11.34893543145377	6.40725790748415	5.79158070411492
O	8.02275224858658	4.87780684787042	2.78246718180625
O	10.63591475033997	1.98030003950873	4.09531179202647
F	6.45619720597593	0.11341826685468	1.84032973524419
F	6.29583349274152	-0.59903216521491	3.88222554164681
F	4.94776960581067	0.94310504178242	3.15906922410493
F	11.23880827952886	0.13128950319516	7.00543625845688
F	11.37991287159554	-0.57350638929721	4.95935535218756
F	12.72126582528954	0.98033807090939	5.66996906035697
F	12.48193576571487	6.47592028576855	5.08810038938939
F	10.70418618940481	7.58178564817101	5.65993182352336
F	11.66397183412649	6.25082567067989	7.08235007087144
F	5.11724754047394	6.45883793778705	3.86626787881982
F	6.87427349103550	7.56246419140846	3.22994508750240
F	5.88034808905759	6.20846228500667	1.85330746254088
H	6.36788326459391	4.22312530941787	10.38821699255786
H	4.99818482816597	3.33305908260099	9.68119658655161
H	6.38149983018907	2.44364996677587	10.36226953653314
H	11.25305353511470	2.49669151927060	-1.47210094127343
H	11.26811416639429	4.27607231150593	-1.50286213006281
H	12.63527066954798	3.38684109927602	-0.78986997474221

Nucleus	Element	Isotropic	Anisotropy
0	C	59.455	29.780
1	C	7.024	-118.815
2	O	126.417	397.647
3	Rh	-7207.440	-6630.554
4	N	40.521	392.273
5	C	63.864	331.189
6	C	185.743	27.179
7	O	136.362	375.886
8	Rh	-7204.243	-6626.351
9	N	40.713	391.677
10	C	63.826	331.125
11	C	185.810	27.045

12	O	145.604	408.207
13	C	6.866	-120.879
14	O	142.635	416.630
15	O	130.274	401.465
16	C	6.997	-118.446
17	C	59.646	30.463
18	O	136.839	411.197
19	C	6.941	-121.359
20	C	59.488	28.971
21	C	59.296	29.078
22	O	134.943	393.283
23	O	148.615	392.459
24	F	266.648	112.126
25	F	256.877	131.054
26	F	255.615	133.366
27	F	264.035	112.166
28	F	254.833	134.909
29	F	255.288	133.631
30	F	263.352	117.185
31	F	250.866	137.684
32	F	260.557	123.190
33	F	264.944	115.359
34	F	253.790	136.464
35	F	261.121	124.217
36	H	29.215	9.920
37	H	29.189	9.901
38	H	29.210	9.963
39	H	29.215	9.919
40	H	29.223	9.902
41	H	29.230	9.951

6. NMR Spectra

Rhodium(III) acetylacetonate ($Rh(acac)_3$): H(C)Rh spectra stacked at variable temperatures (10mM, $CDCl_3$)

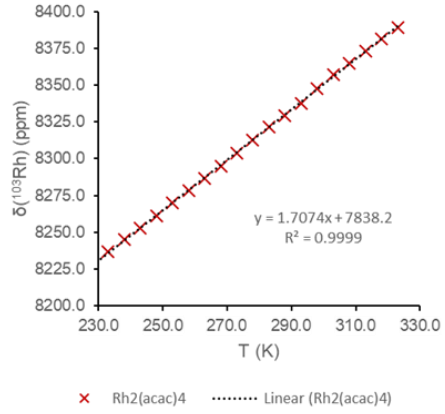

T(K)	$\delta(^{103}Rh)$ (ppm)
223.0	8219.5
228.0	8228.1
233.0	8236.8
238.0	8244.9
243.0	8252.7
248.0	8261.0
253.0	8270.1
258.0	8278.5
263.0	8286.4
268.0	8295.1
273.0	8303.8
278.0	8312.8
283.0	8321.4
288.0	8329.5
293.0	8337.8
298.0	8347.4
303.0	8357.3
308.0	8364.8
313.0	8372.9
318.0	8381.1
323.0	8389.4

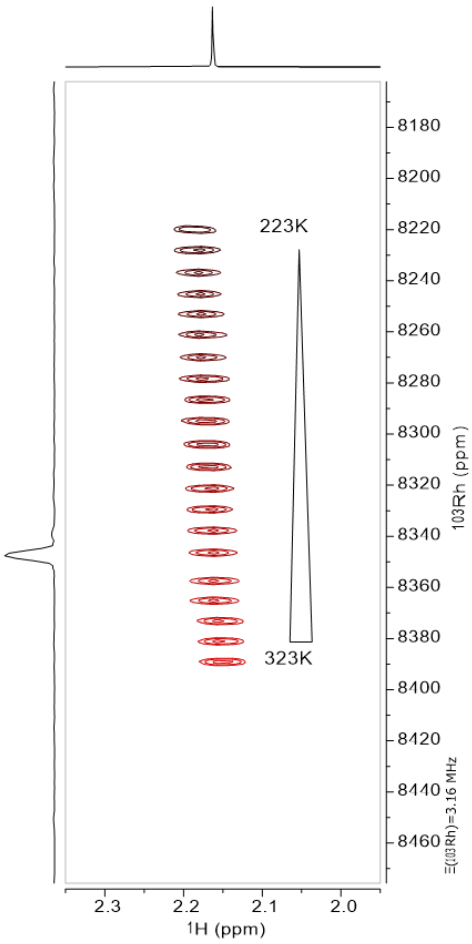

Dirhodium(II) tetra(acetate) ($Rh_2(OAc)_4$) (1) : ^{1}H-NMR (500 MHz, CD_3CN)

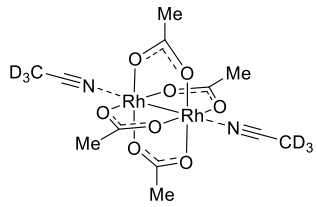

Dirhodium(II) tetra(acetate) ($Rh_2(OAc)_4$) (1) : H(C)Rh spectrum (CD_3CN)

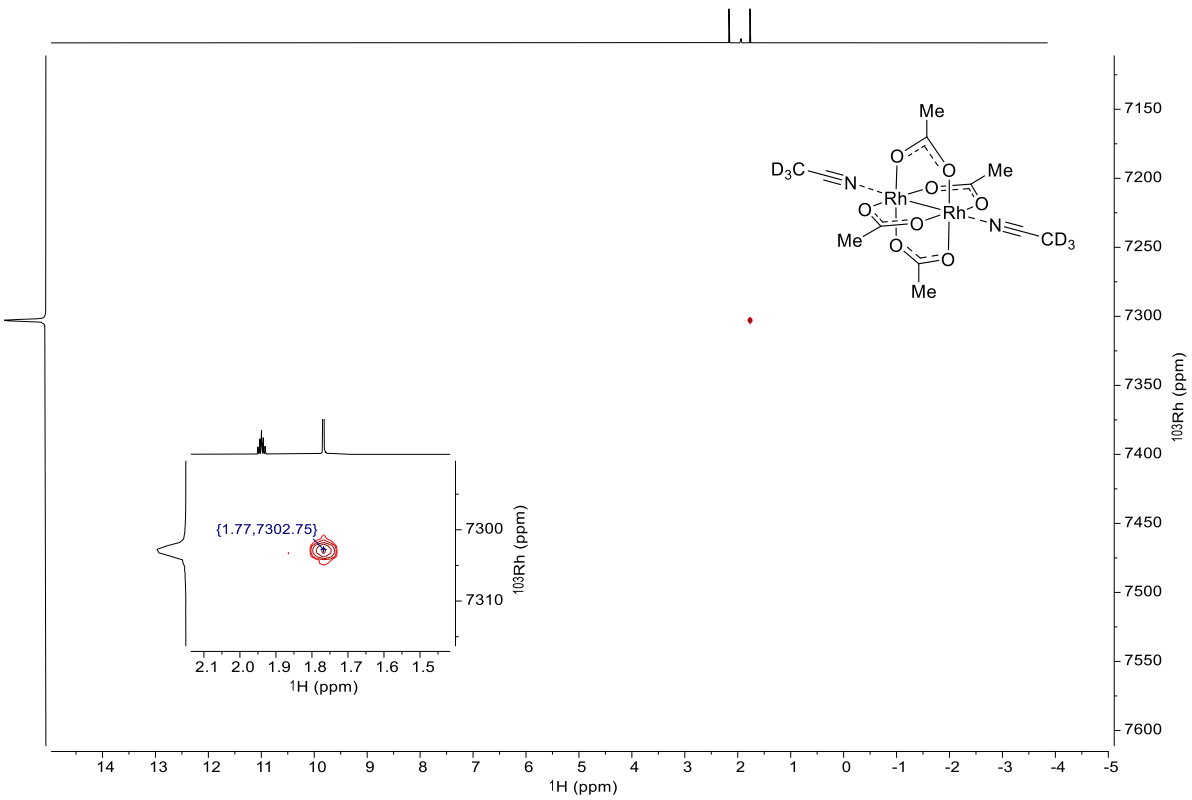

Dirhodium(II) tetra(acetate) ($Rh_2(OAc)_4$) (1) : H(C)Rh spectra stacked at variable temperatures (CD_3CN)

T(K)	δ(^{103}Rh) (ppm)
298	7303.0
293	7296.5
283	7283.4
273	7269.9
263	7256.1
253	7242.8
243	7229.9
233	7217.3

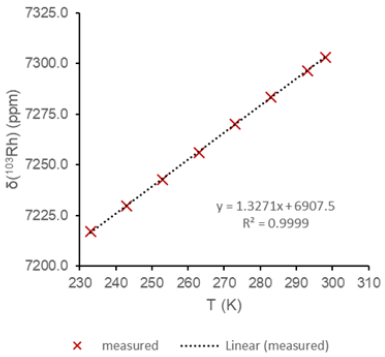

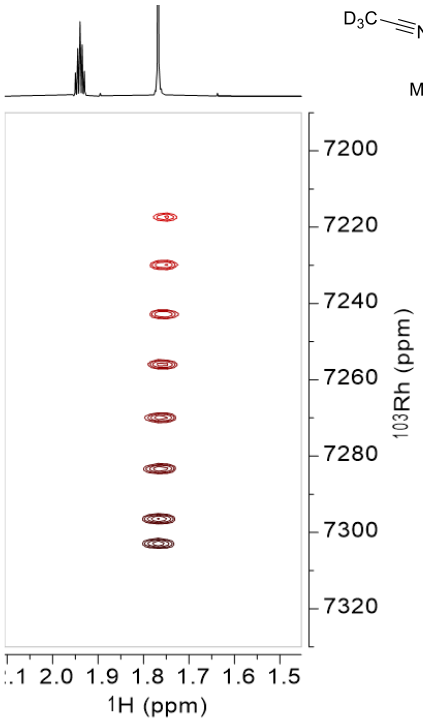

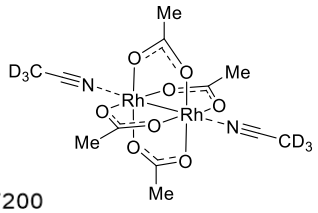

Dirhodium(II) tetra(acetate) ($Rh_2(OAc)_4$) (1): ^{1}H-NMR (500 MHz, [D_8]-THF)

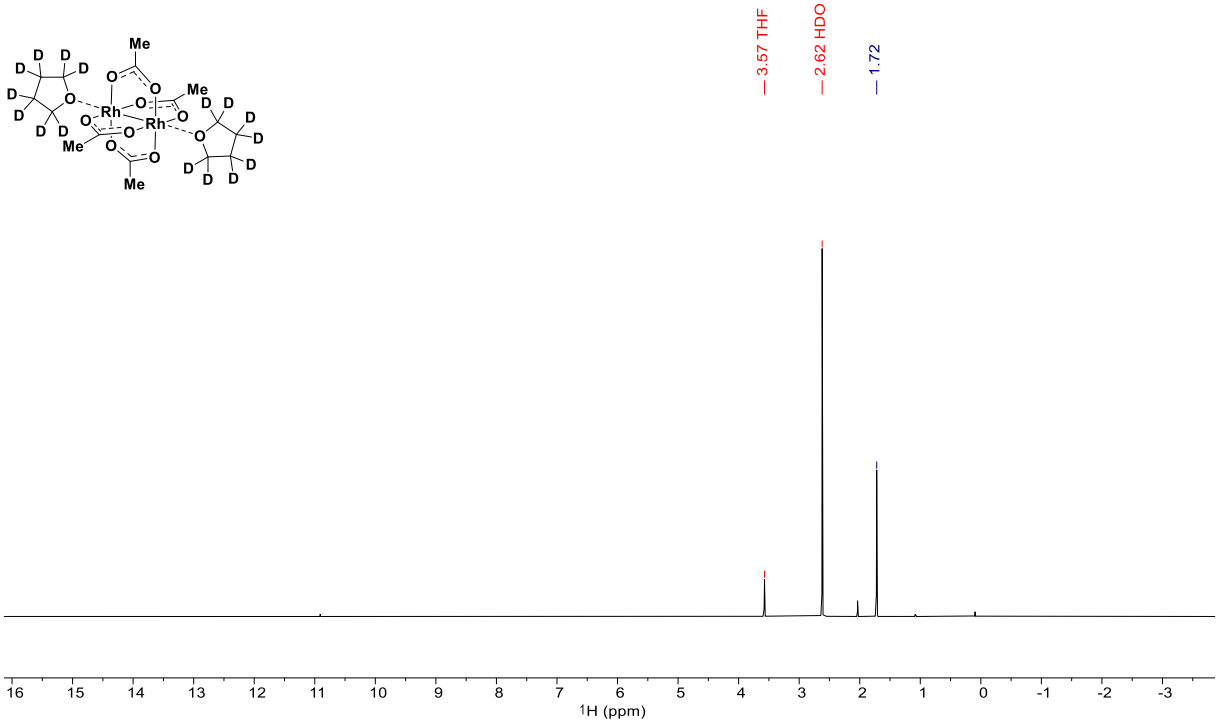

Dirhodium(II) tetra(acetate) ($Rh_2(OAc)_4$) (1): 2D H(C)Rh spectrum ([D_8]-THF)

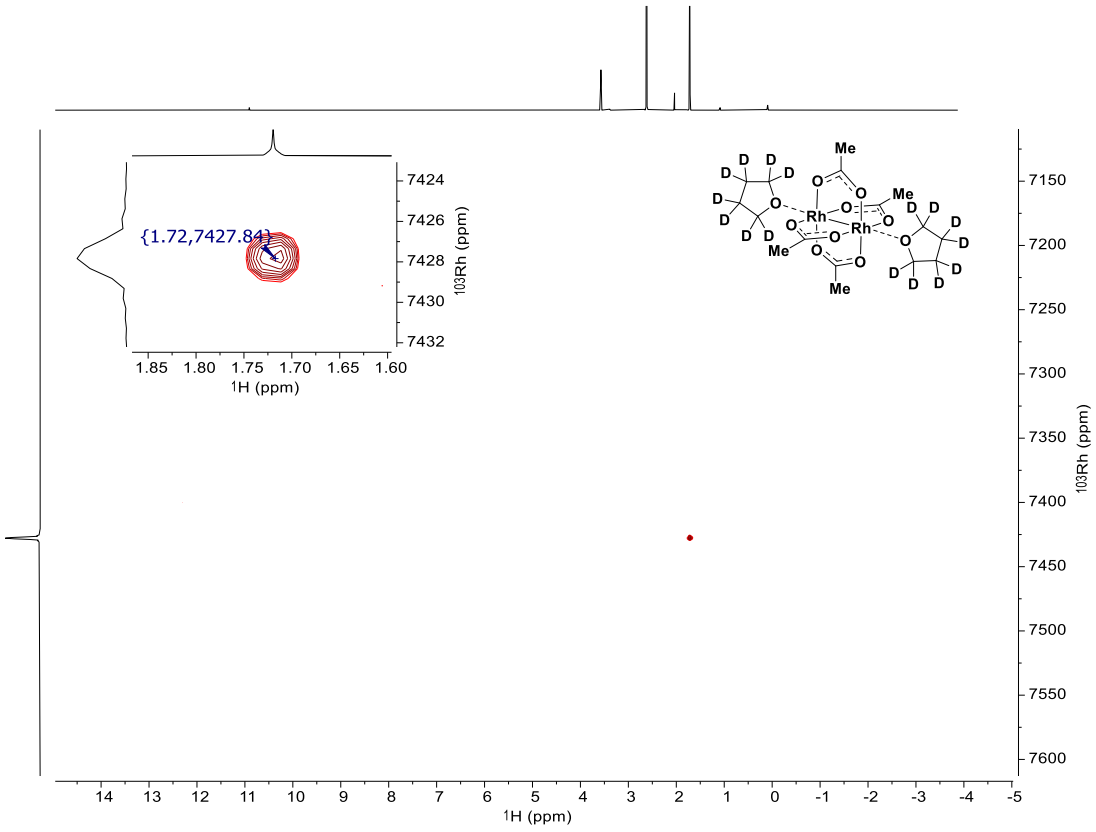

Dirhodium(II) tetra(acetate) ($Rh_2(OAc)_4$) (1): ^{1}H-NMR (500 MHz, [D_6]-acetone)

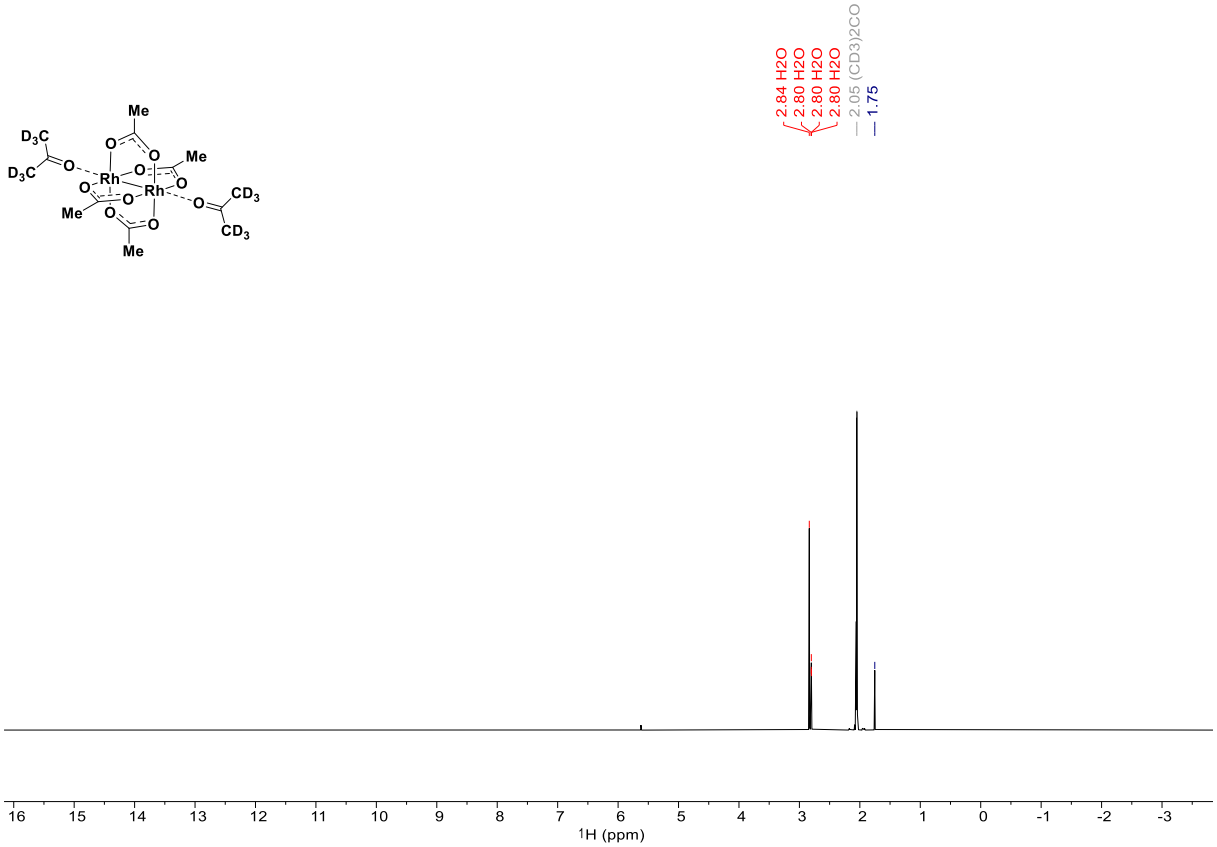

Dirhodium(II) tetra(acetate) ($Rh_2(OAc)_4$) (1): 2D H(C)Rh spectrum ([D_6]-acetone)

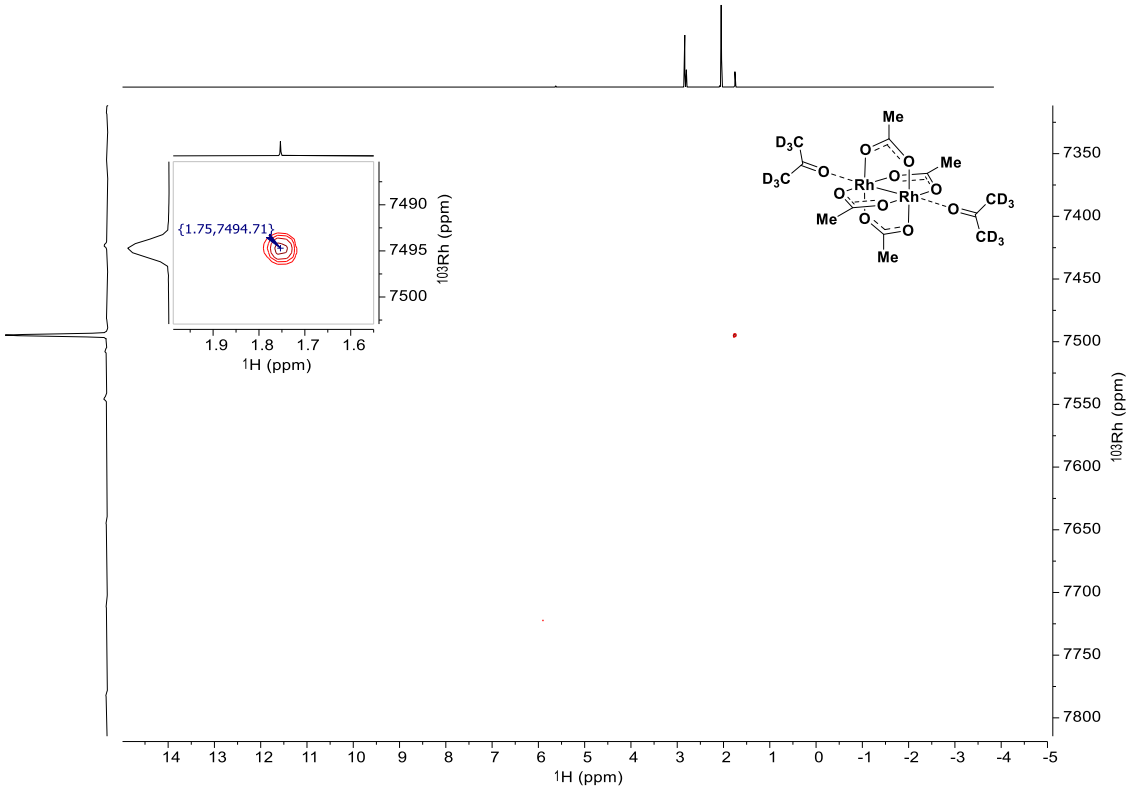

$[Rh_2(OAc)_4]\cdot PPh_3$ (1·PPh_3): ^{1}H-NMR (500 MHz, CD_2Cl_2)

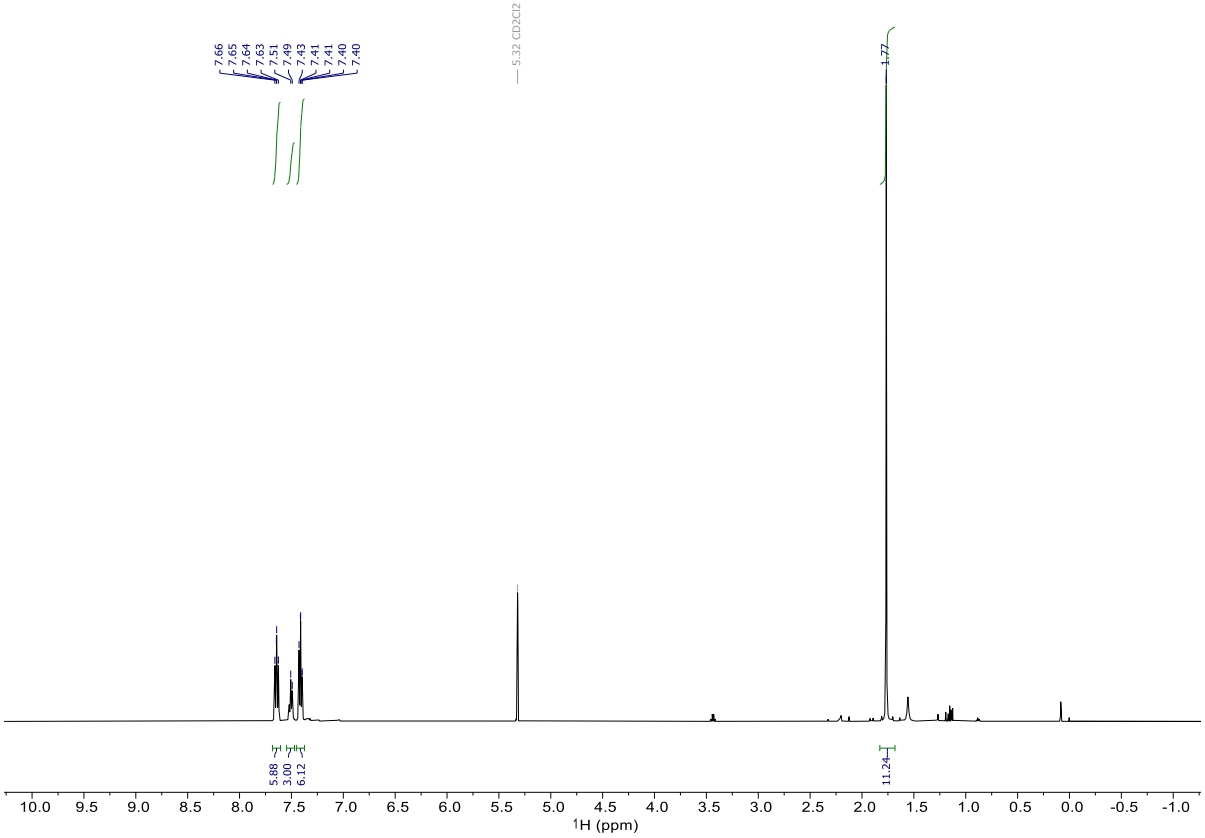

$[Rh_2(OAc)_4]\cdot PPh_3$ (1·PPh_3): ^{31}P-NMR (202 MHz, CD_2Cl_2)

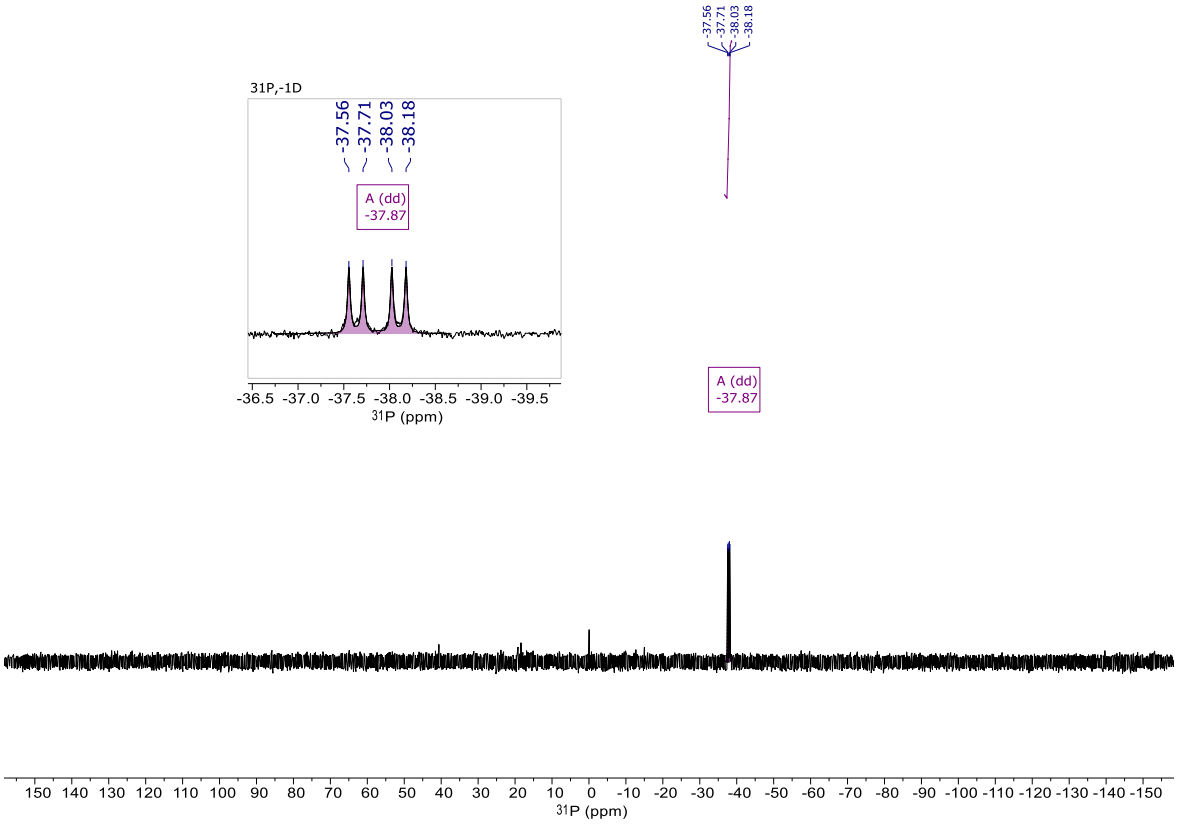

$[Rh_2(OAc)_4]\cdot PPh_3$ ($1\cdot PPh_3$): 2D H(C)Rh spectrum (CD_2Cl_2)

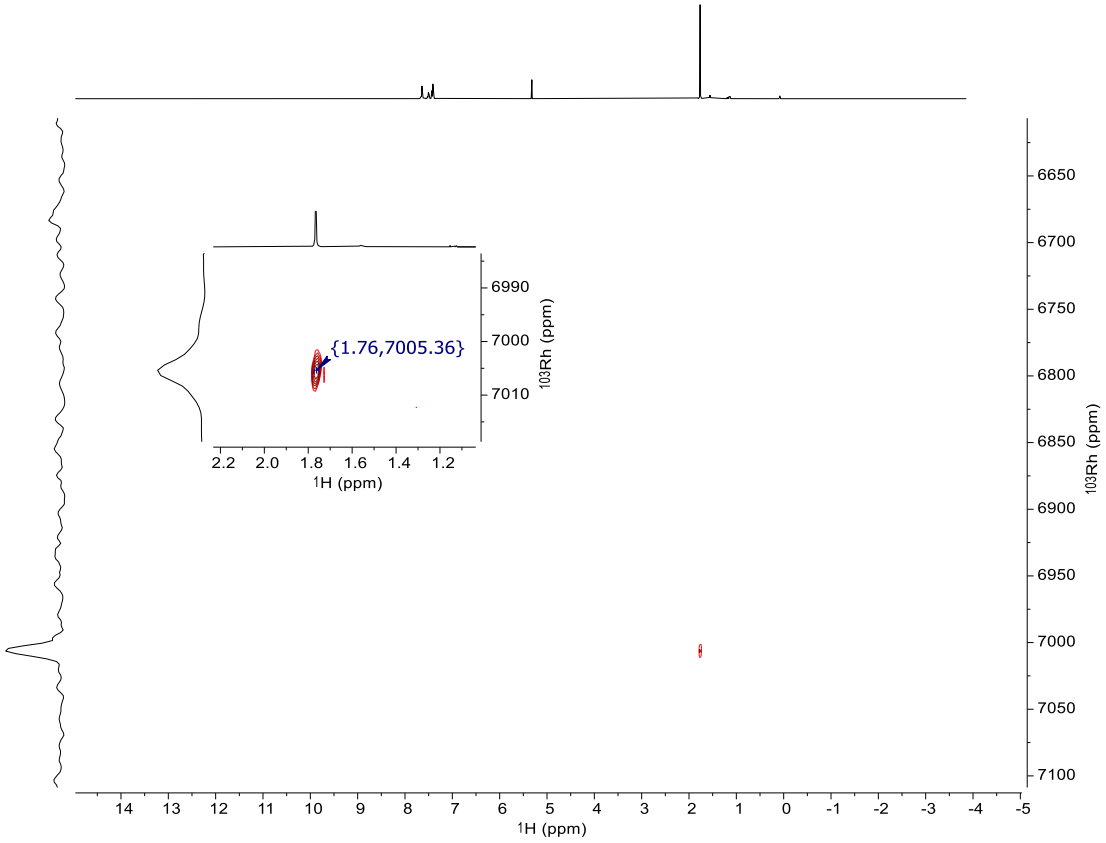

Dirhodium(II) tetra(acetate-2-^{13}C) (2-^{13}C-1): ^{1}H-NMR (400 MHz, CD_3CN)

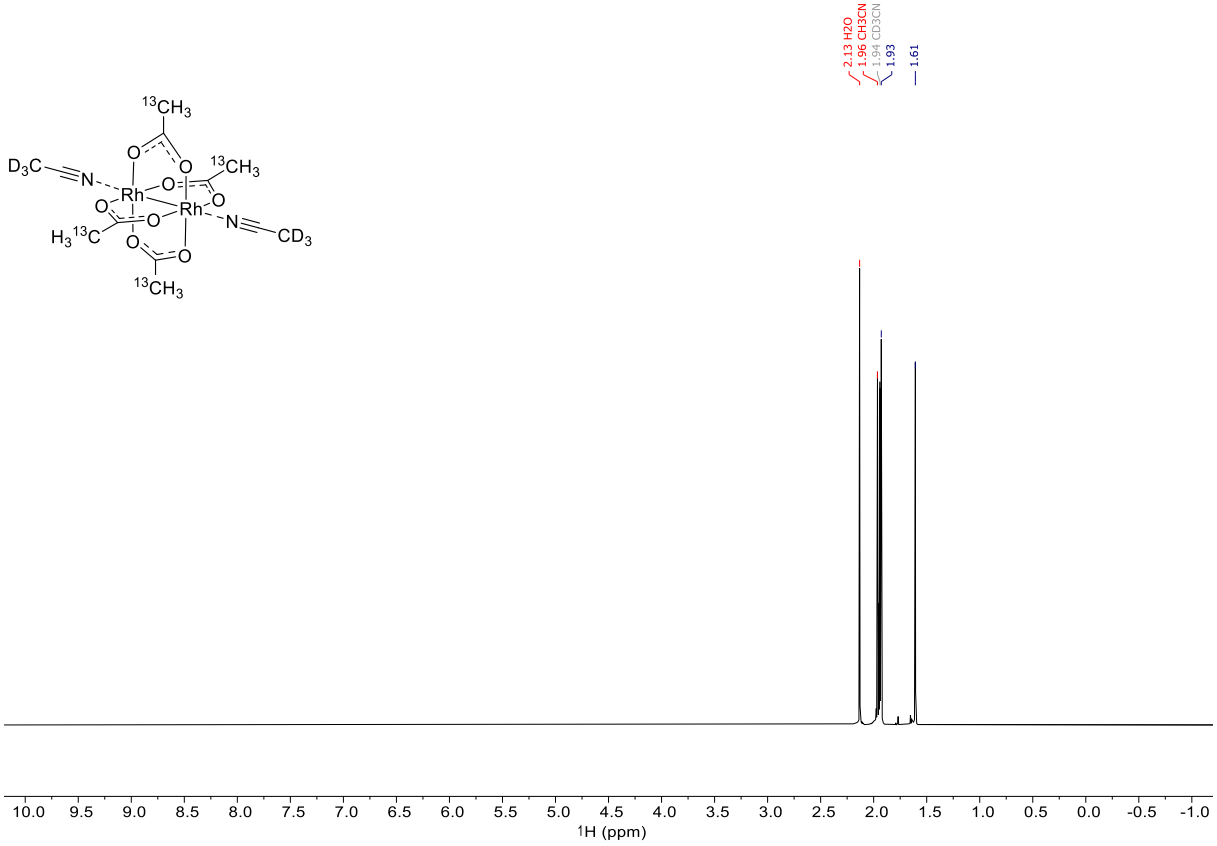

Dirhodium(II) tetra(acetate-2-^{13}C) (2-^{13}C-1): ^{13}C{^{1}H}-NMR (101 MHz, CD_3CN)

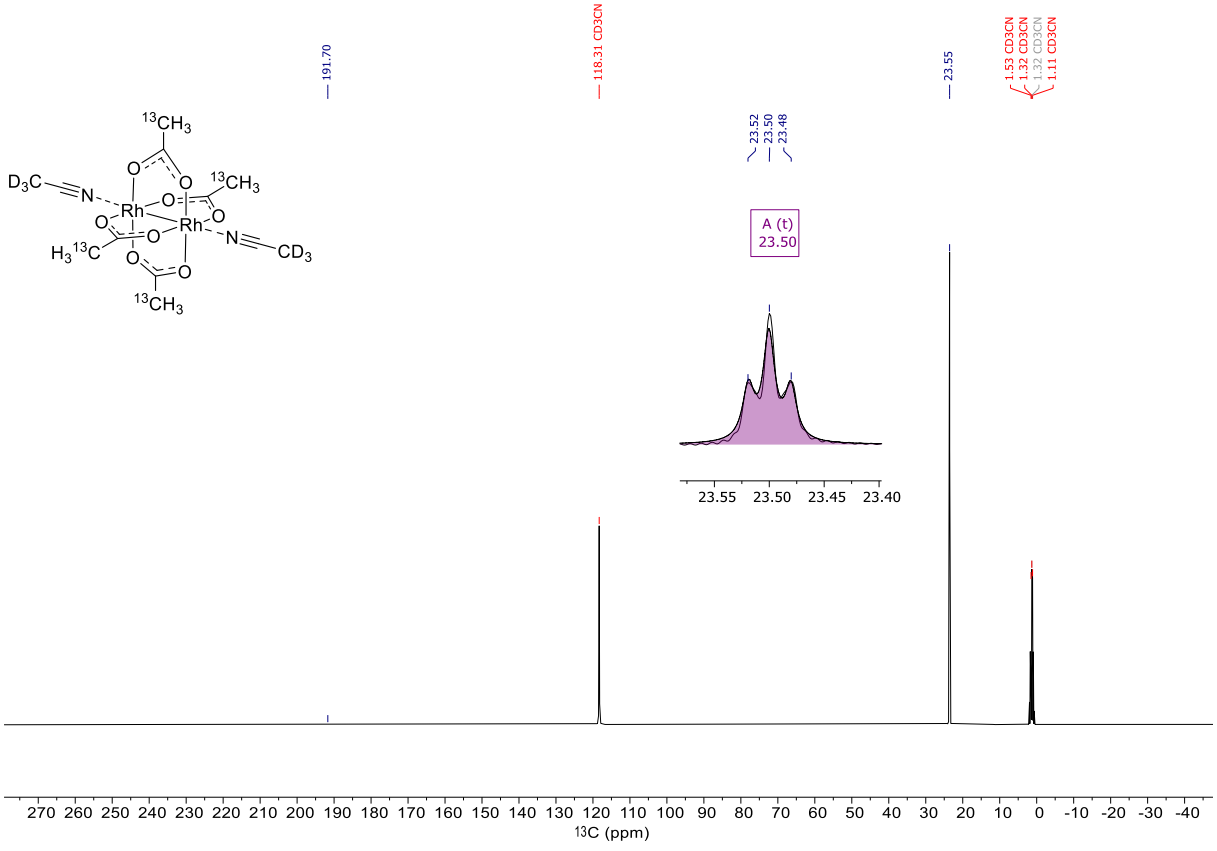

Dirhodium(II) tetra(acetate-2-^{13}C): Left: ^{13}C{^{1}H}-NMR (126 MHz, CD_3CN); Right: ^{13}C{^{1}H, ^{103}Rh}-NMR (126 MHz, CD_3CN)

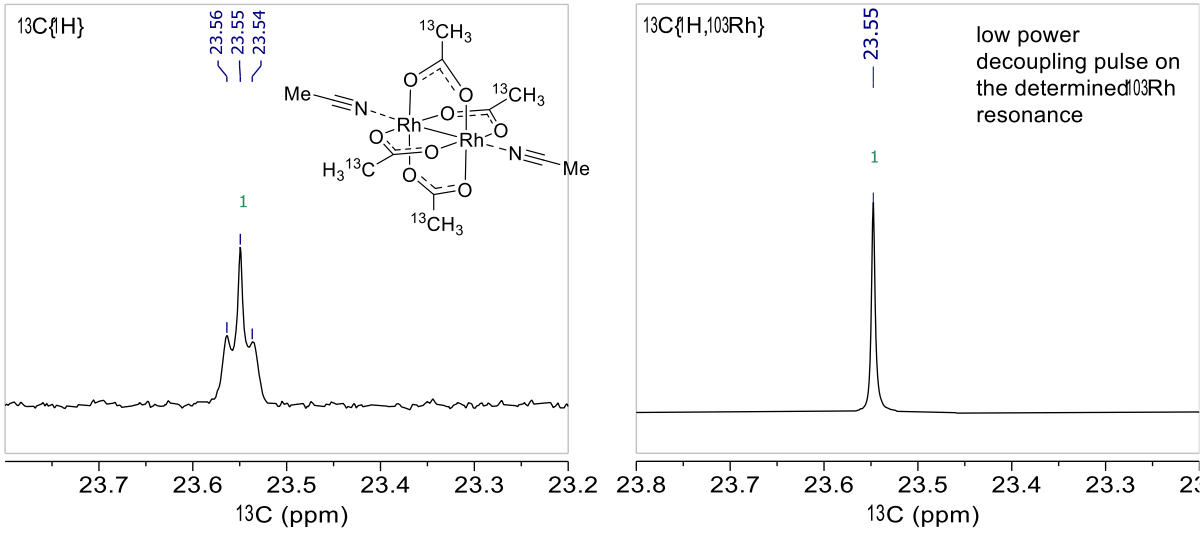

Dirhodium(II) tetra(acetate-2-^{13}C) (2-^{13}C-1): ^{13}C{^{1}H}-^{103}Rh-HMBC (CD_3CN)

To verify that the ^{103}Rh NMR signal is not folded, two spectra with the same offset, but a different spectral width in the indirect dimension were measured. By comparing the spectra, the signal appears at almost the same position (within 1 ppm). This confirms that the cross peaks is not folded and the correct ^{103}Rh resonance was found.

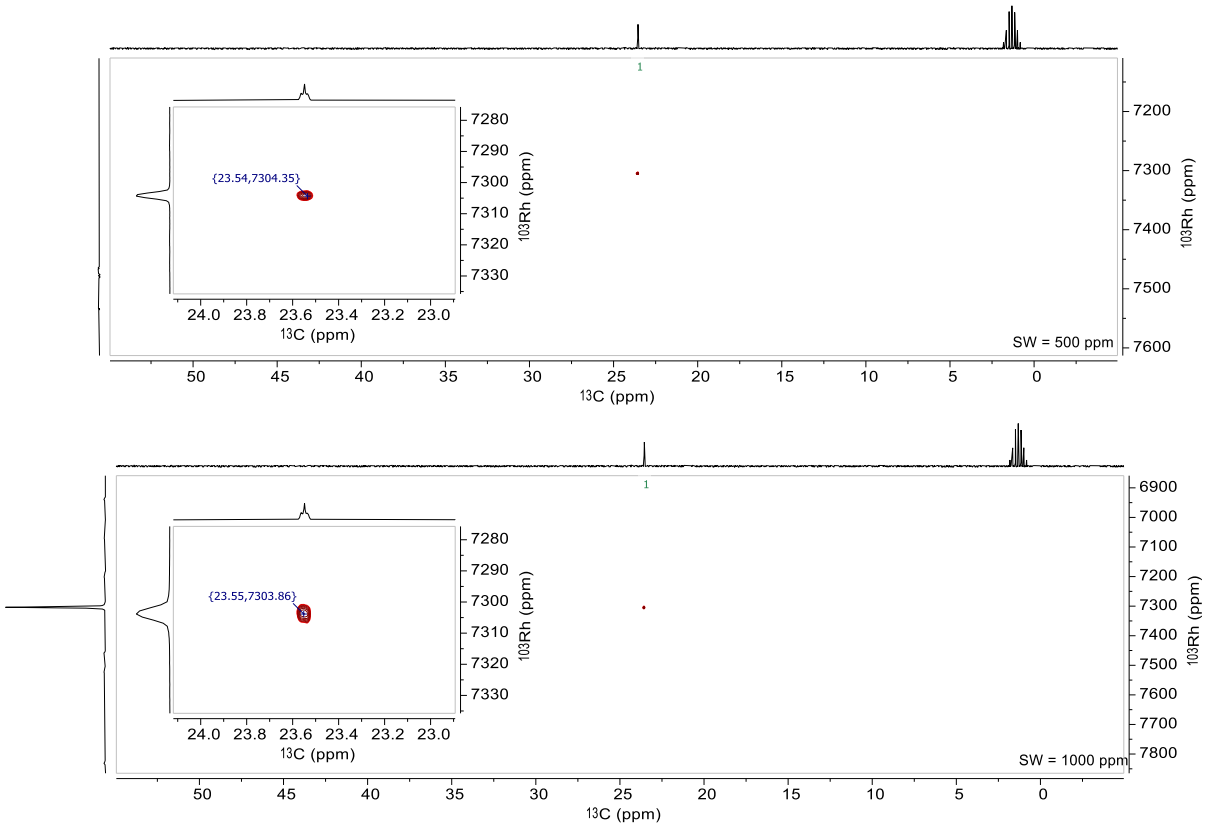

Dirhodium(II) tetra(acetate-1-^{13}C) (1-^{13}C-1): ^{1}H-NMR (400 MHz, CD_3CN)

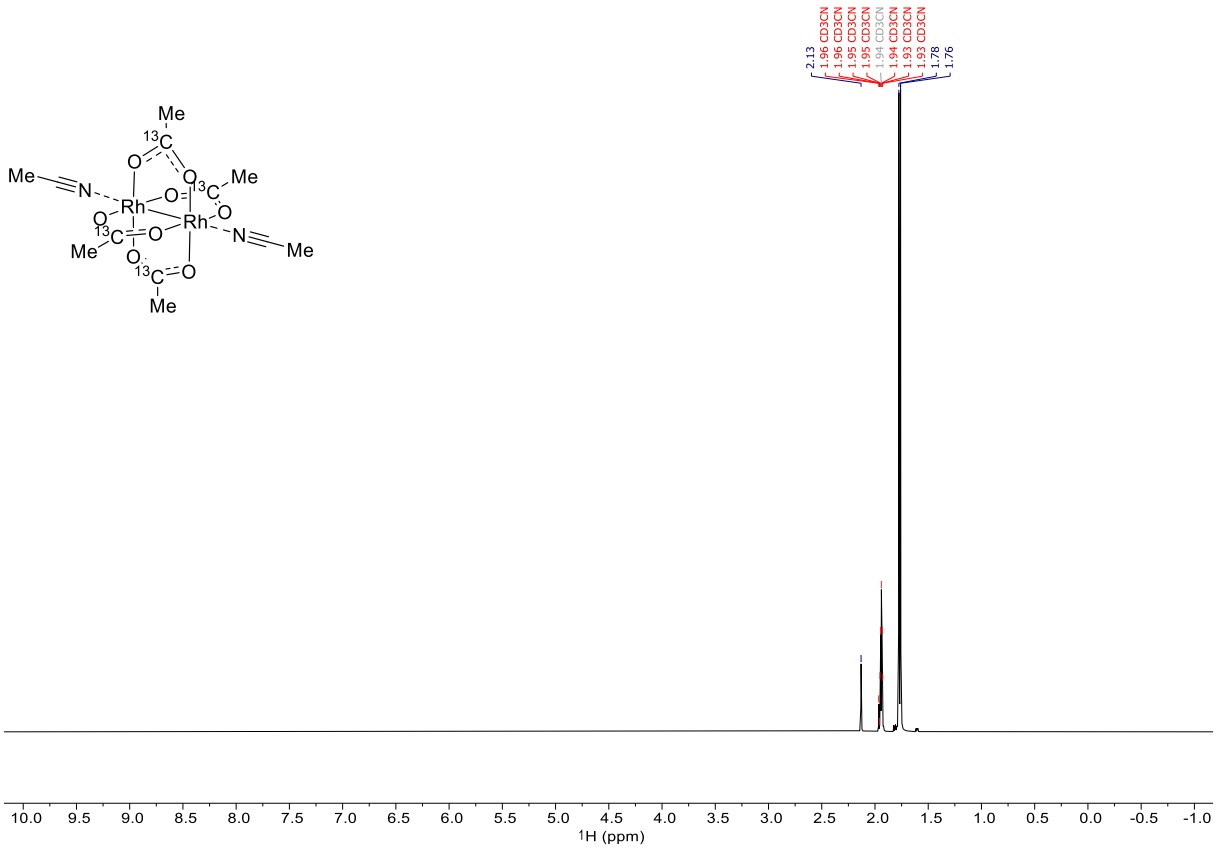

Dirhodium(II) tetra(acetate-1-^{13}C) (1-^{13}C-1): ^{13}C{^{1}H}-NMR (101 MHz, CD_3CN)

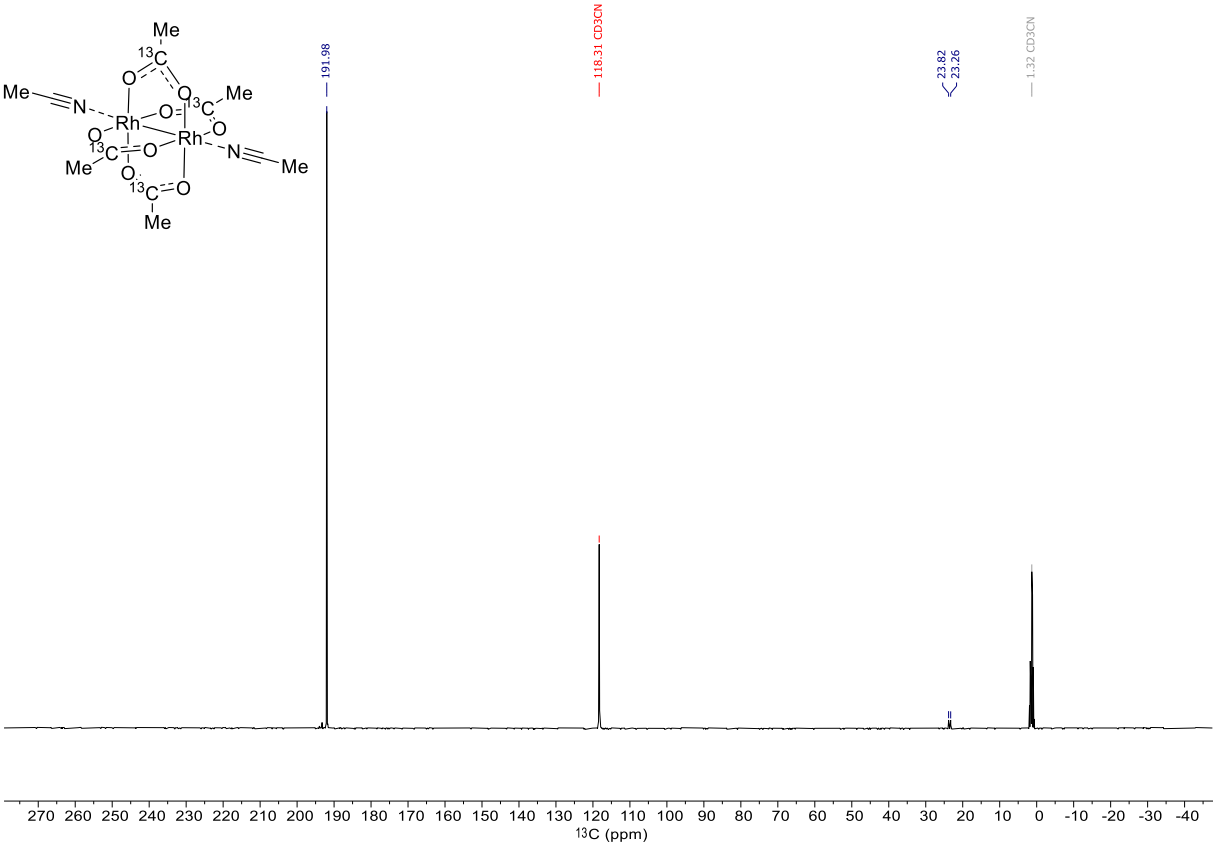

$Rh_2(OAc)_3(OTfa)$ (2): ^{1}H-NMR (500 MHz, CD_3CN)

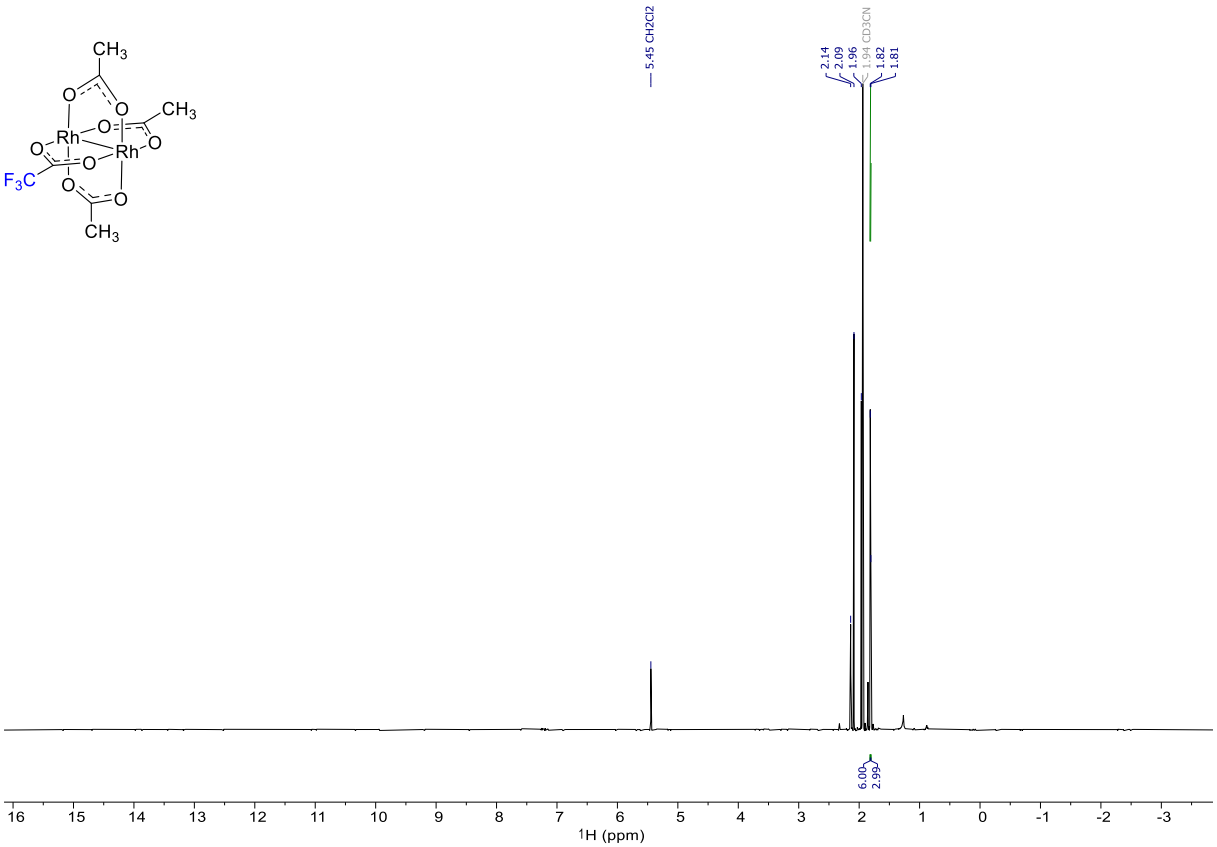

$Rh_2(OAc)_3(OTfa)$ (2): ^{19}F-NMR (565 MHz, CD_3CN)

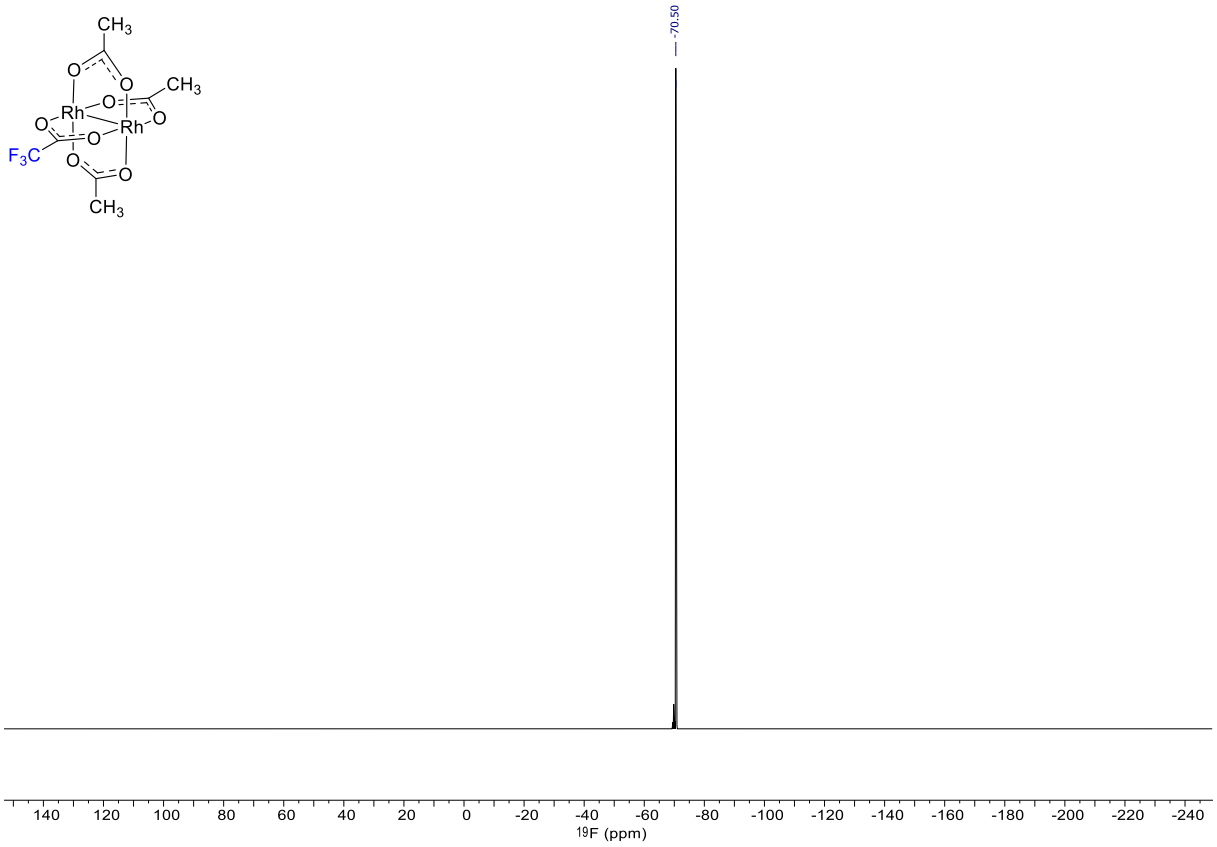

$Rh_2(OAc)_3(OTfa)$ (2): ^{13}C-NMR (151 MHz, CD_3CN)

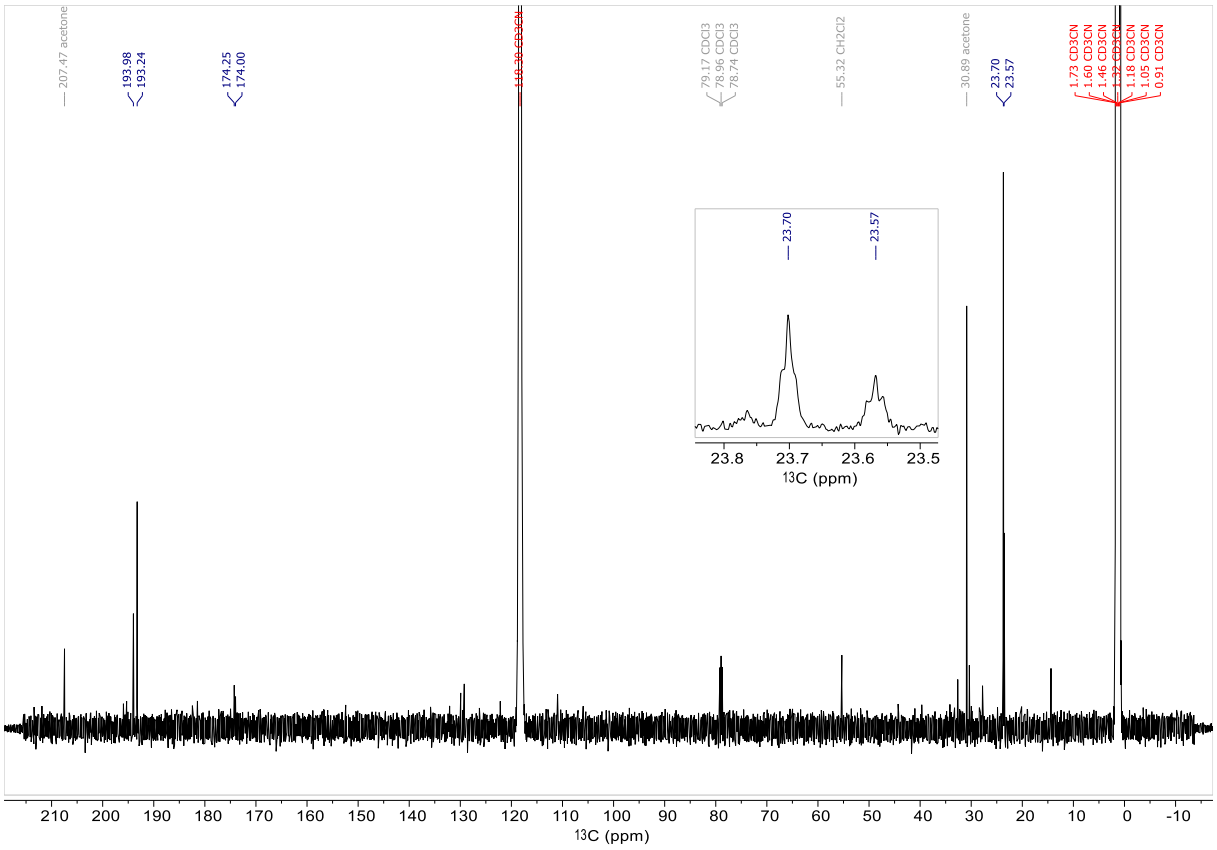

$Rh_2(OAc)_3(OTfa)$ (2): ^{1}H-^{13}C-*edited*-HSQC (CD_3CN)

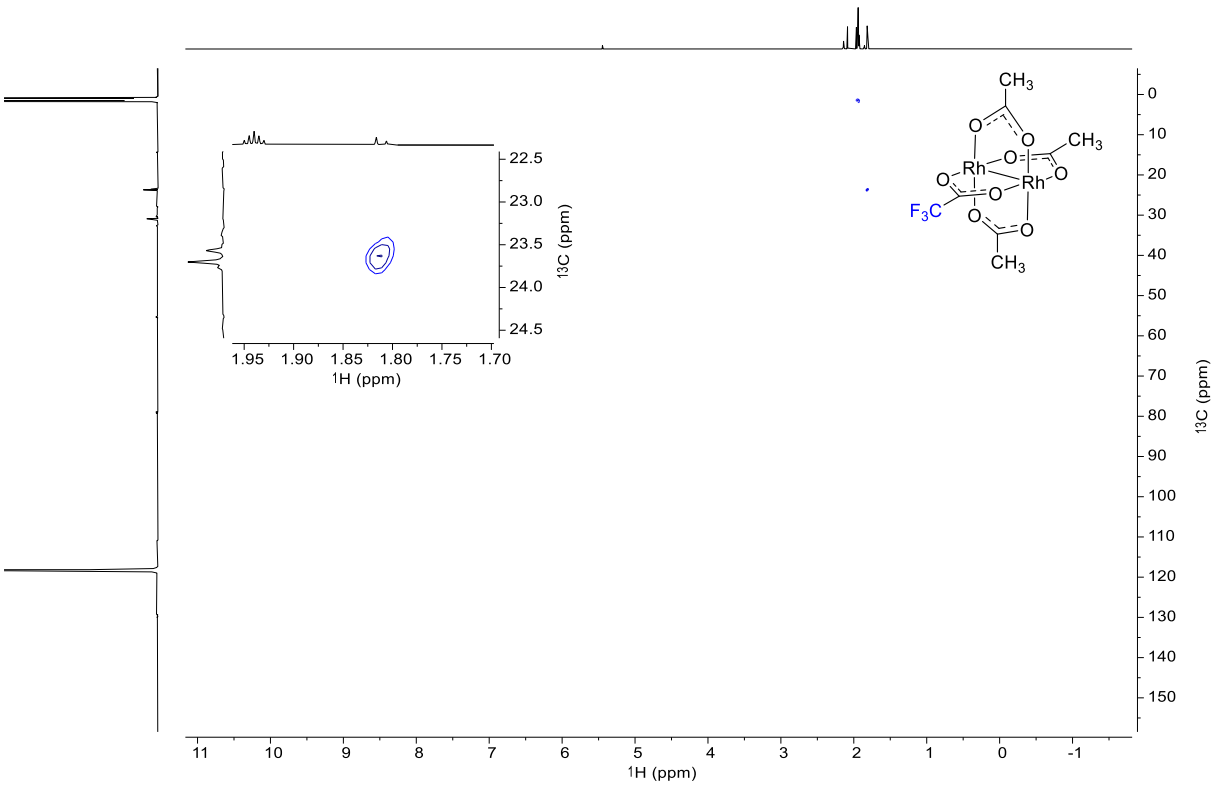

$Rh_2(OAc)_3(OTfa)$ (2): ^{1}H-^{13}C-HMBC (CD_3CN)

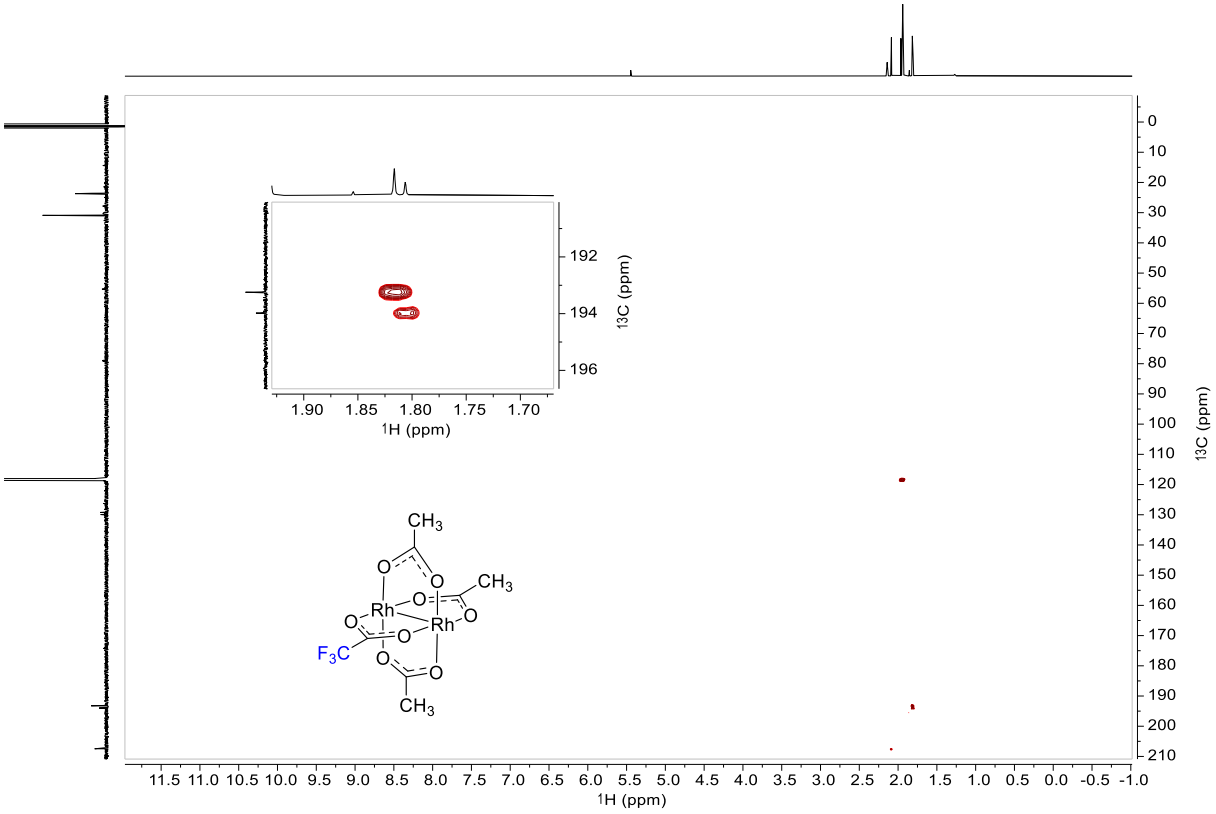

$Rh_2(OAc)_3(OTfa)$ (2): H(C)Rh (CD_3CN)

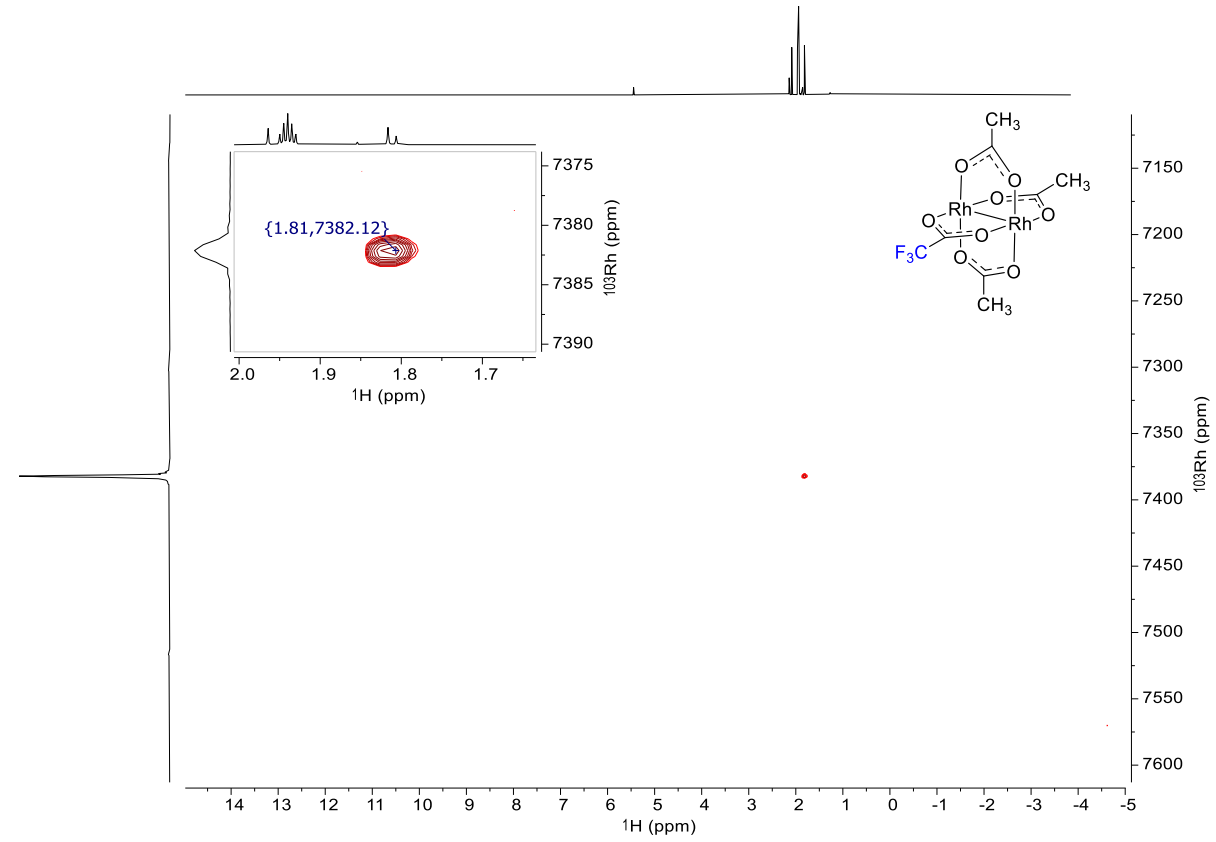

***cis*-Rh$_2$(OAc)$_2$(OTfa)$_2$ (3): ^{1}H-NMR (600 MHz, CD$_3$CN)**

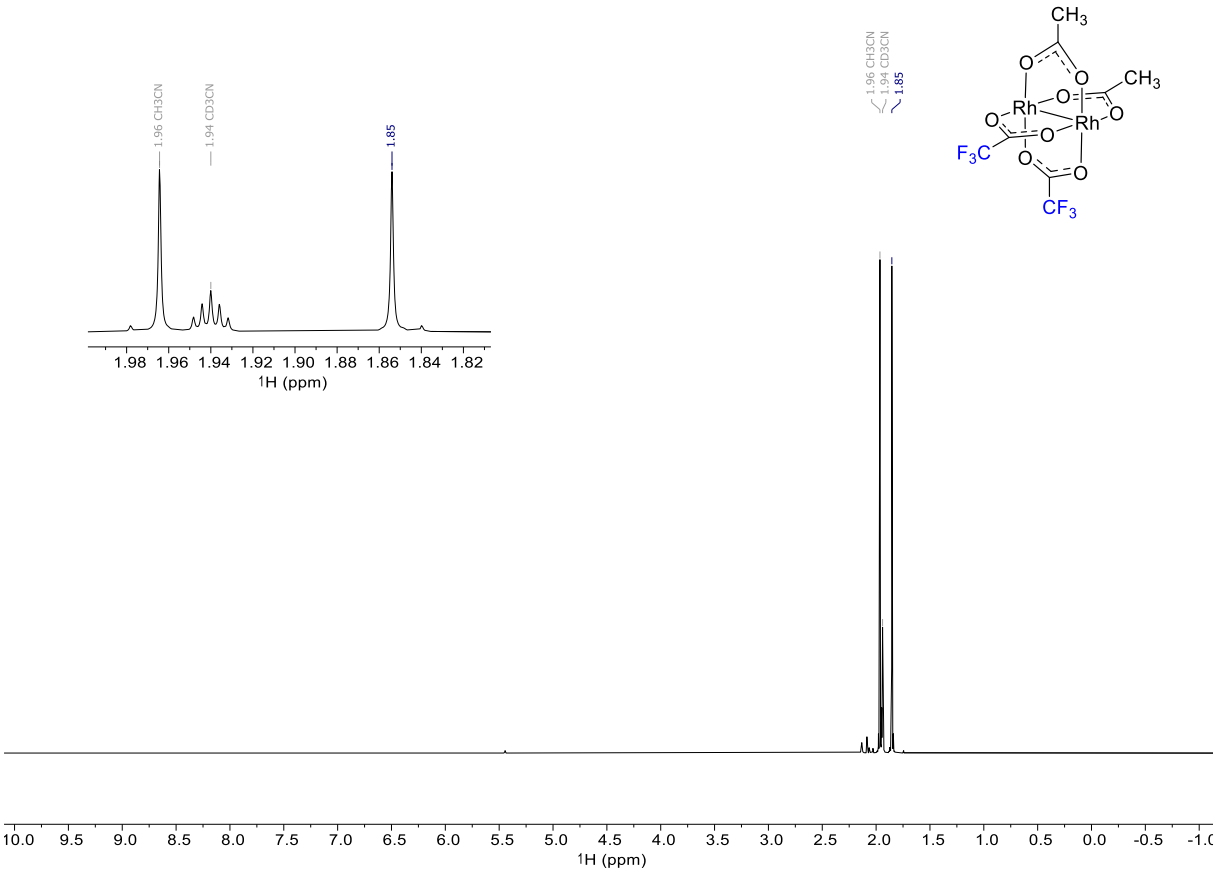

***cis*-Rh$_2$(OAc)$_2$(OTfa)$_2$ (3): ^{13}C{^{1}H}-NMR (151 MHz, CD$_3$CN)**

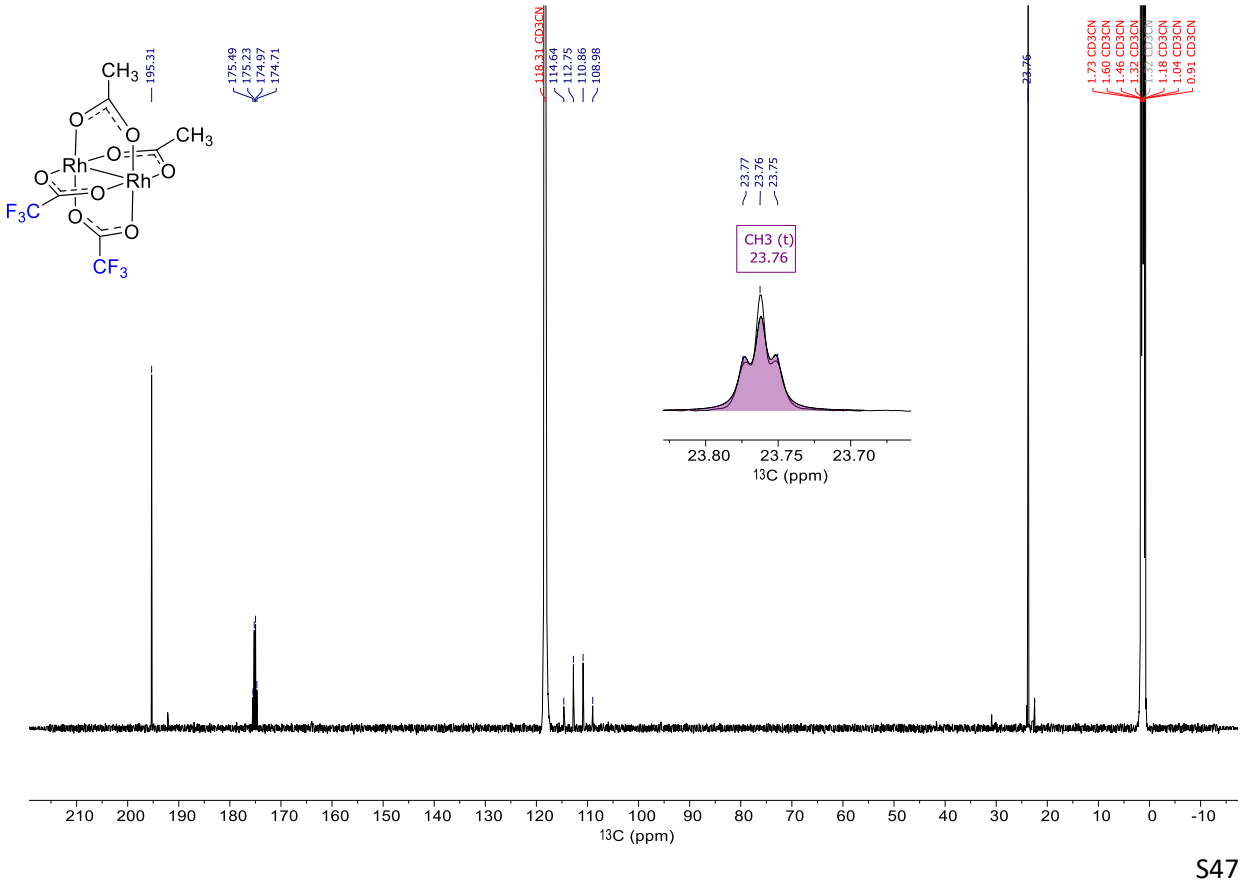

***cis*-Rh$_2$(OAc)$_2$(OTfa)$_2$ (3): ^{19}F-NMR (565 MHz, CD$_3$CN)**

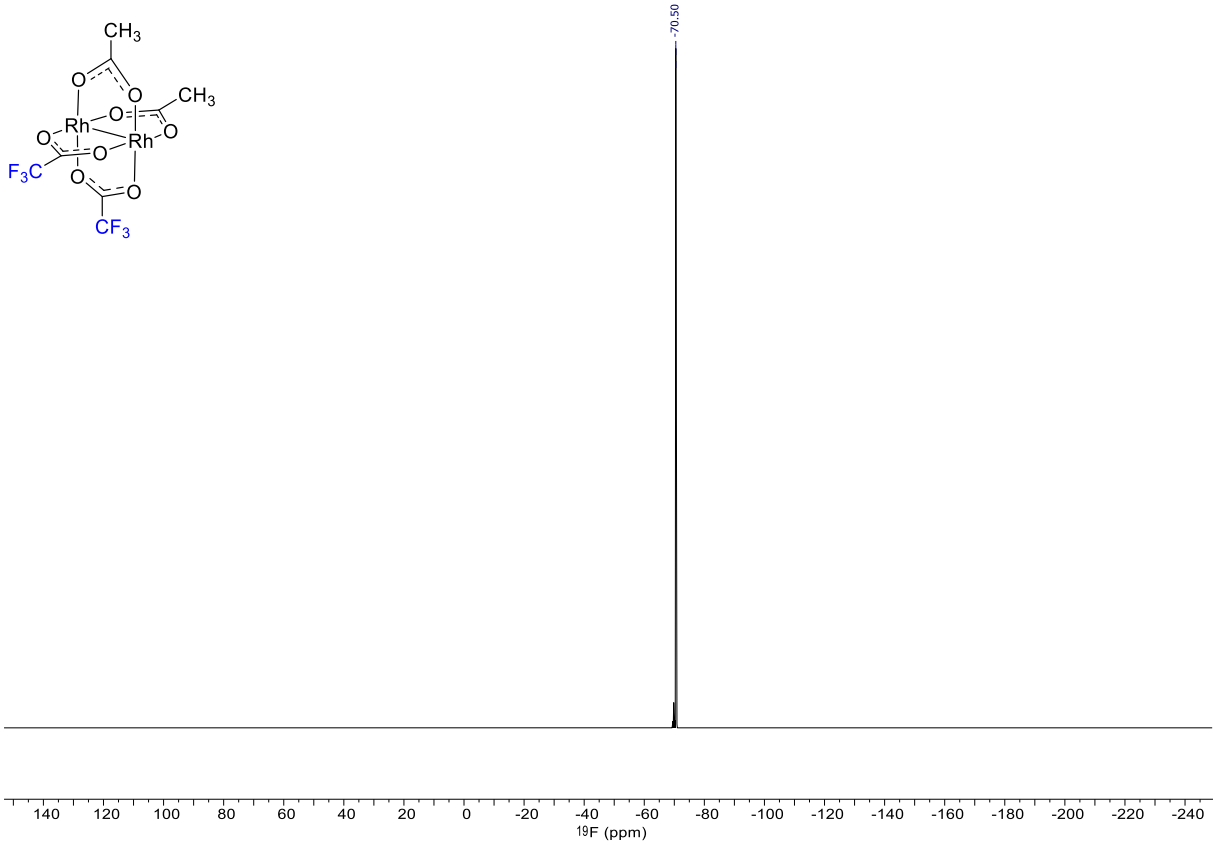

***cis*-Rh$_2$(OAc)$_2$(OTfa)$_2$ (3): H(C)Rh (CD$_3$CN)**

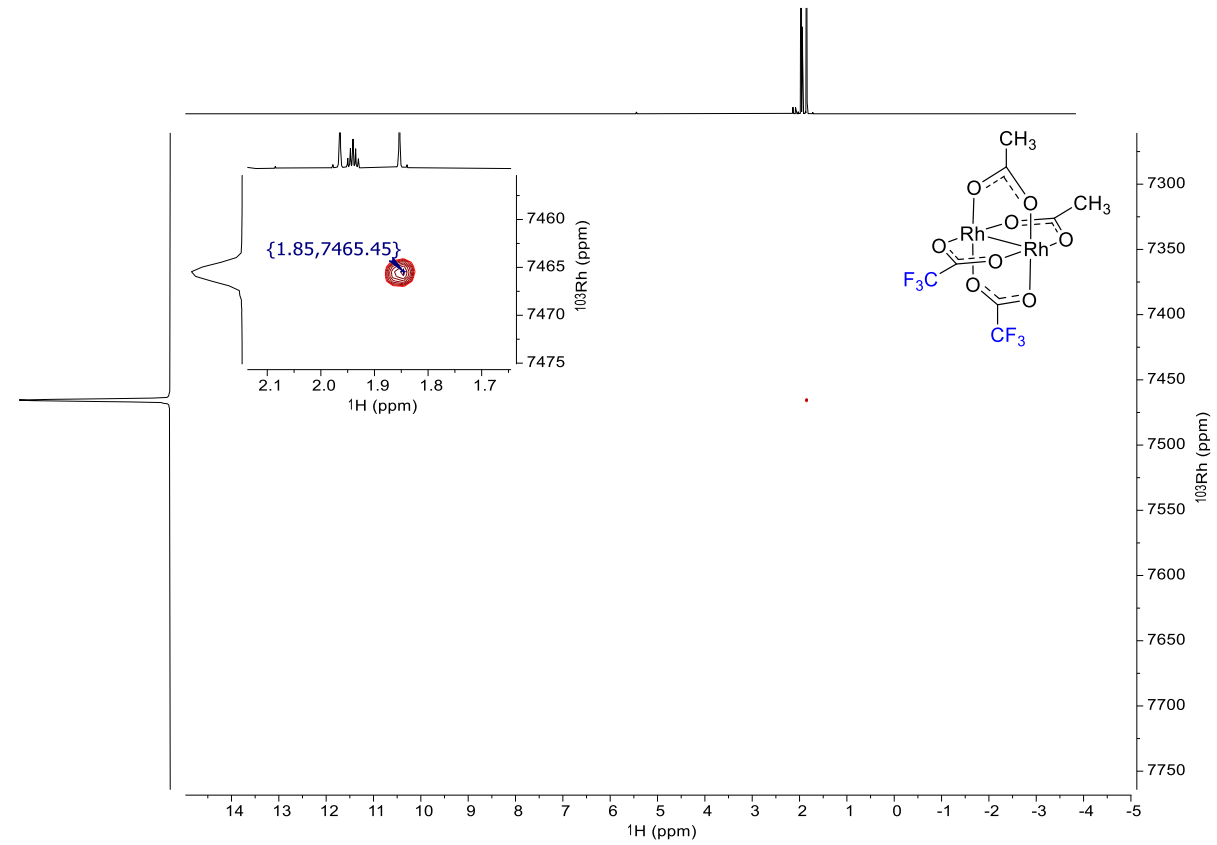

***trans*-$Rh_2(OAc)_2(OTfa)_2$ (4): ^{1}H-NMR (600 MHz, CD_3CN)**

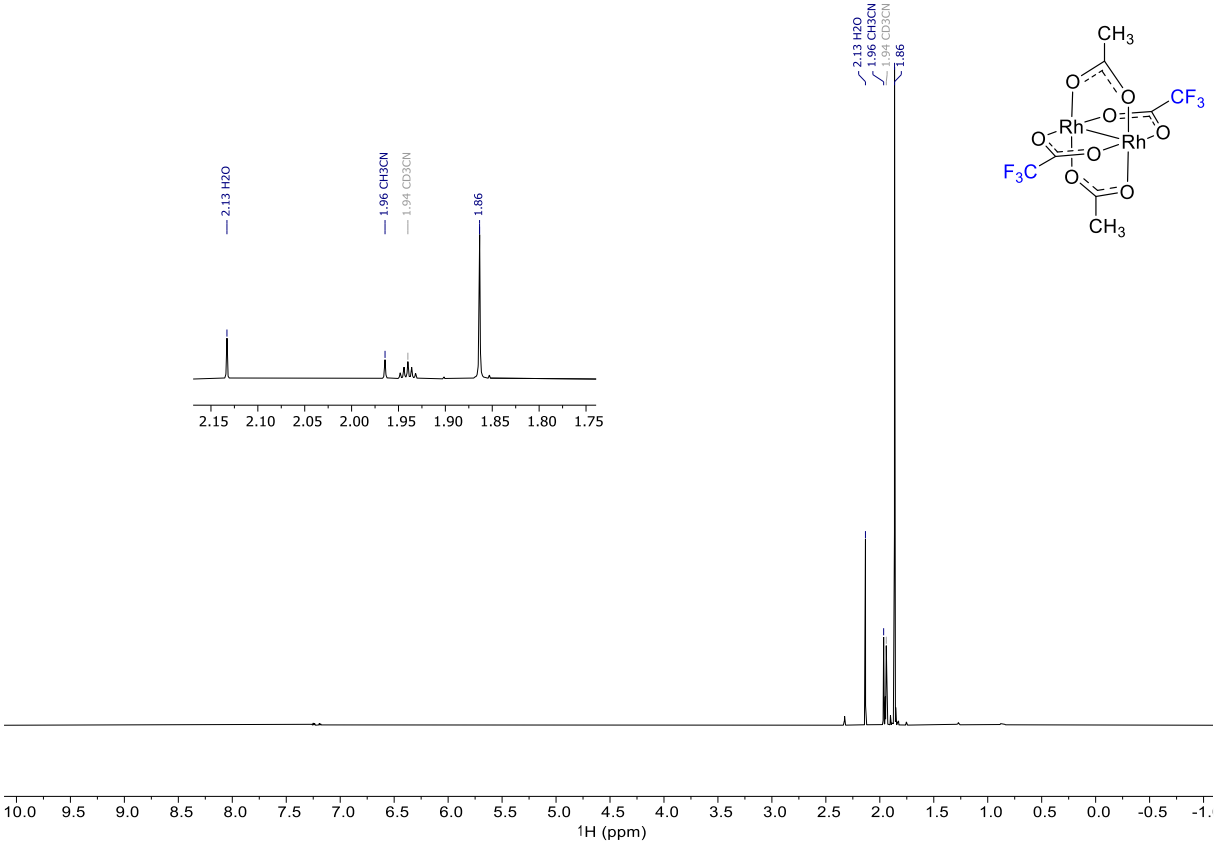

***trans*-$Rh_2(OAc)_2(OTfa)_2$ (4): $^{13}C\{^1H\}$-NMR (151 MHz, CD_3CN)**

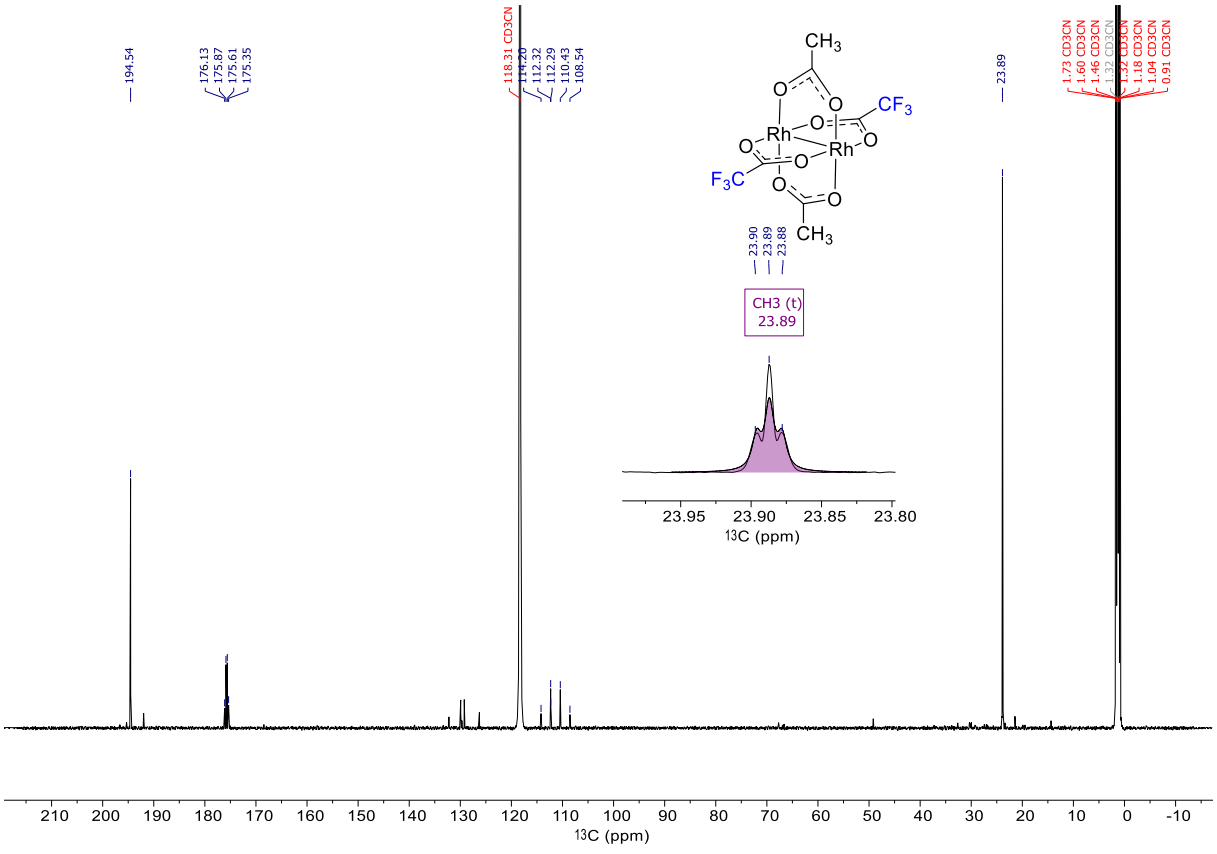

trans-$Rh_2(OAc)_2(OTfa)_2$ (4): ^{19}F-NMR (565 MHz, CD_3CN)

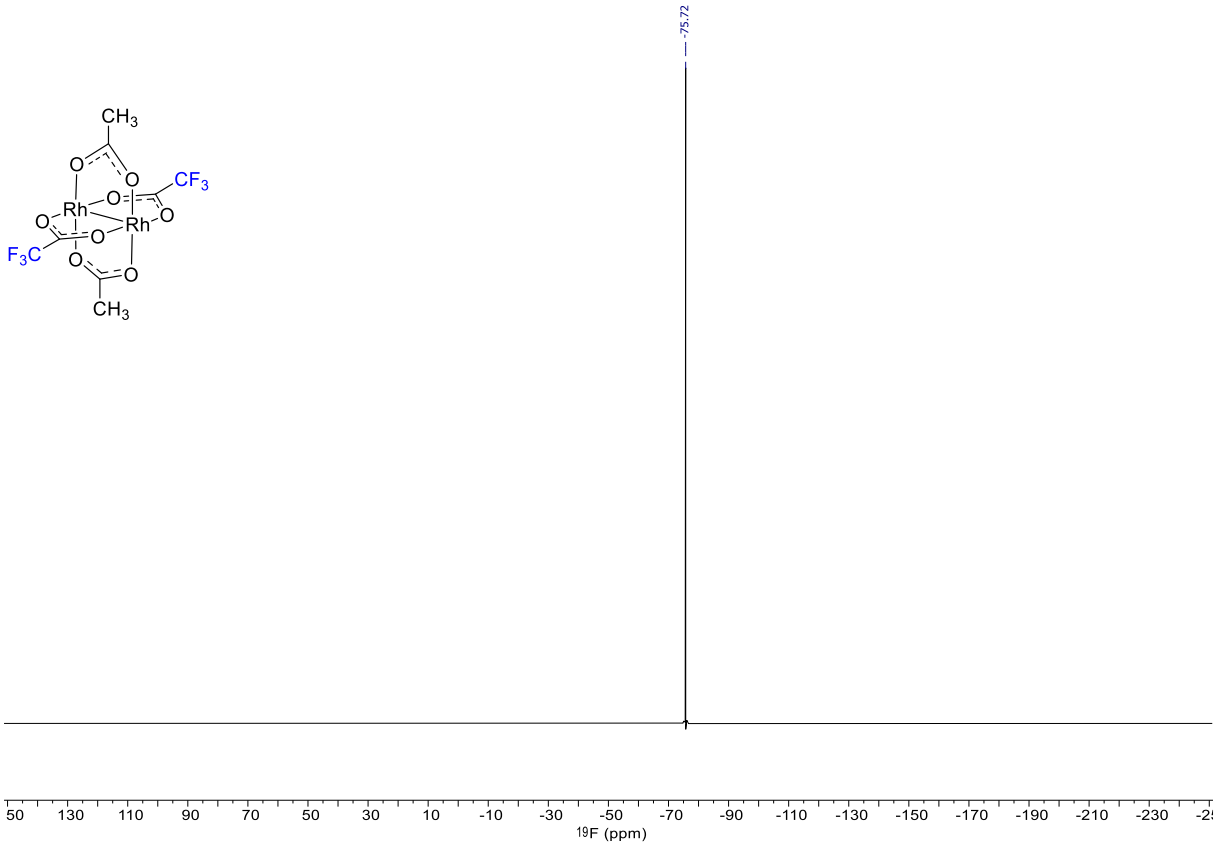

trans-$Rh_2(OAc)_2(OTfa)_2$ (4): H(C)Rh (CD_3CN)

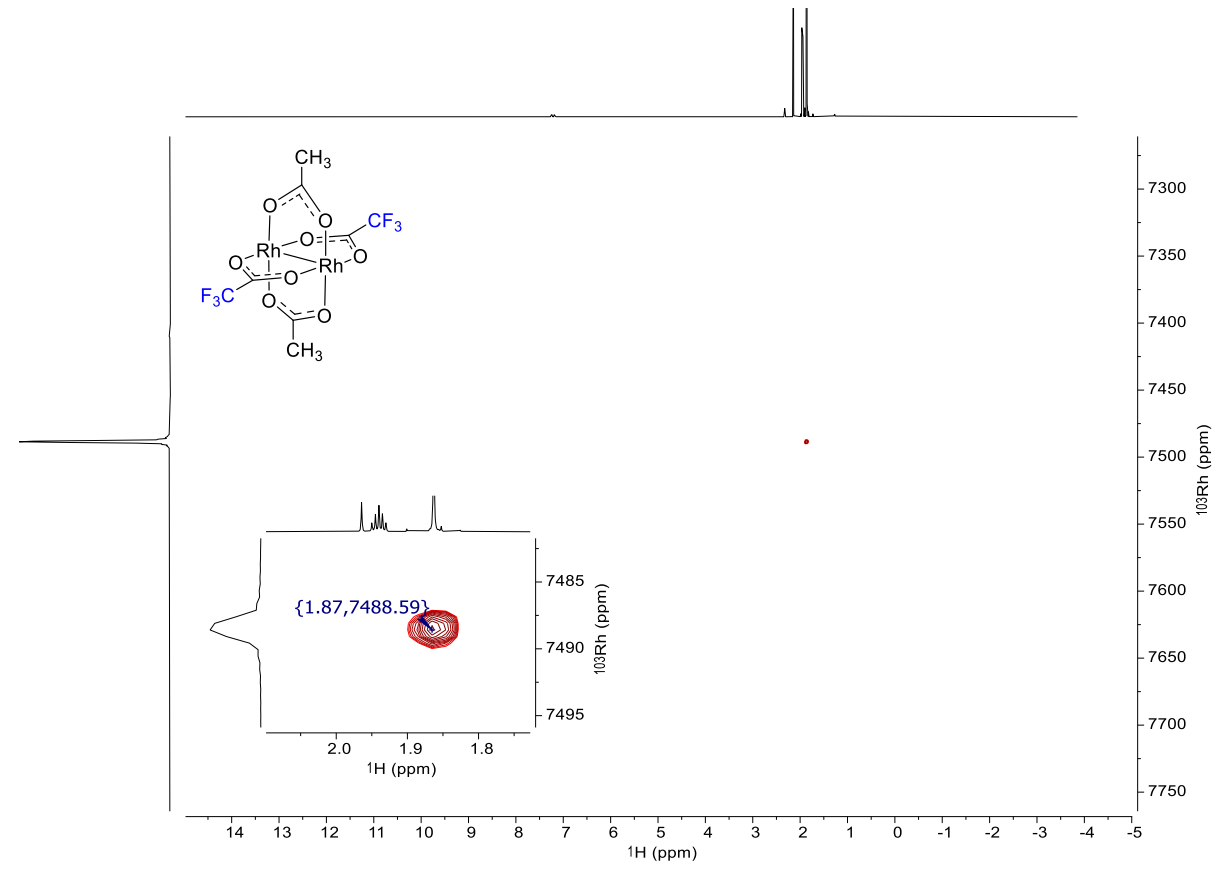

$Rh_2(OAc)(OTfa)_3$ (5): ^{1}H-NMR (500 MHz, CD_3CN)

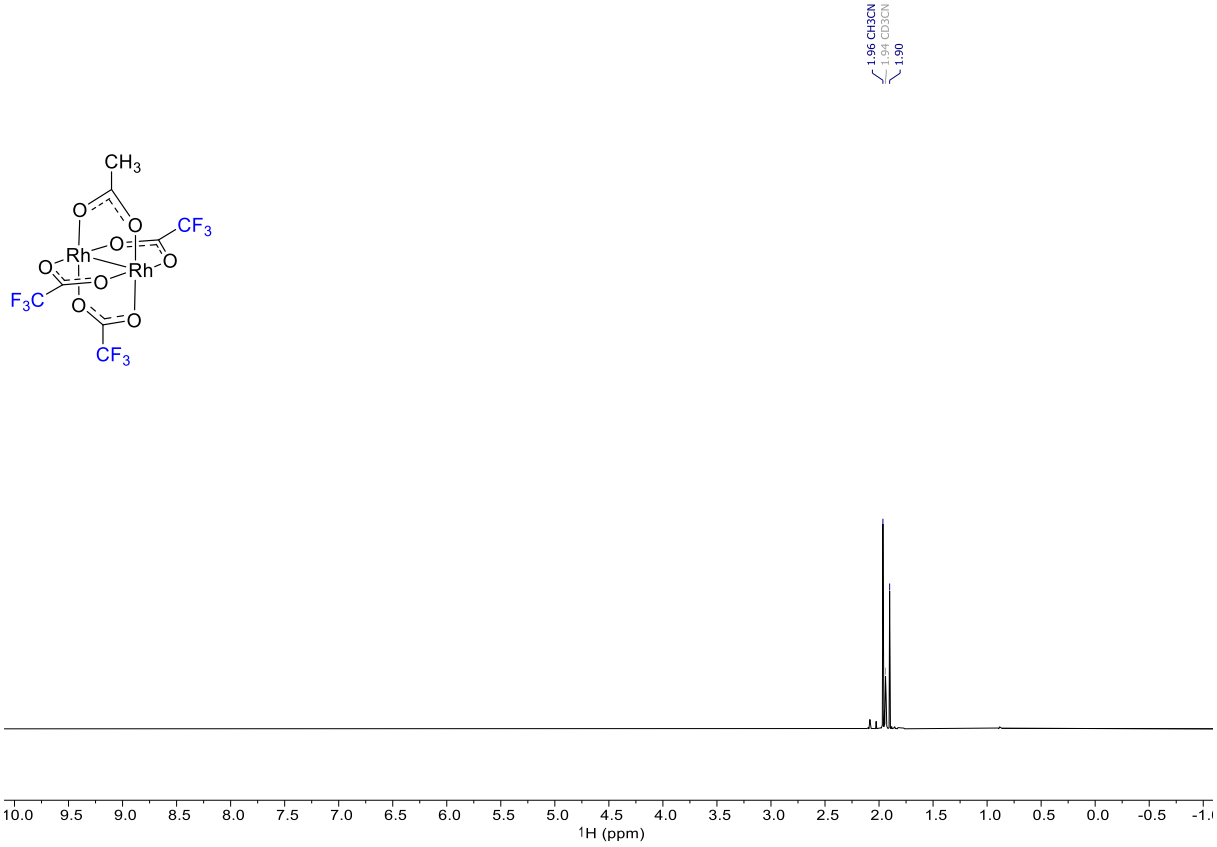

$Rh_2(OAc)(OTfa)_3$ (5): $^{13}C\{^1H\}$-NMR (151 MHz, CD_3CN)

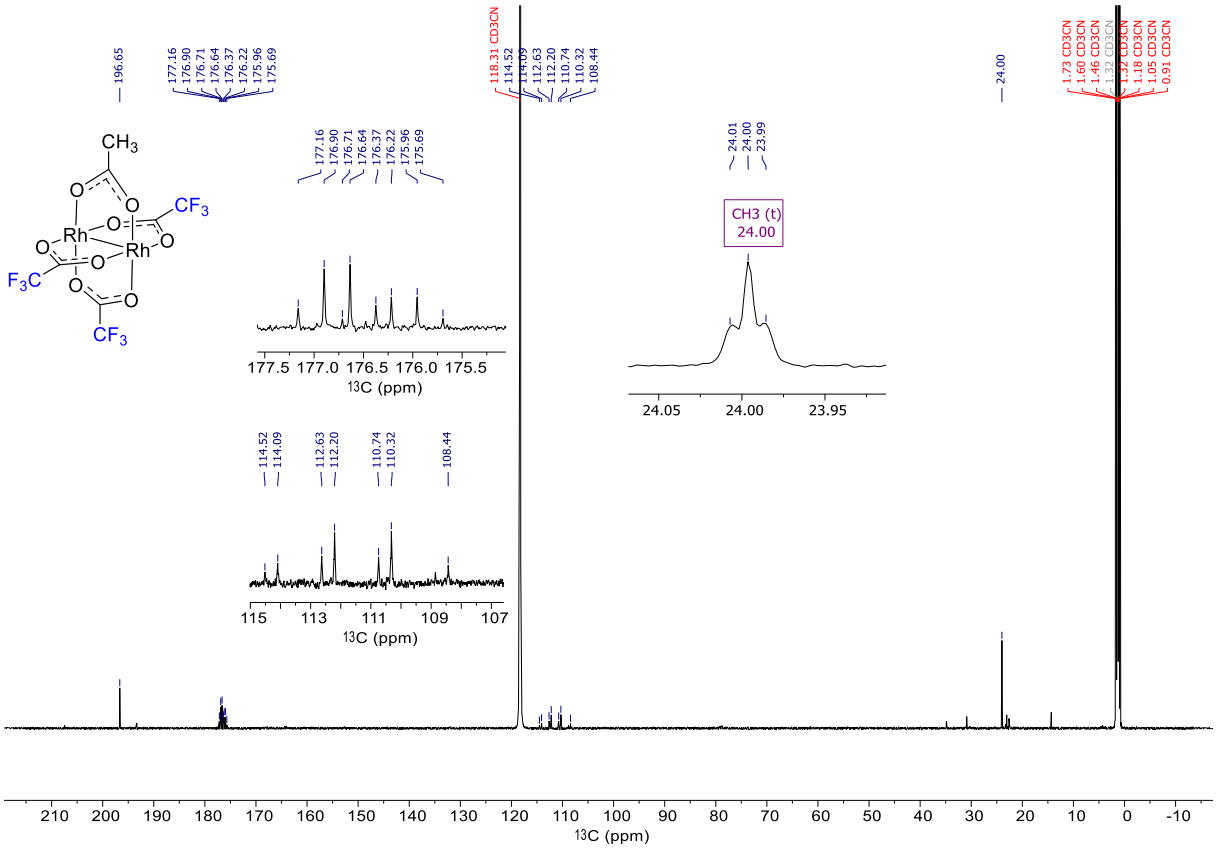

$Rh_2(OAc)(OTfa)_3$ (5): ^{19}F-NMR (565 MHz, CD_3CN)

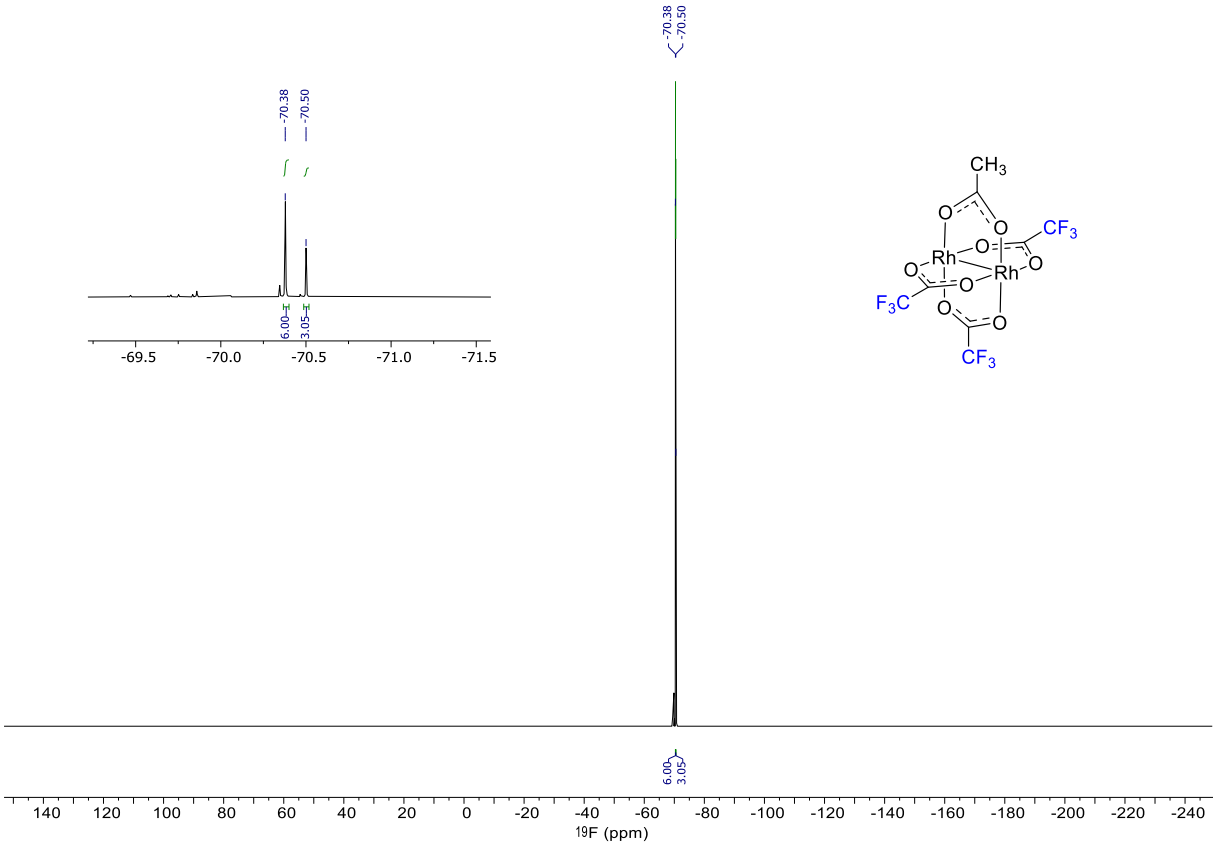

$Rh_2(OAc)(OTfa)_3$ (5): H(C)Rh (CD_3CN)

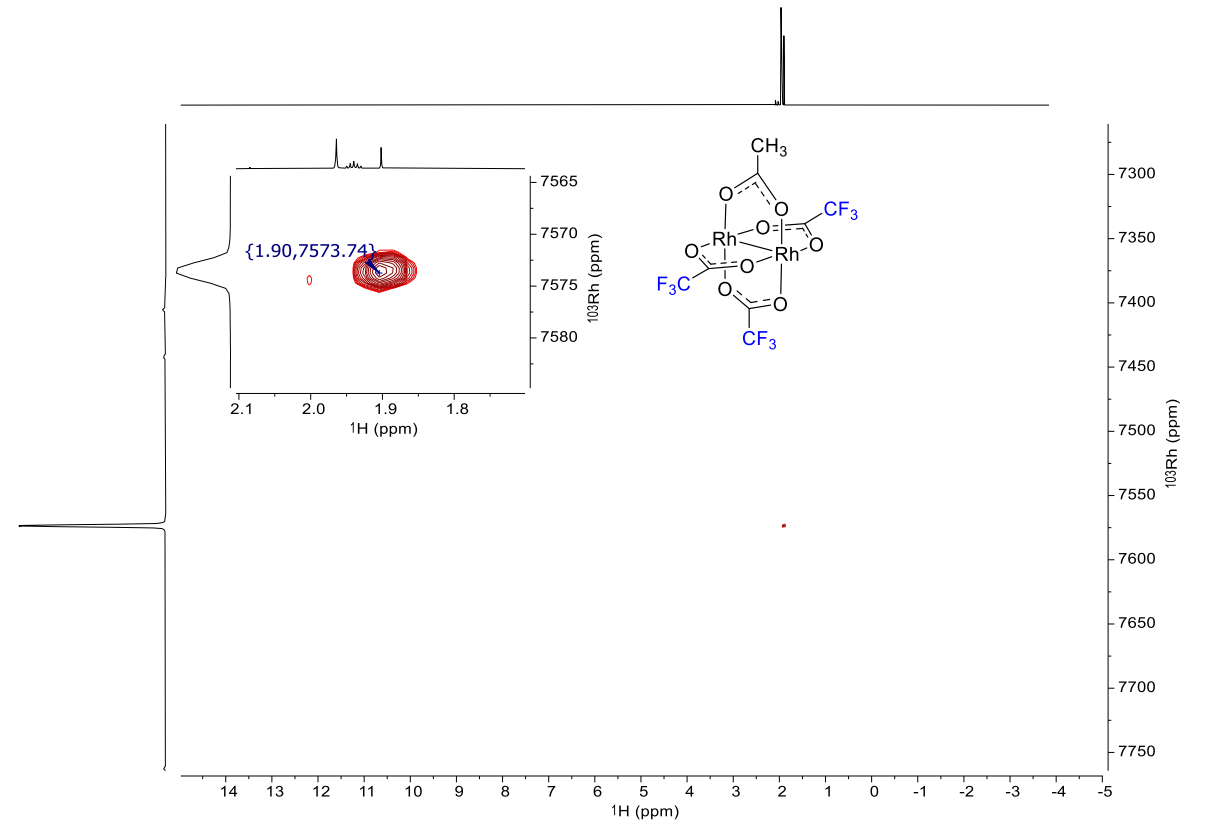

Dirhodium(II) tetra(trifluoracetate) ($Rh_2(OTfa)_4$) (6): ^{19}F-NMR (565 MHz, CD_3CN)

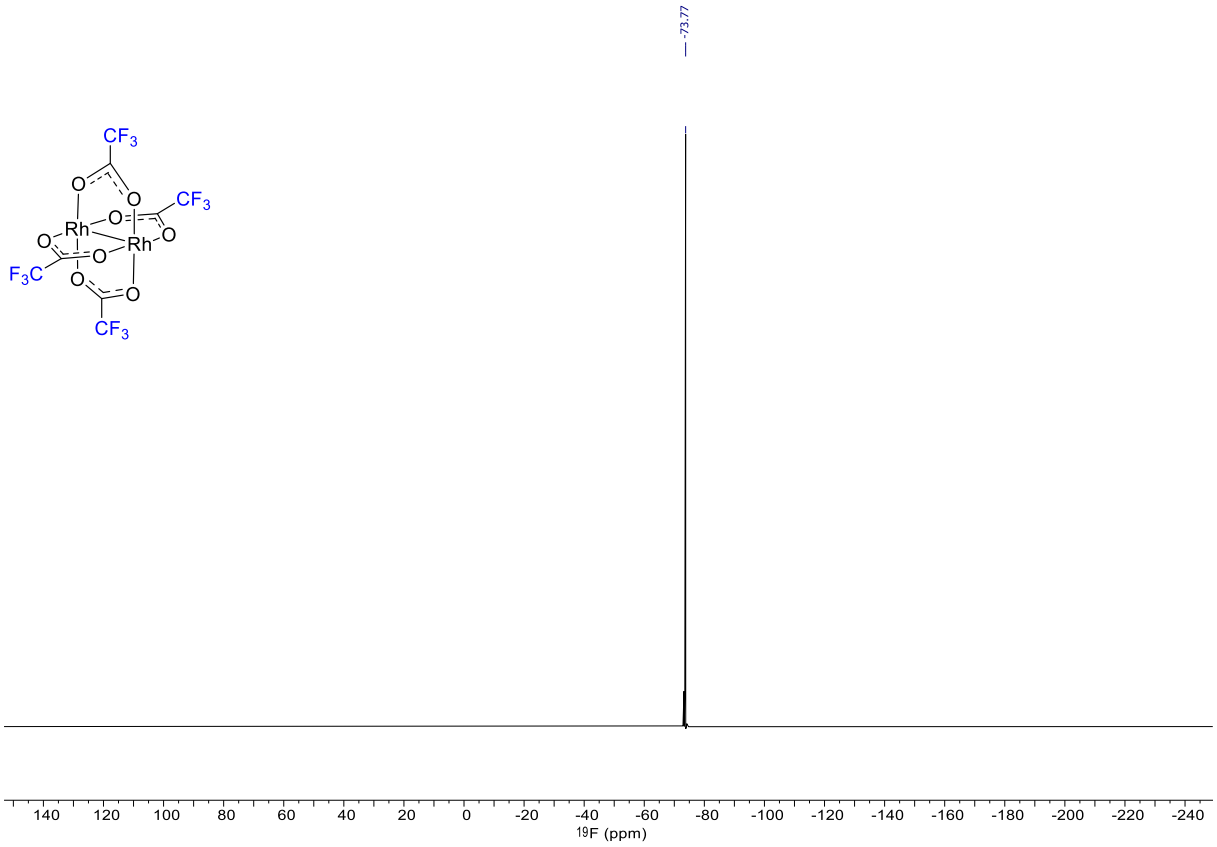

Dirhodium(II) tetra(trifluoracetate) ($Rh_2(OTfa)_4$) (6): ^{13}C-NMR (151 MHz, CD_3CN)

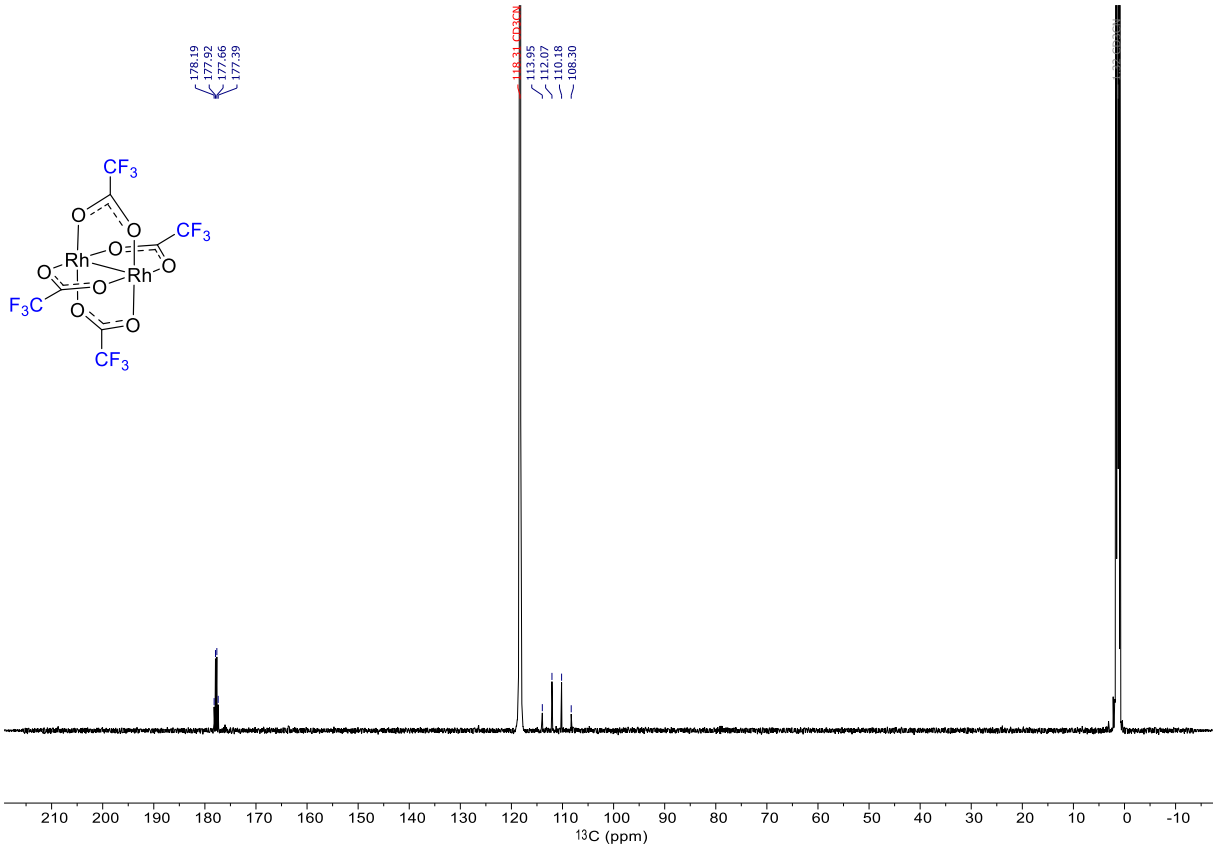

Dirhodium(II) tetra(trifluoracetate) ($Rh_2(OTfa)_4$) (6): ^{103}Rh-NMR (15.92 MHz, CD_3CN)

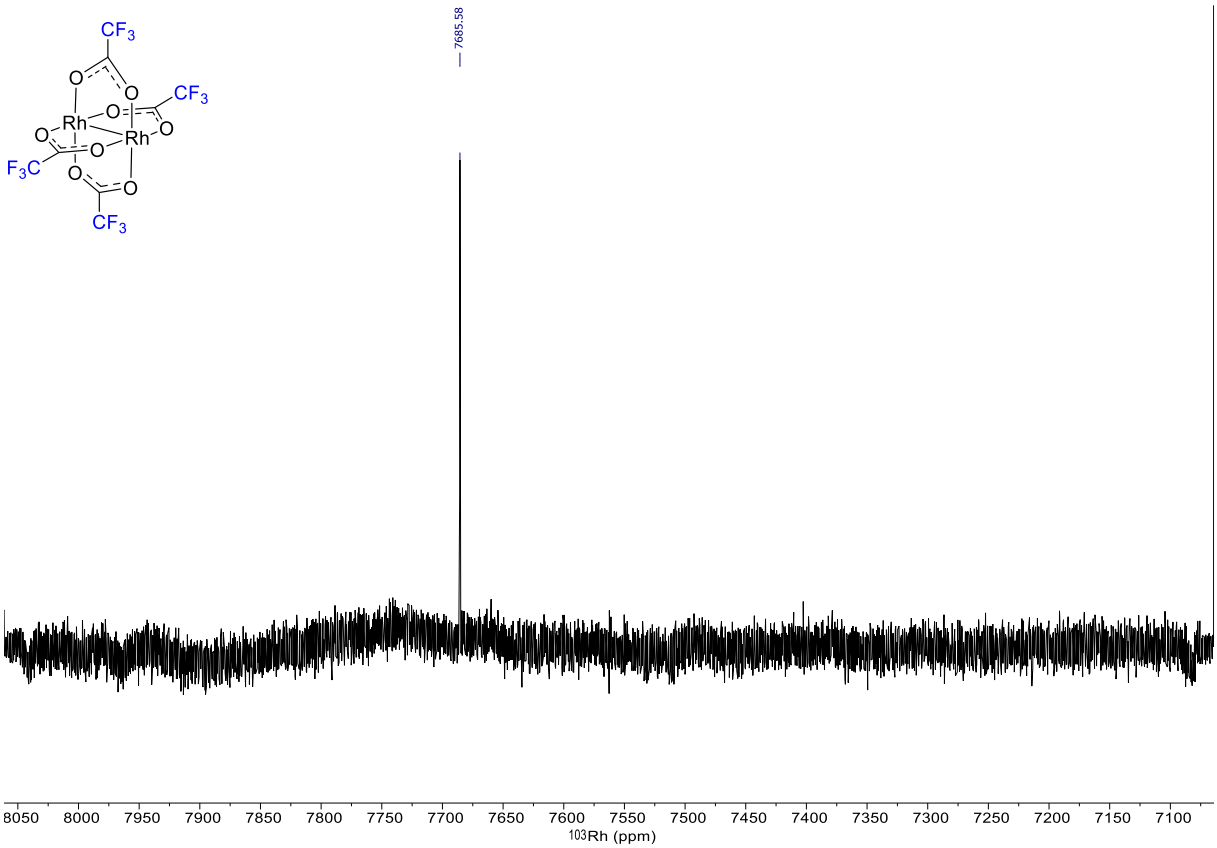

$Rh_2(OPiv)_4$ (7): ^{1}H-NMR (400 MHz, CD_3CN)

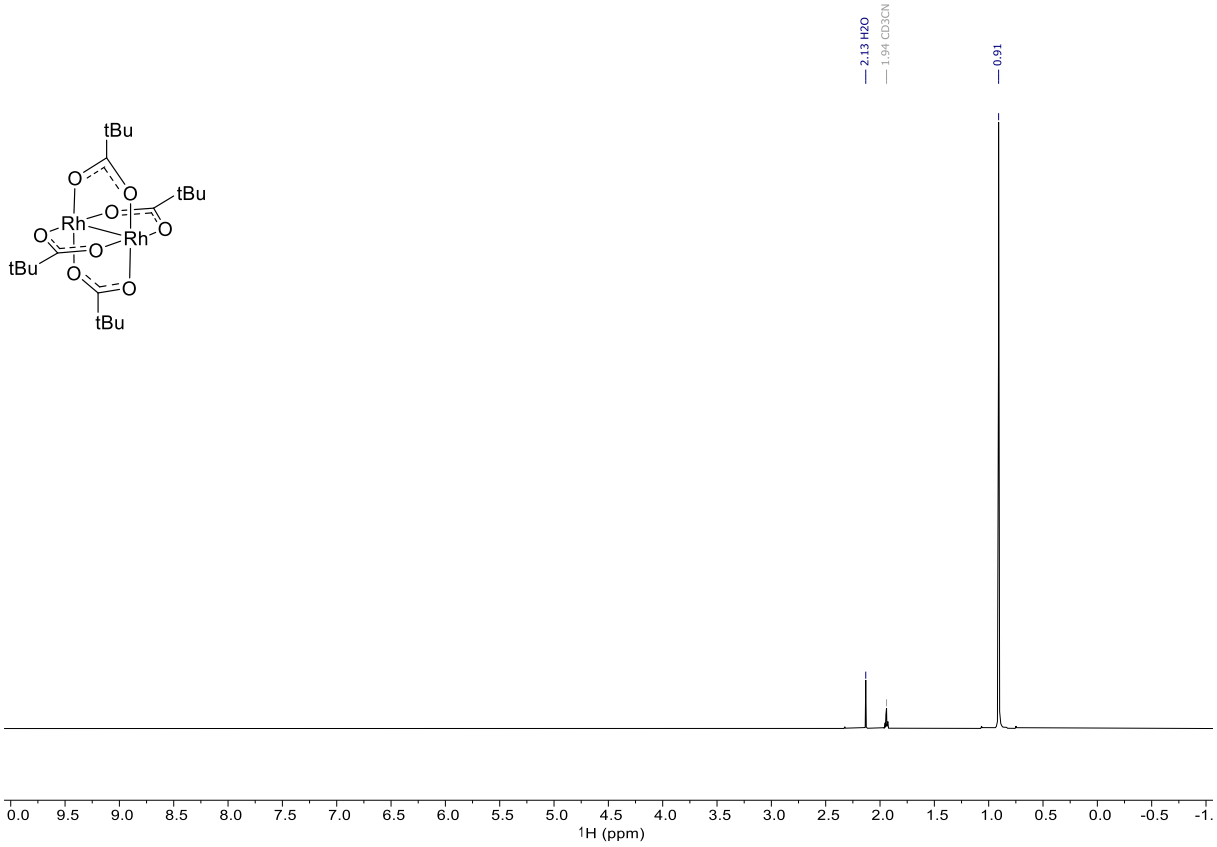

$Rh_2(OPiv)_4$ (7): H(C)Rh (CD_3CN)

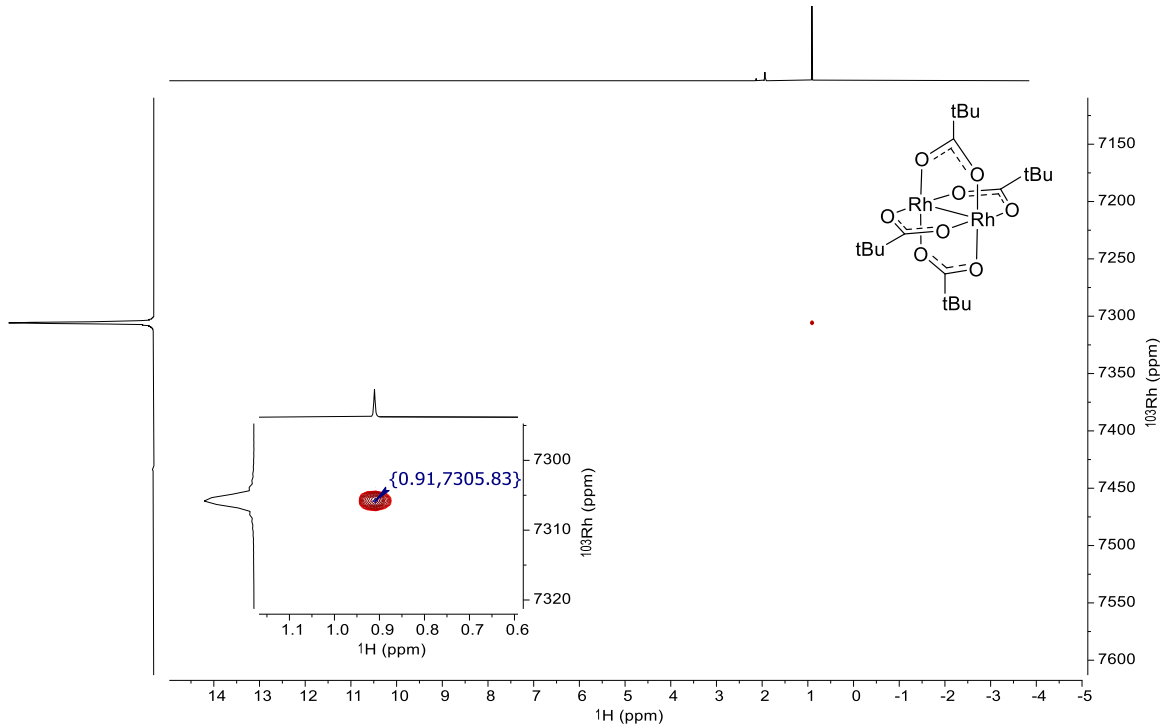

$Rh_2(HCO_2)_4$ (8): ^{1}H-NMR (400 MHz, CD_3CN)

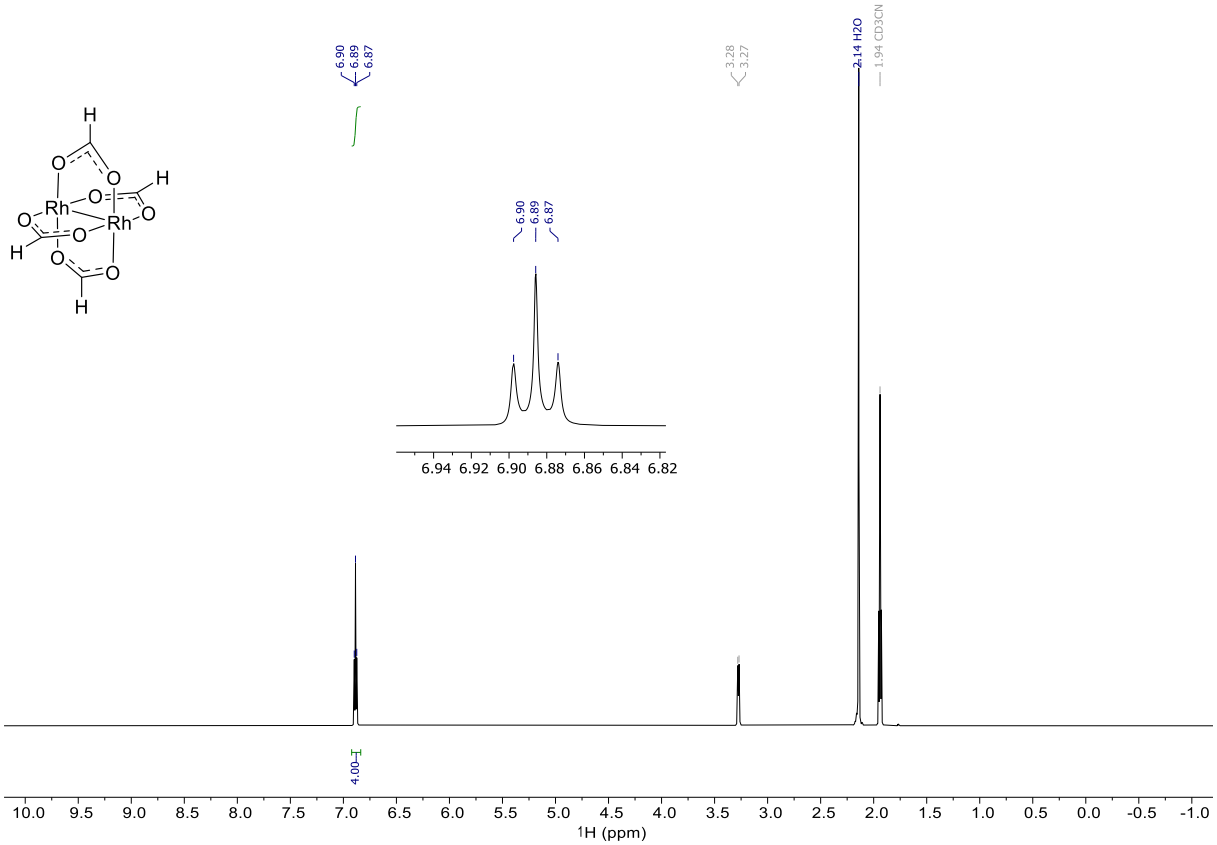

$Rh_2(HCO_2)_4$ (8): $^{13}C\{^1H\}$-NMR (101 MHz, CD_3CN)

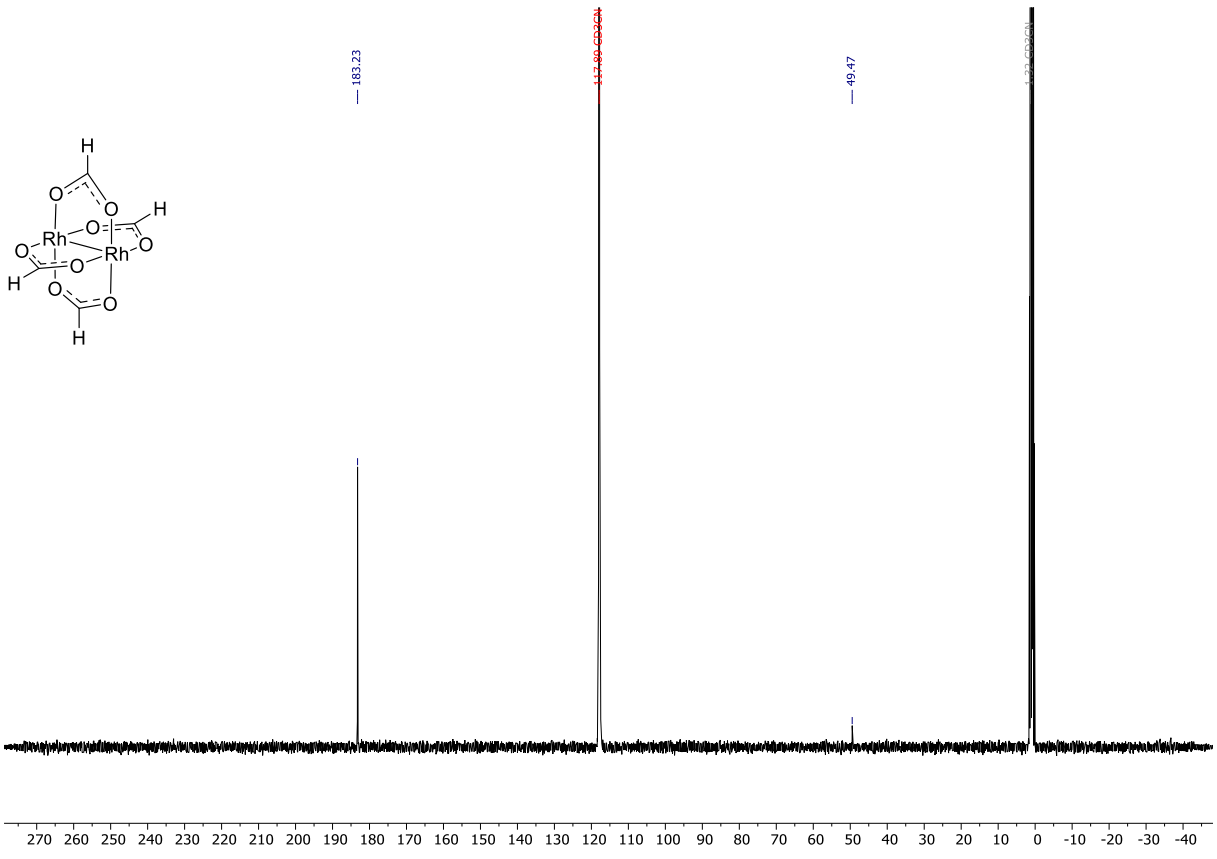

$Rh_2(HCO_2)_4$ (8): ^{1}H-^{13}C-*edited*-HSQC (CD_3CN)

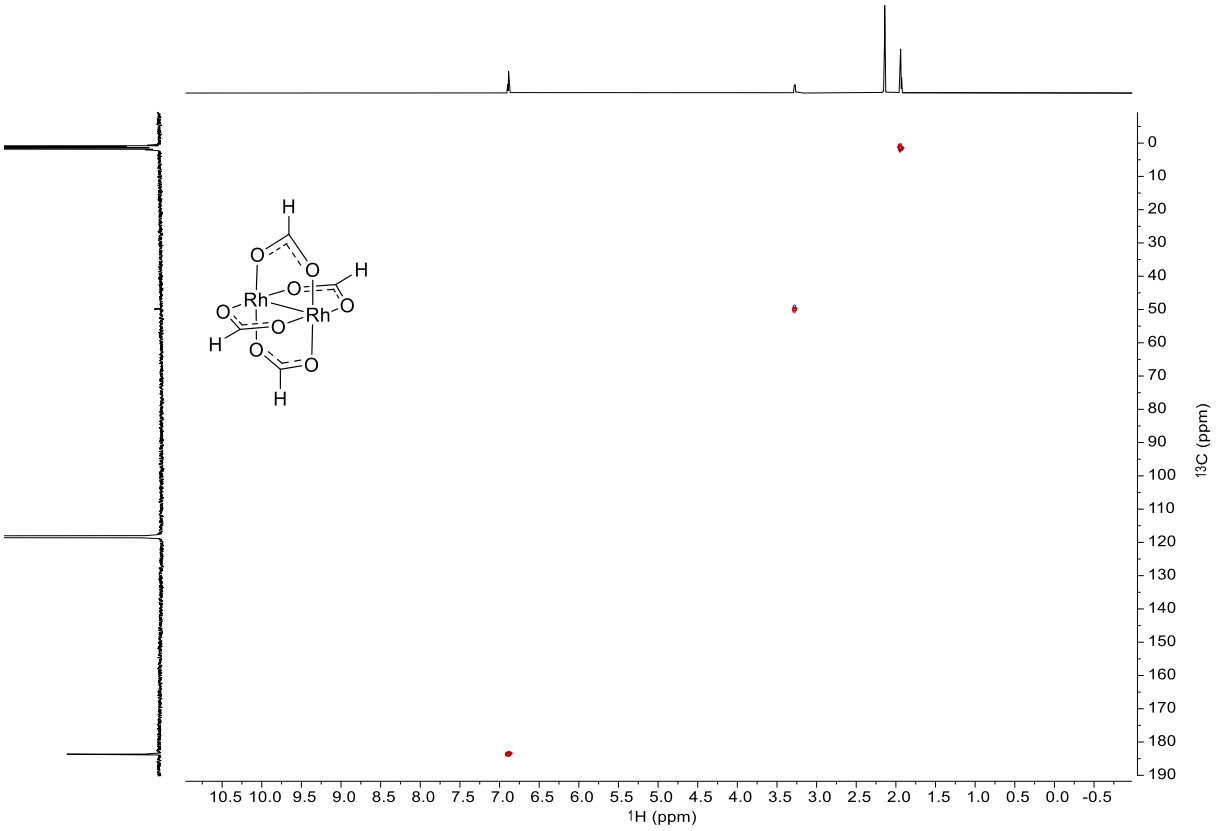

$Rh_2(HCO_2)_4$ (8): ^{1}H-^{103}Rh-HMBC (CD_3CN)

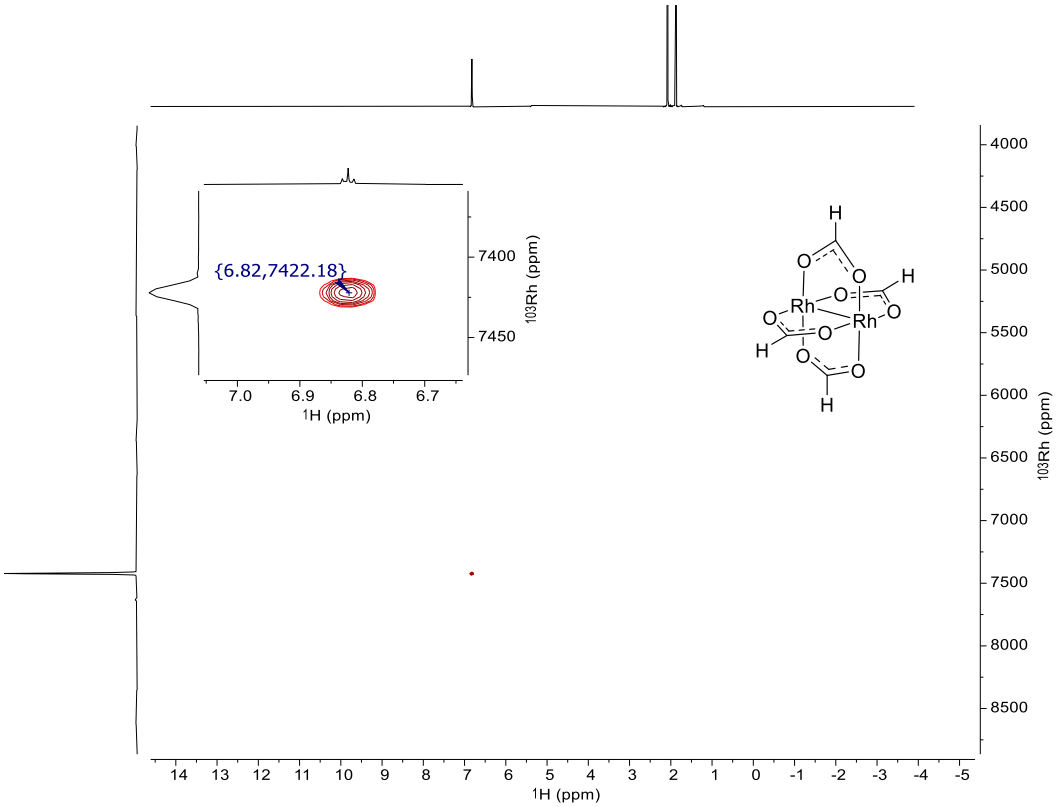
{6.82,7422.18}
7400
7450
103Rh (ppm)
7.0
6.9
6.8
6.7
1H (ppm)
H
O
O
H
O
Rh
O
Rh
O
O
H
O
O
H
4000
4500
5000
5500
6000
6500
7000
7500
8000
8500
103Rh (ppm)
14
13
12
11
10
9
8
7
6
5
4
3
2
1
0
-1
-2
-3
-4
-5
1H (ppm)

$Rh_2(OBz)_4$ (9): ^{1}H-NMR (400 MHz, CD_3CN)

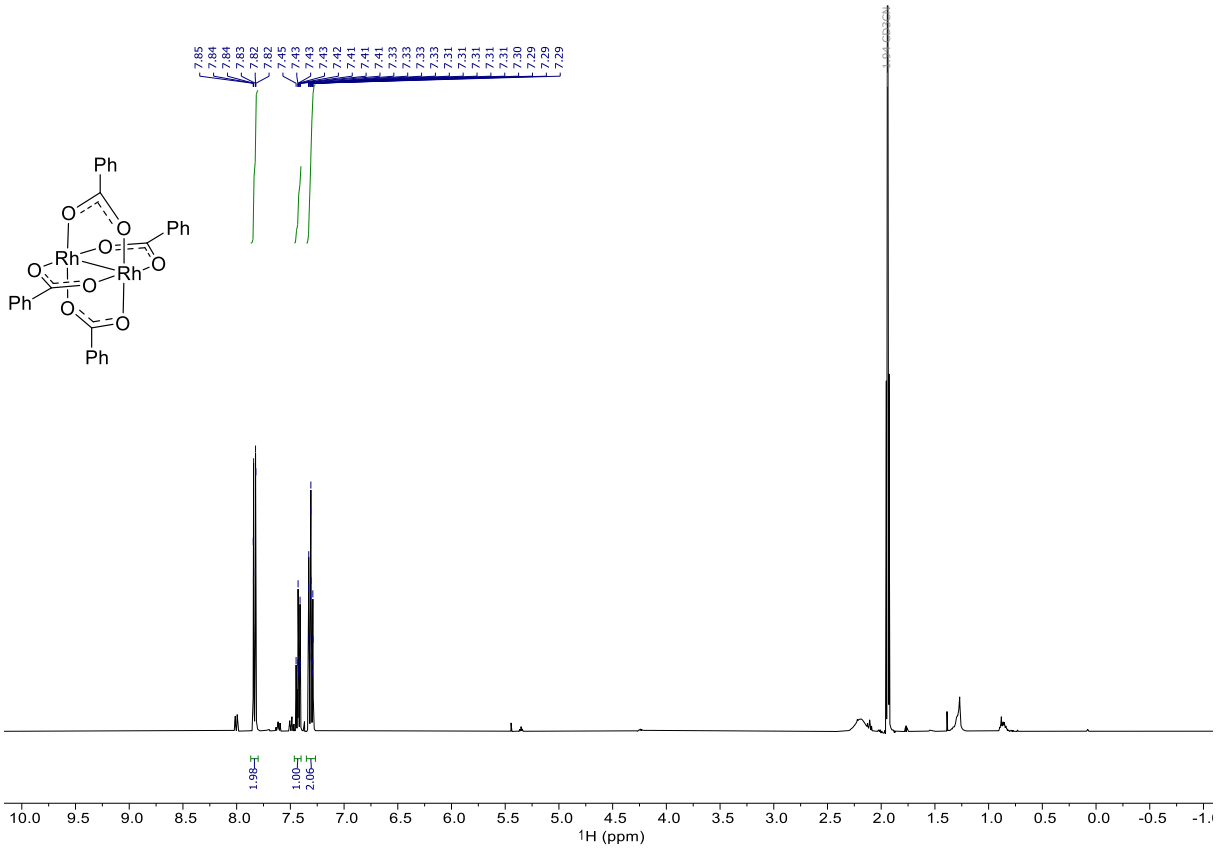

$Rh_2(OBz)_4$ (9): $^{13}C\{^1H\}$-NMR (101 MHz, CD_3CN)

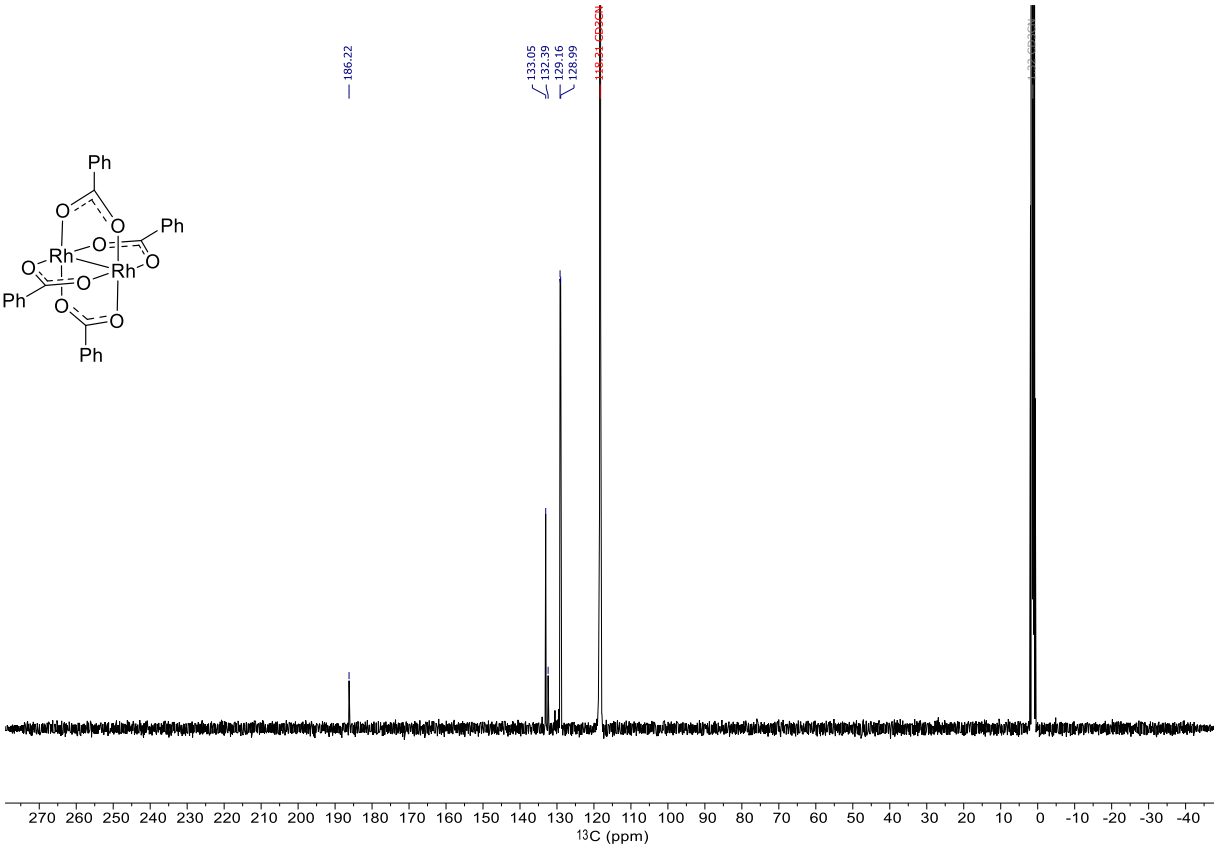

$Rh_2(OBz)_4$ (9): H(C)Rh (CD_3CN)

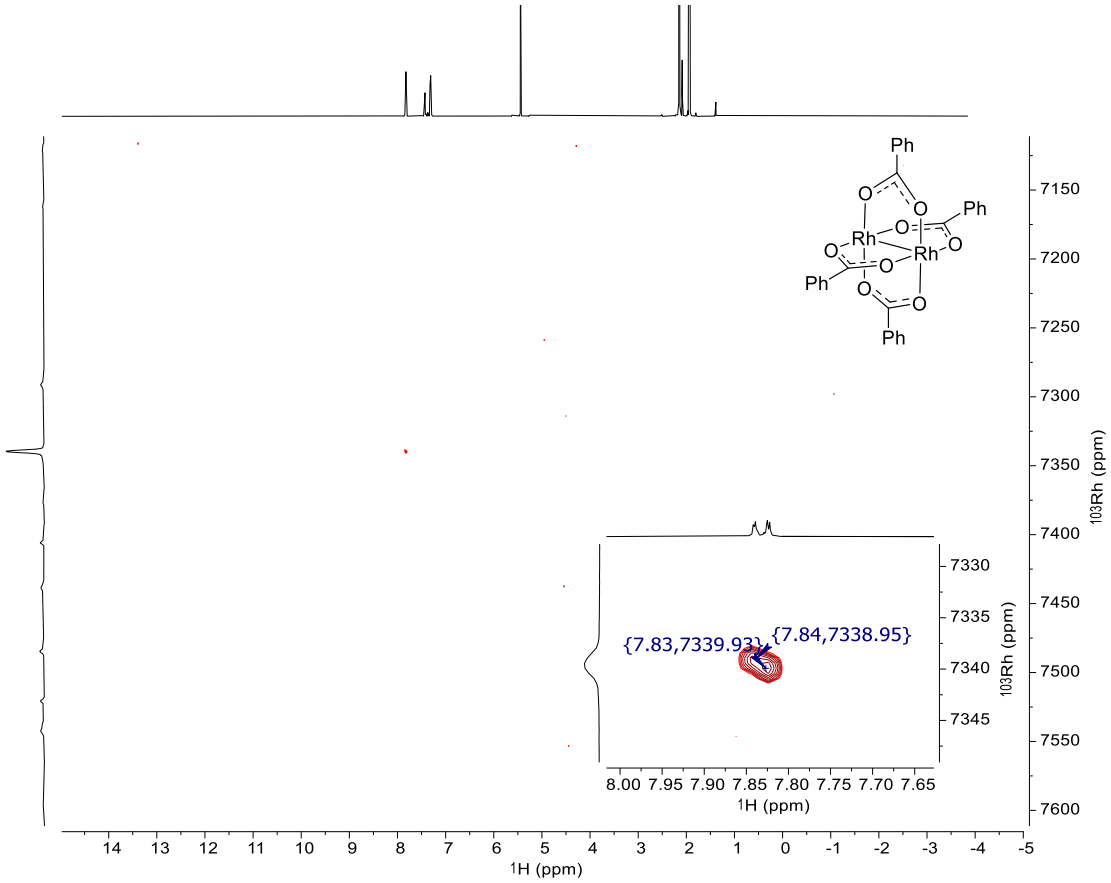

$Rh_2(OBz)_4$ (9): ^{1}H-NMR (500 MHz, [D_8]-THF)

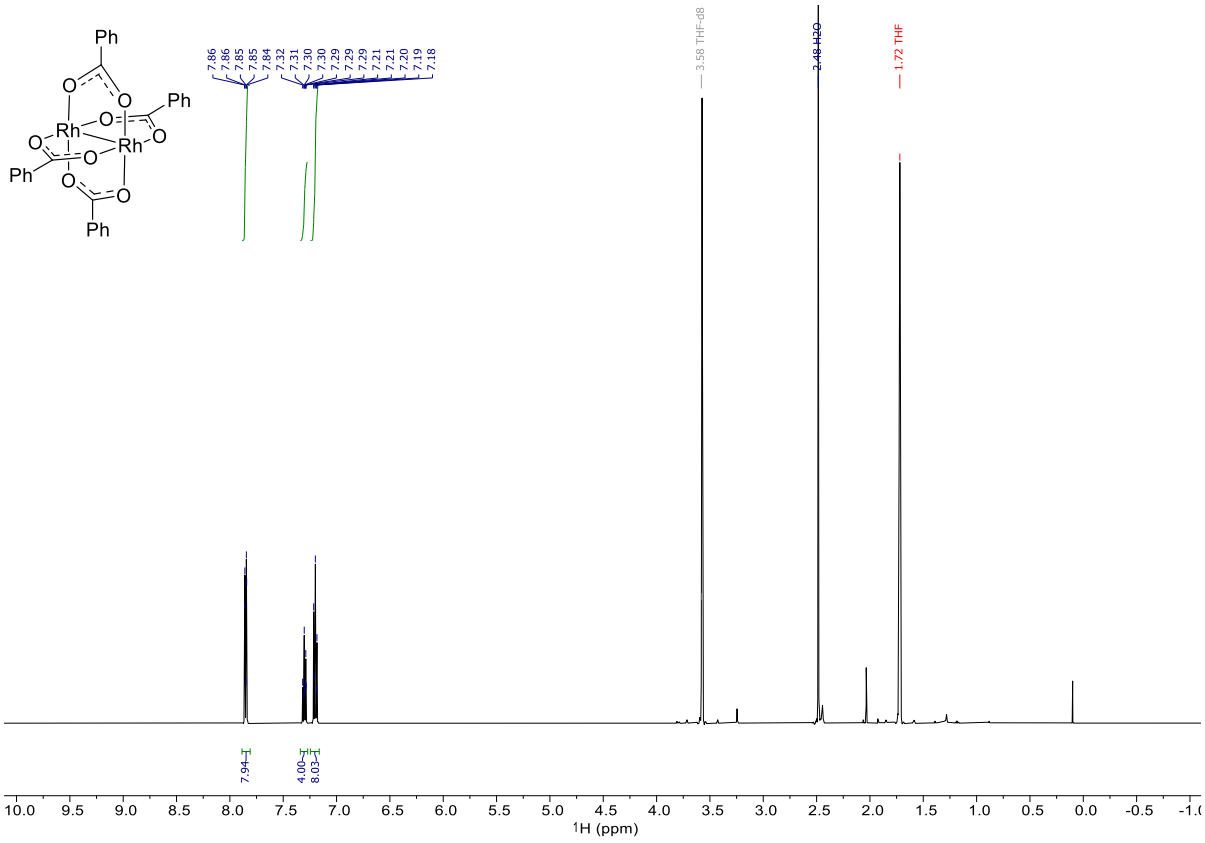

$Rh_2(OBz)_4$ (9): H(C)Rh ([D_8]-THF)

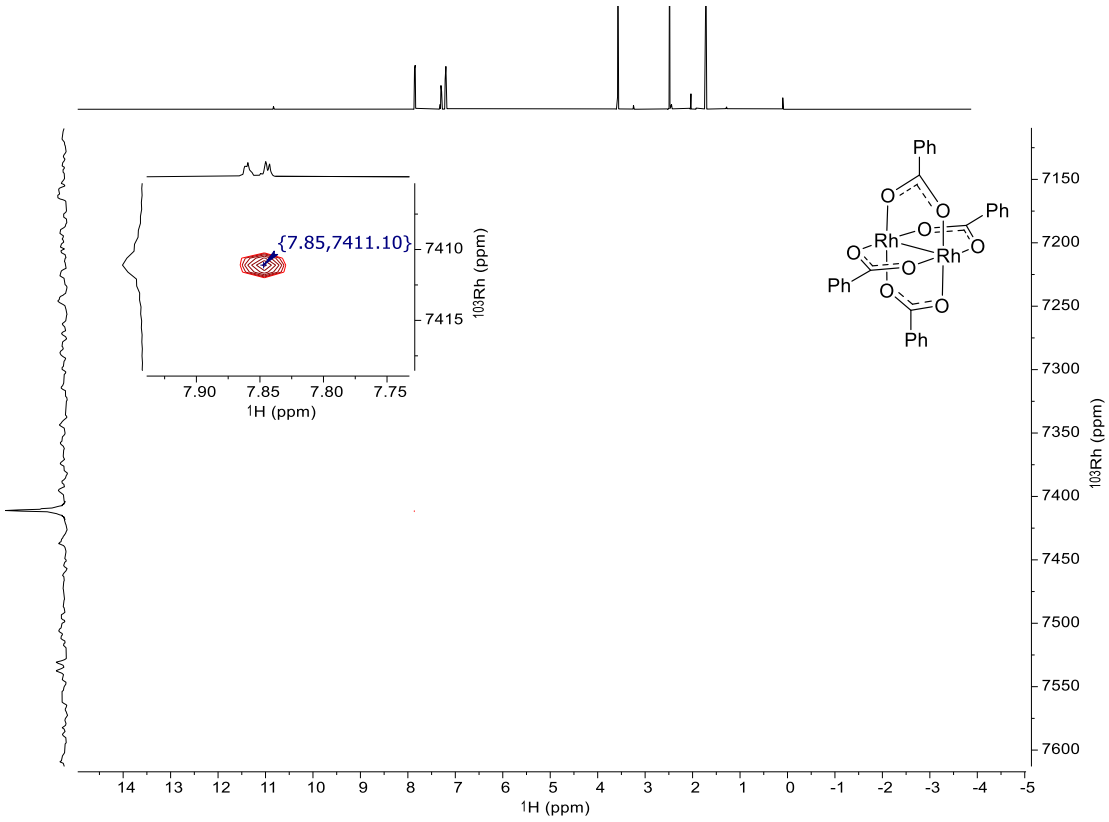

$Rh_2(p\text{-}FC_6H_4COO)_4$ (10): ^{1}H-NMR (400 MHz, [D_8]-THF)

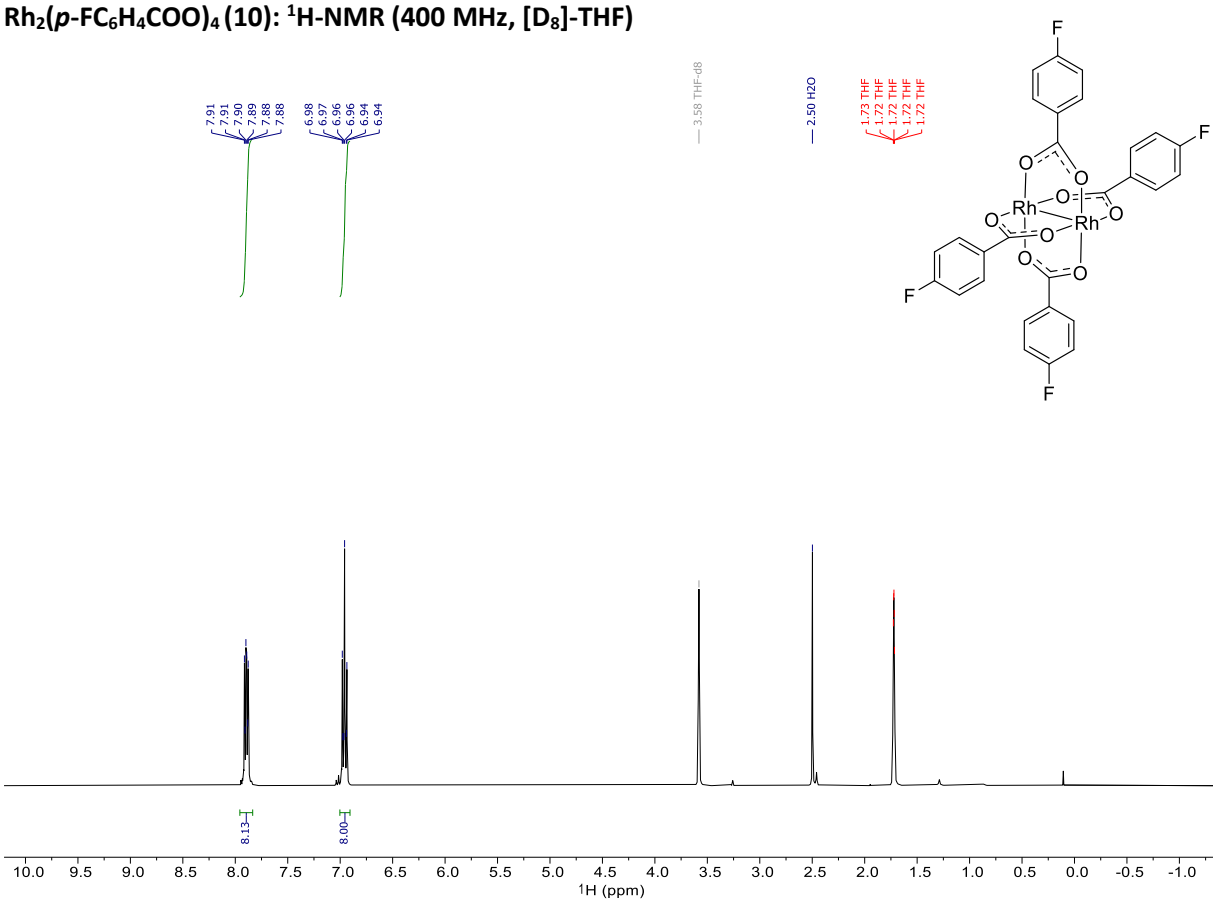

$Rh_2(p\text{-}FC_6H_4COO)_4$ (10): H(C)Rh ([D_8]-THF)

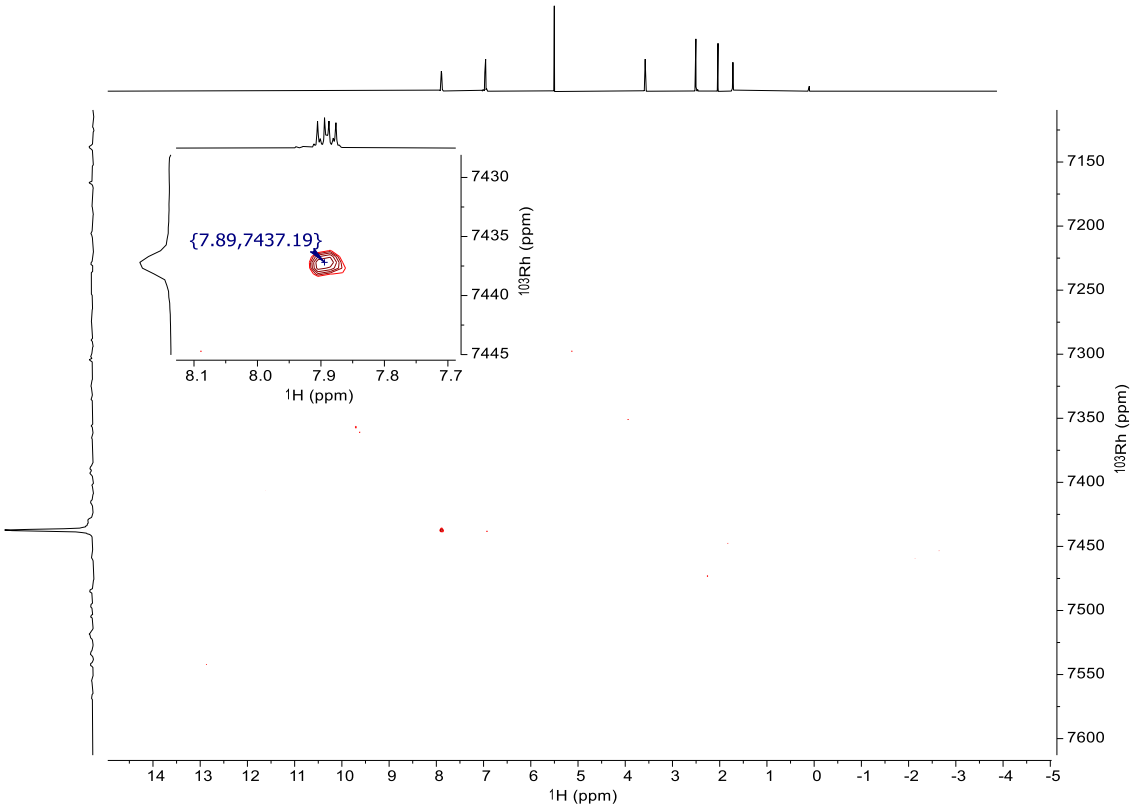

$Rh_2(p\text{-}F_3CC_6H_4COO)_4$ (11): ^{1}H-NMR (400 MHz, [D_8]-THF)

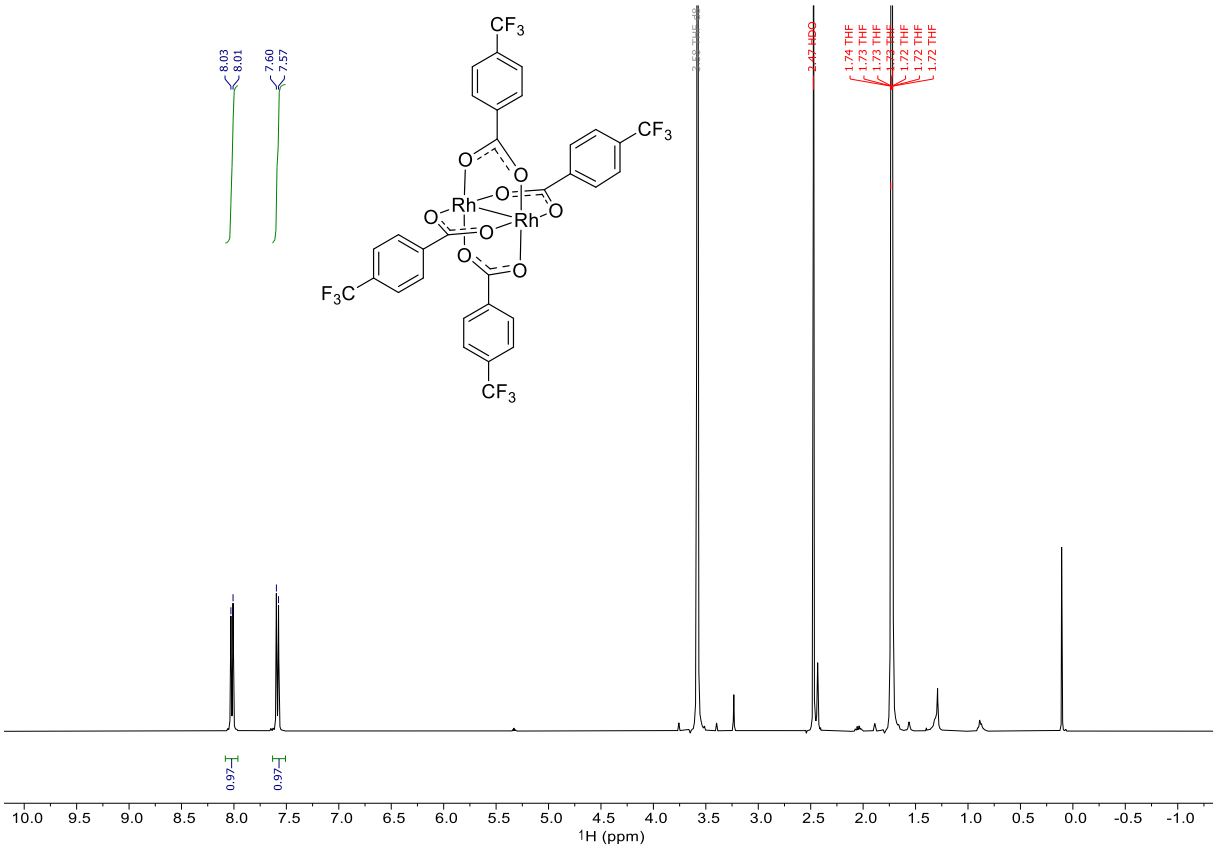

$Rh_2(p\text{-}F_3CC_6H_4COO)_4$ (11): H(C)Rh ([D_8]-THF)

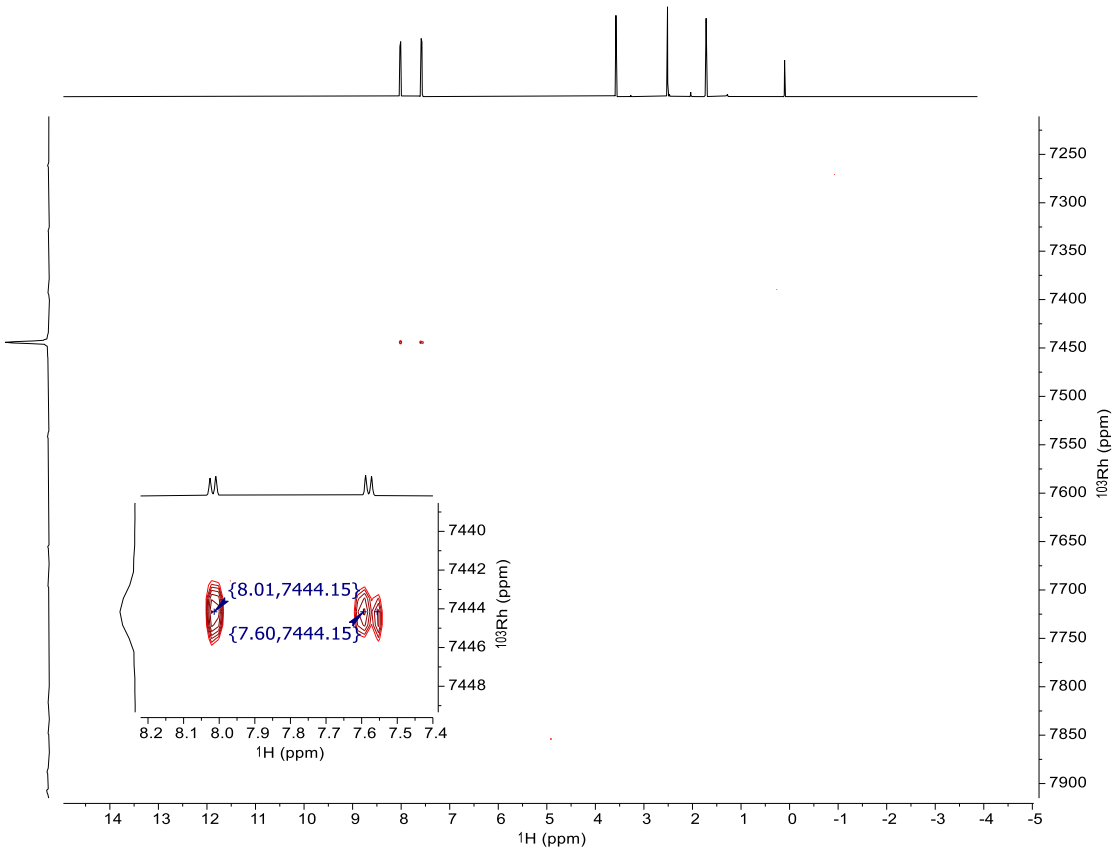

$Rh_2(ClCH_2CO_2)_4$ (12): ^{1}H-NMR (600 MHz, CD_3CN)

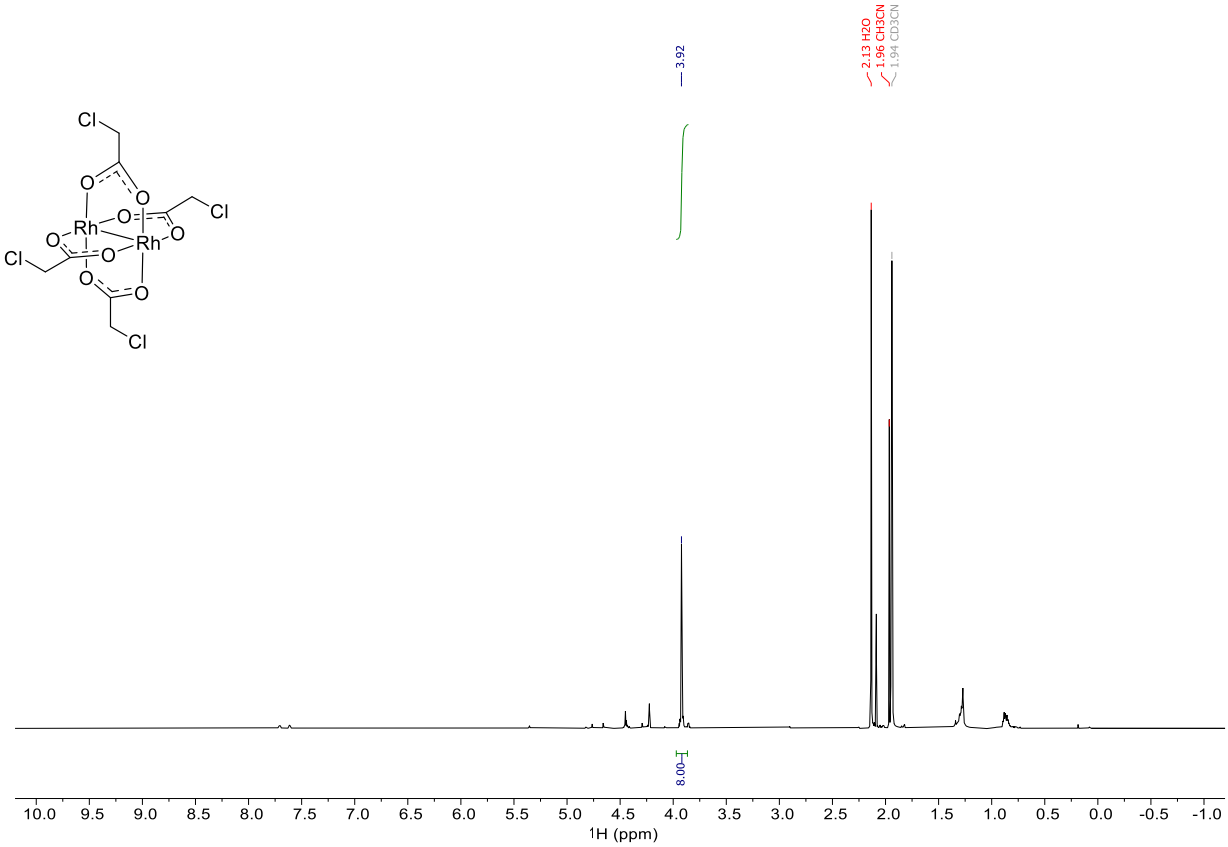

$Rh_2(ClCH_2CO_2)_4$ (12): ^{13}C-NMR (151 MHz, CD_3CN)

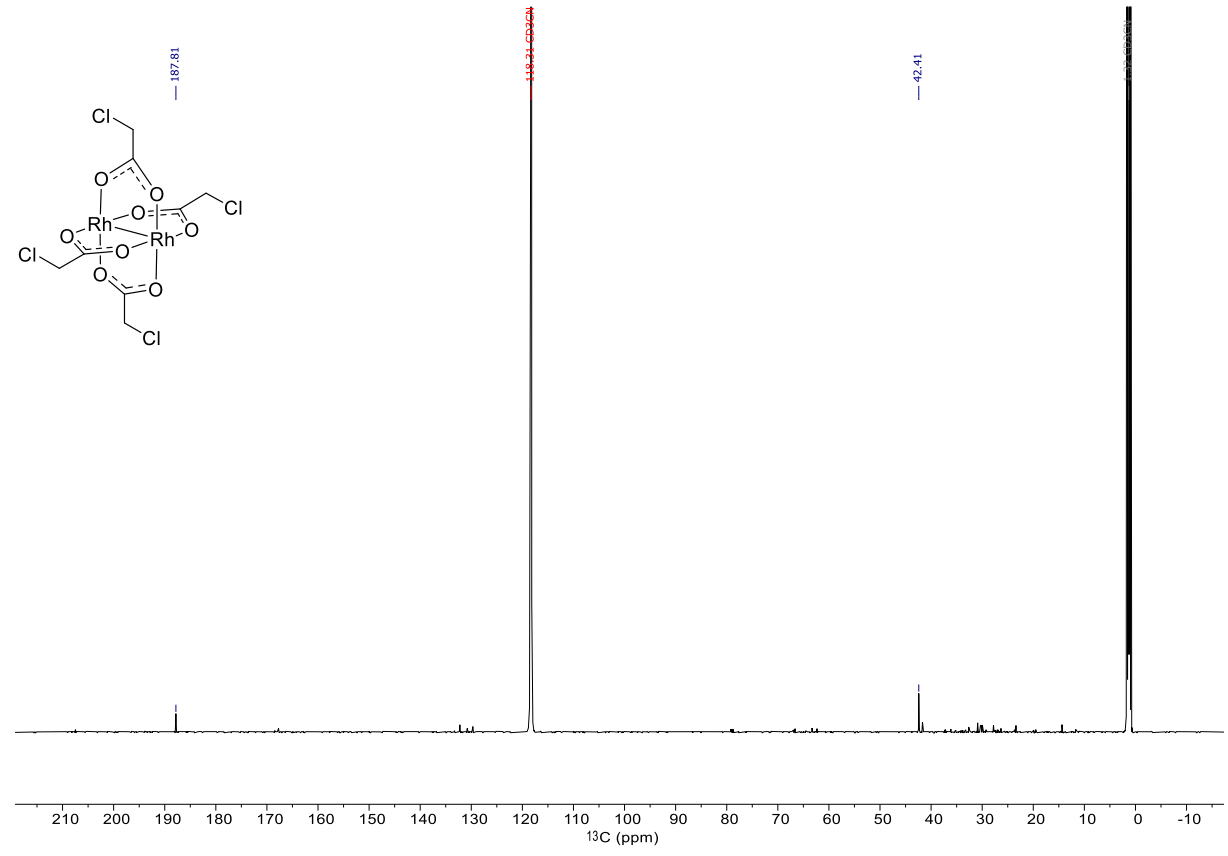

$Rh_2(ClCH_2CO_2)_4$ (12): H(C)Rh (CD_3CN)

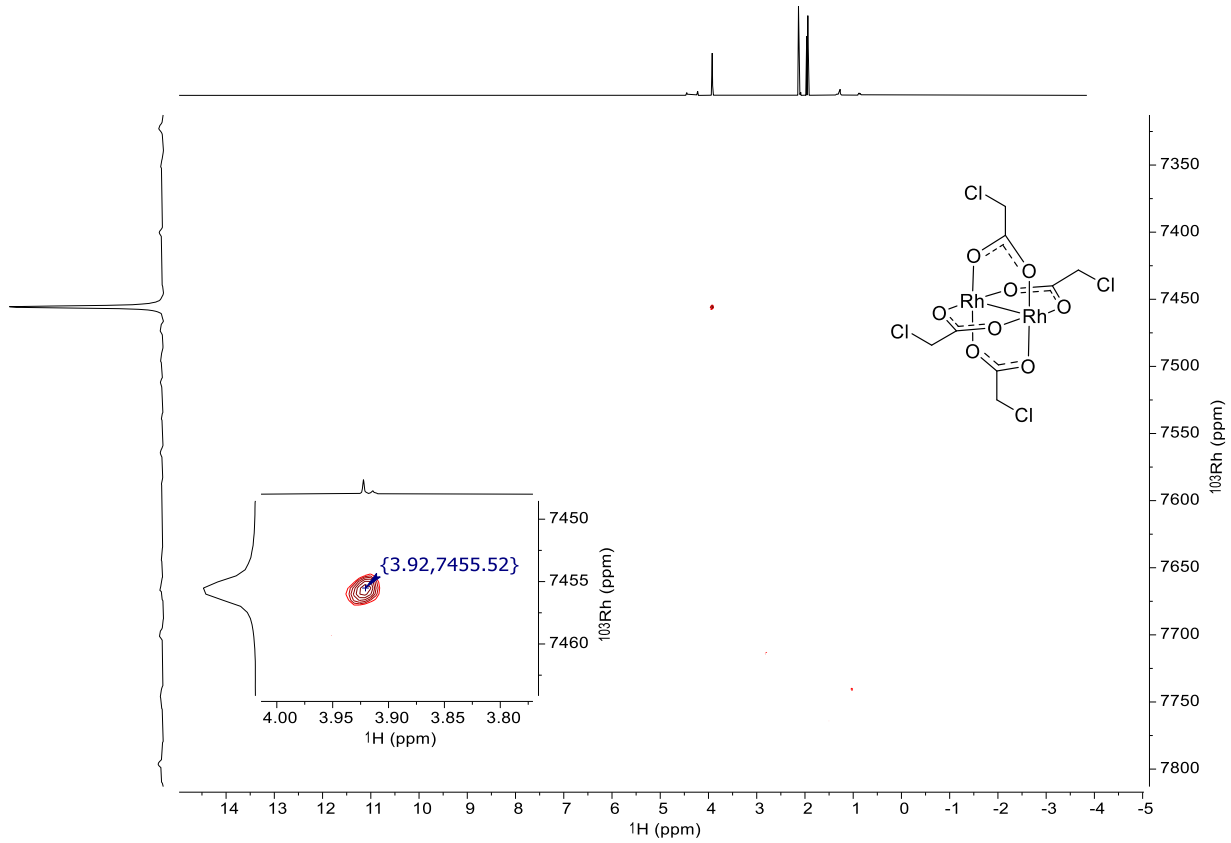

Rh_2(triphenylacetate)$_4$ (13): ^{1}H-NMR (500 MHz, [D_8]-THF)

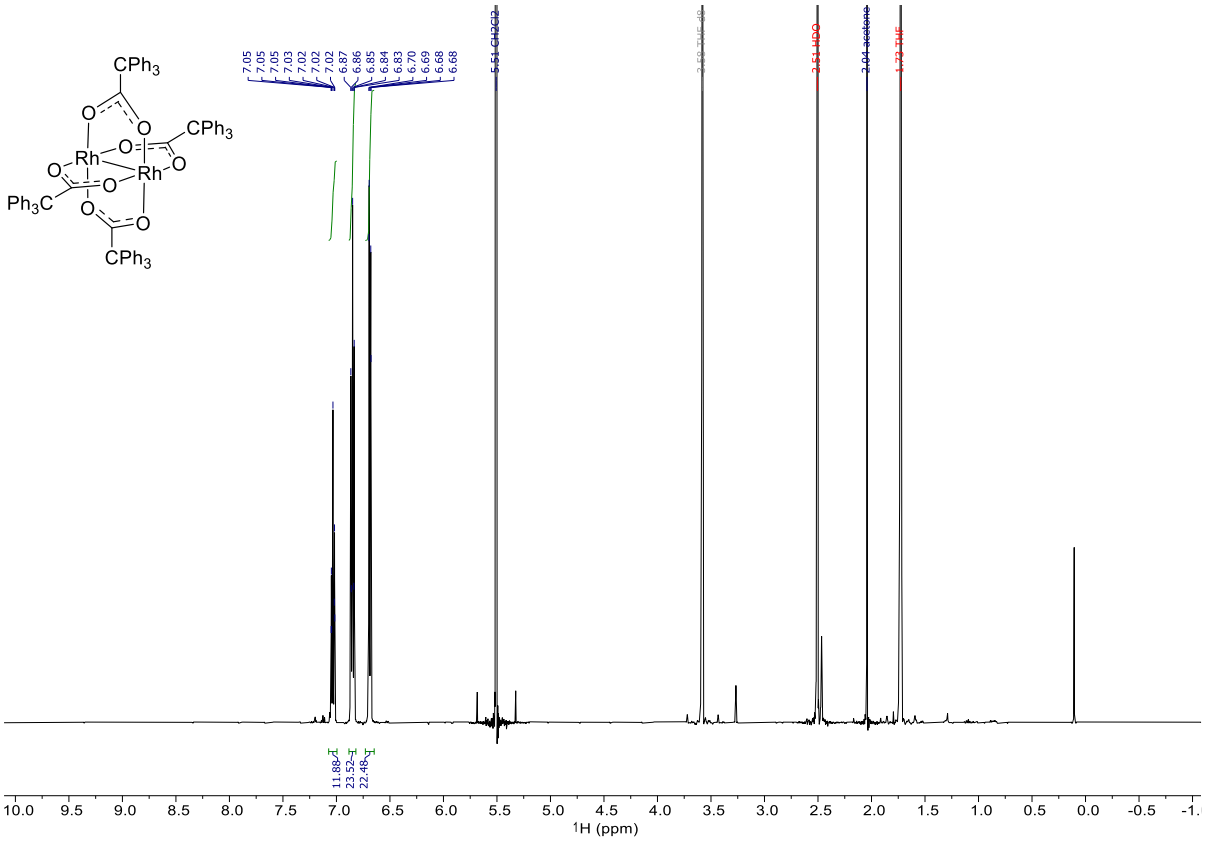

Rh_2(triphenylacetate)$_4$ (13): H(C)Rh ([D_8]-THF)

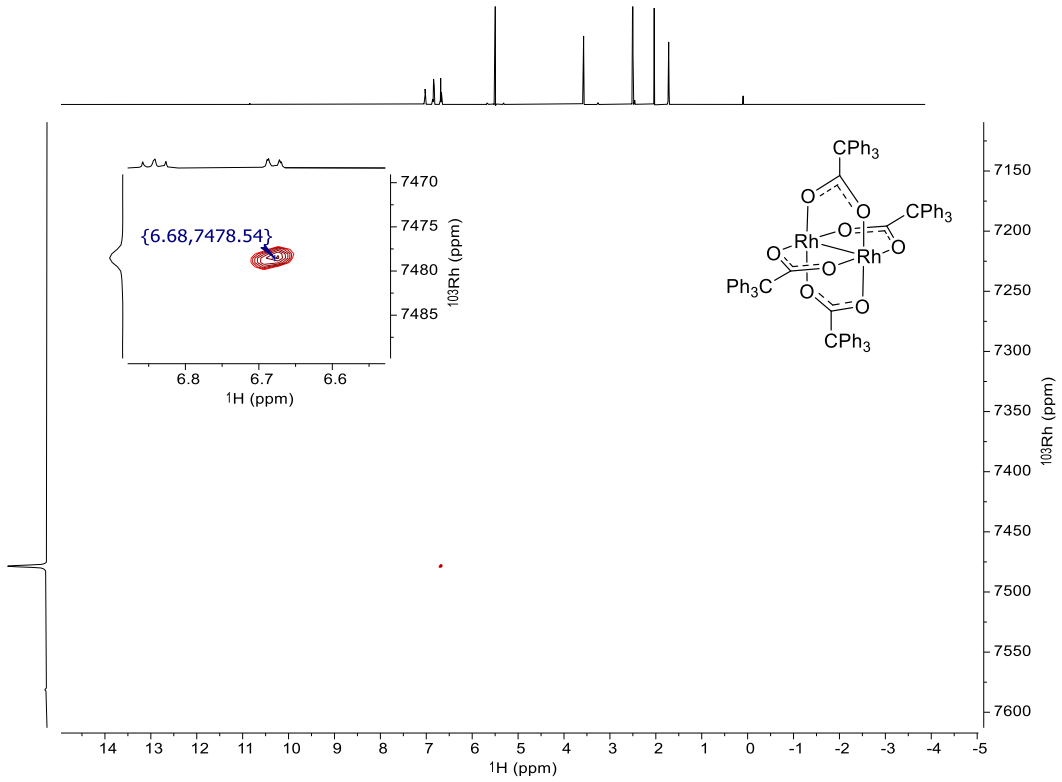

$Rh_2(esp)_2$ (14): ^{1}H-NMR (500 MHz, CD_3CN)

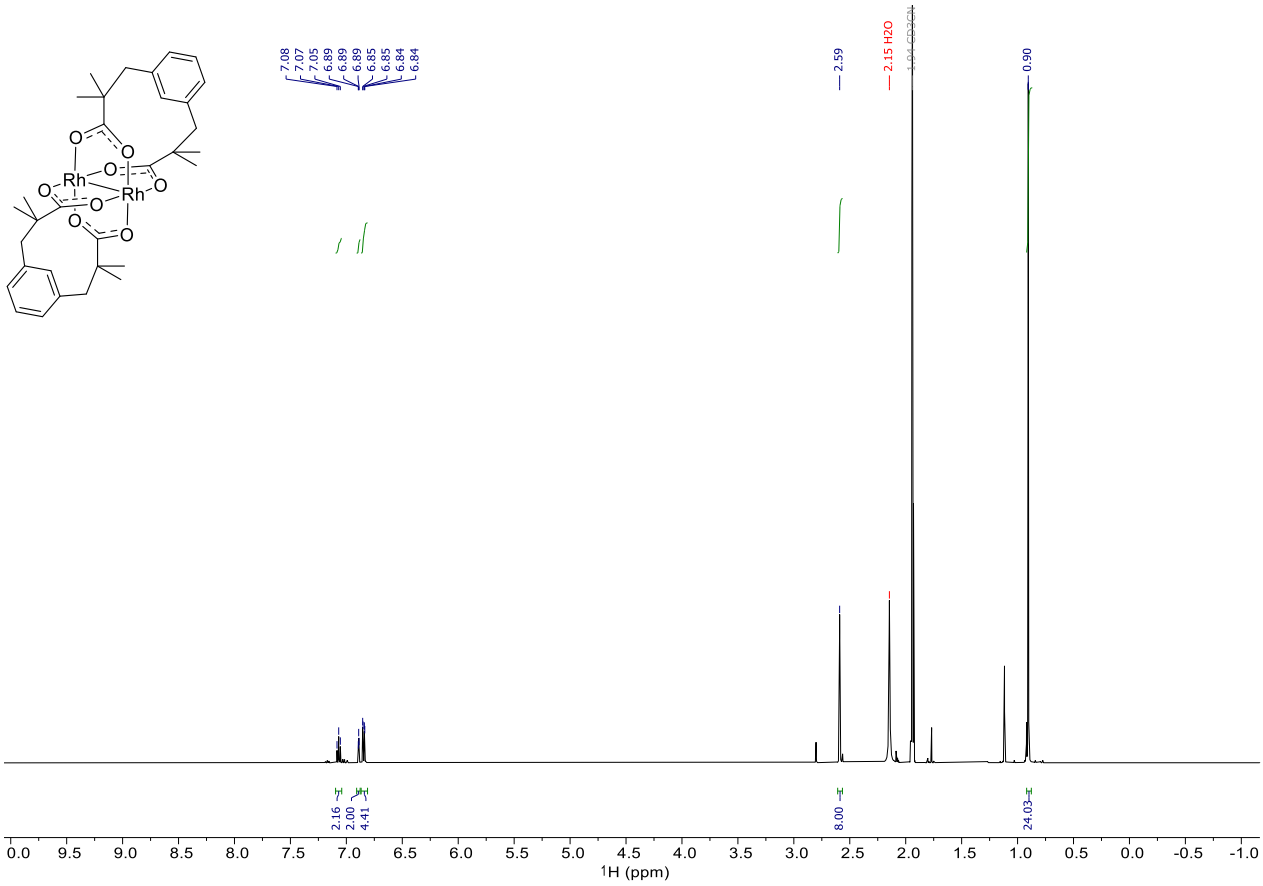

$Rh_2(esp)_2$ (14): H(C)Rh (CD_3CN)

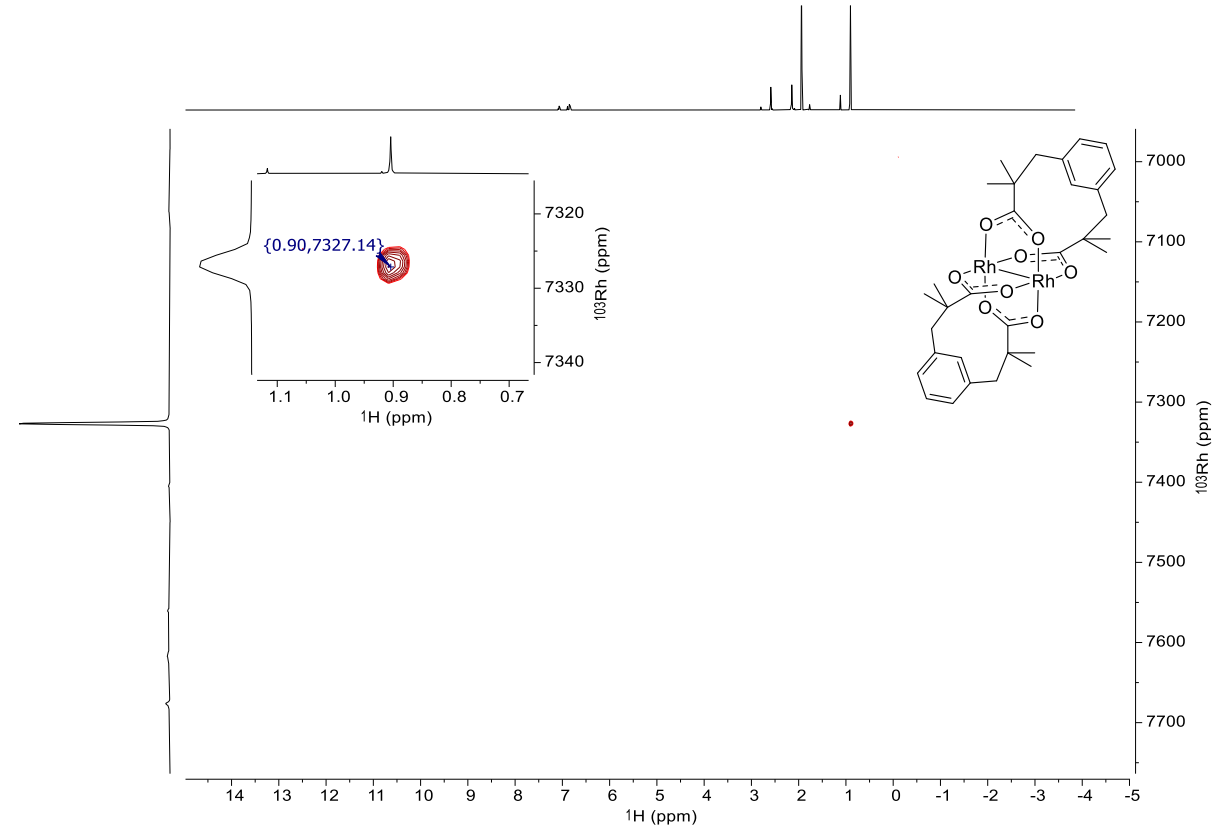

Rh_2(*S*-PTTL)$_4$ (15): ^{1}H-NMR (500 MHz, CD_3CN)

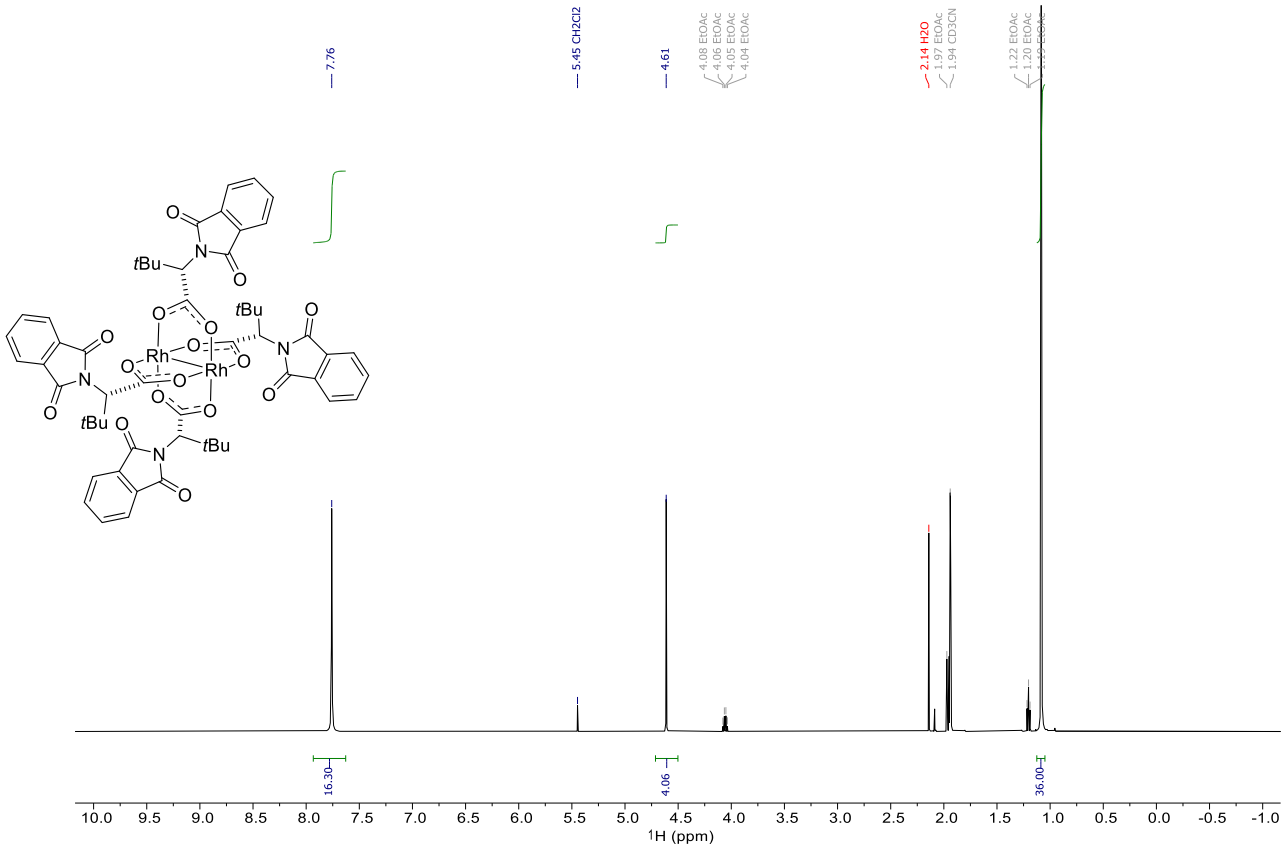

Rh_2(*S*-PTTL)$_4$ (15): H(C)Rh (CD_3CN)

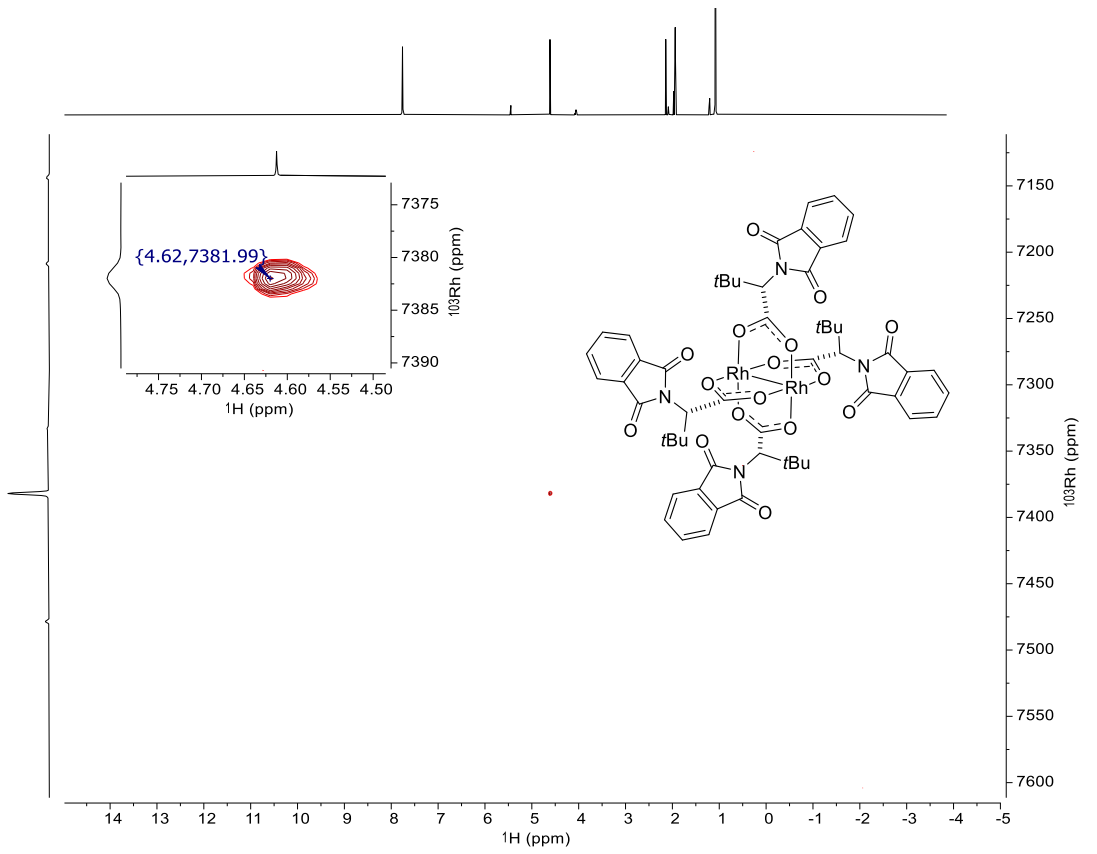

Rh_2(ACAM)(OPiv)$_3$ (16): ^{1}H-NMR (600 MHz, CD_3CN)

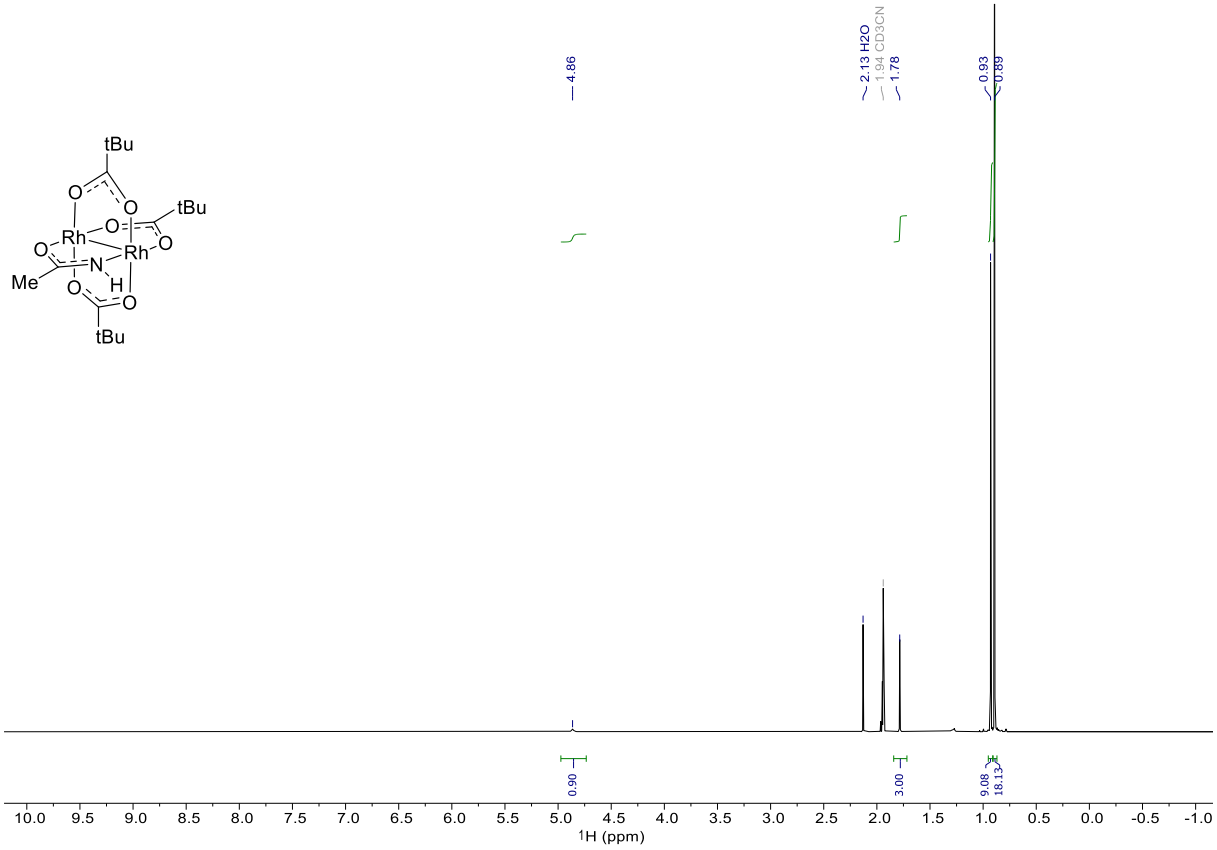

Rh_2(ACAM)(OPiv)$_3$ (16): $^{13}C\{^1H\}$-NMR (151 MHz, CD_3CN)

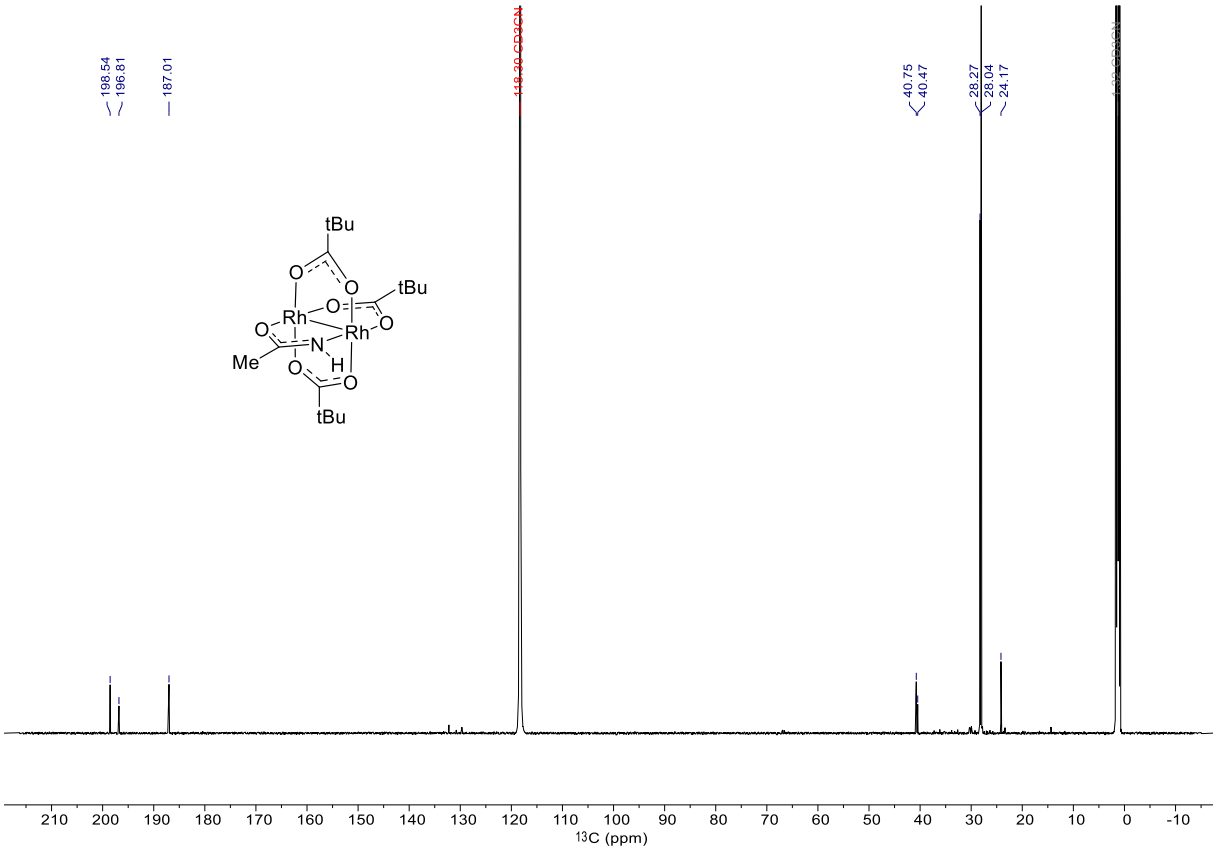

Rh_2(ACAM)(OPiv)$_3$ (16): ^{1}H-^{15}N-HMBC (CD_3CN)

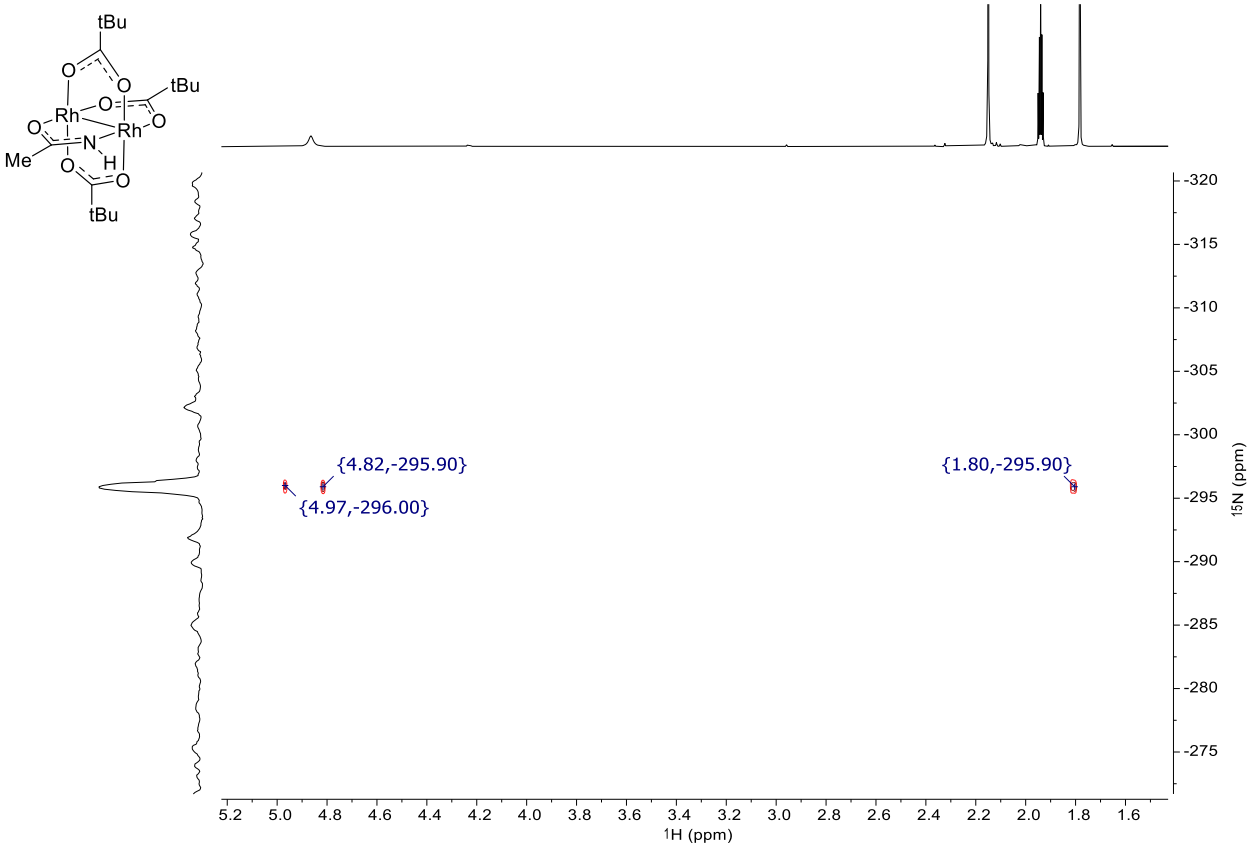

Rh_2(ACAM)(OPiv)$_3$ (16): H(C)Rh (CD_3CN)

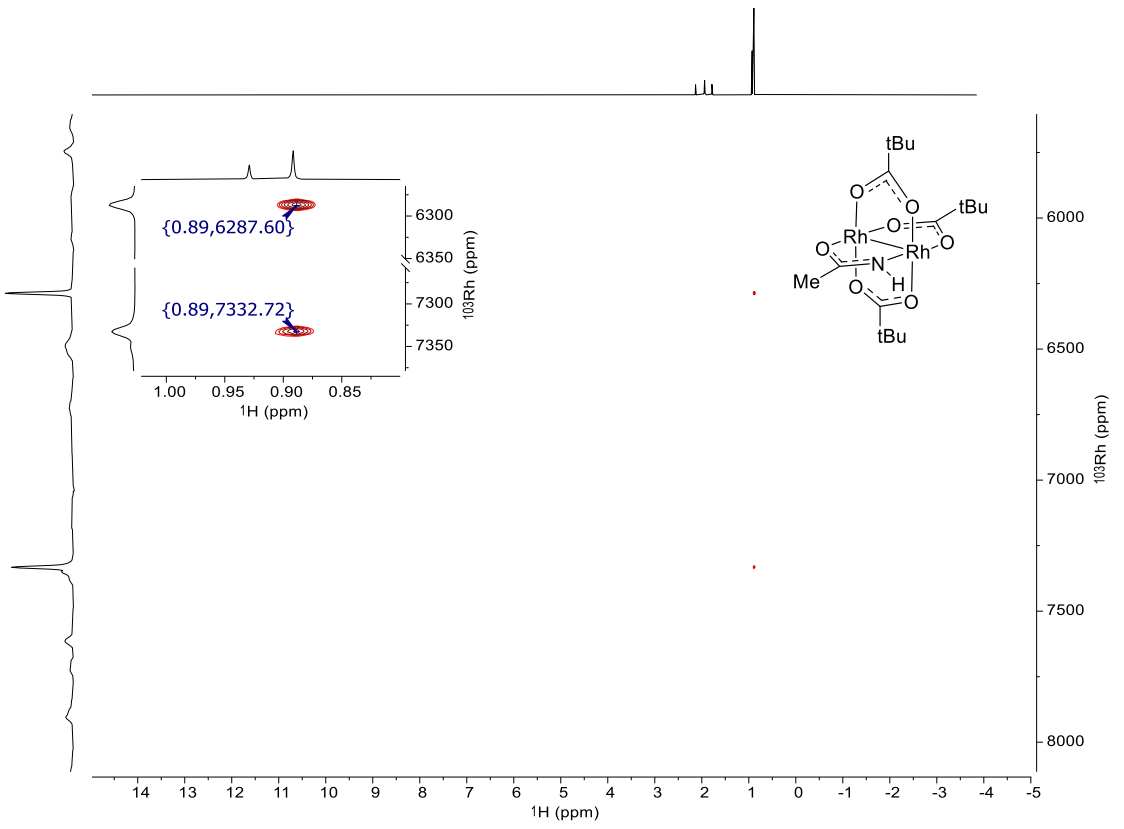

$Rh_2(mhp)_4$ (17): H(C)Rh (CD_2Cl_2/CD_3CN, 50:50 *v/v*)

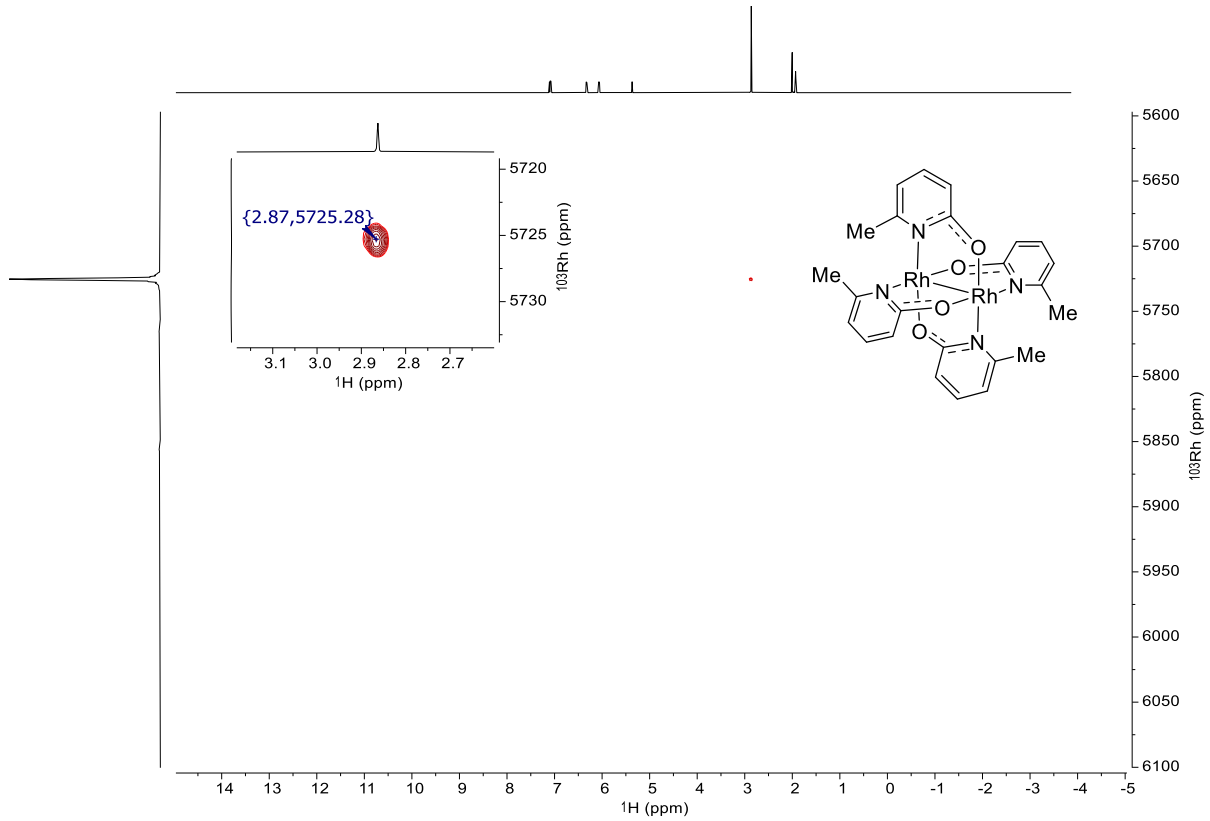

$Rh_2(mhp)_4$ (17): ^{1}H-^{103}Rh HMBC (CD_2Cl_2/CD_3CN, 50:50 *v/v*)

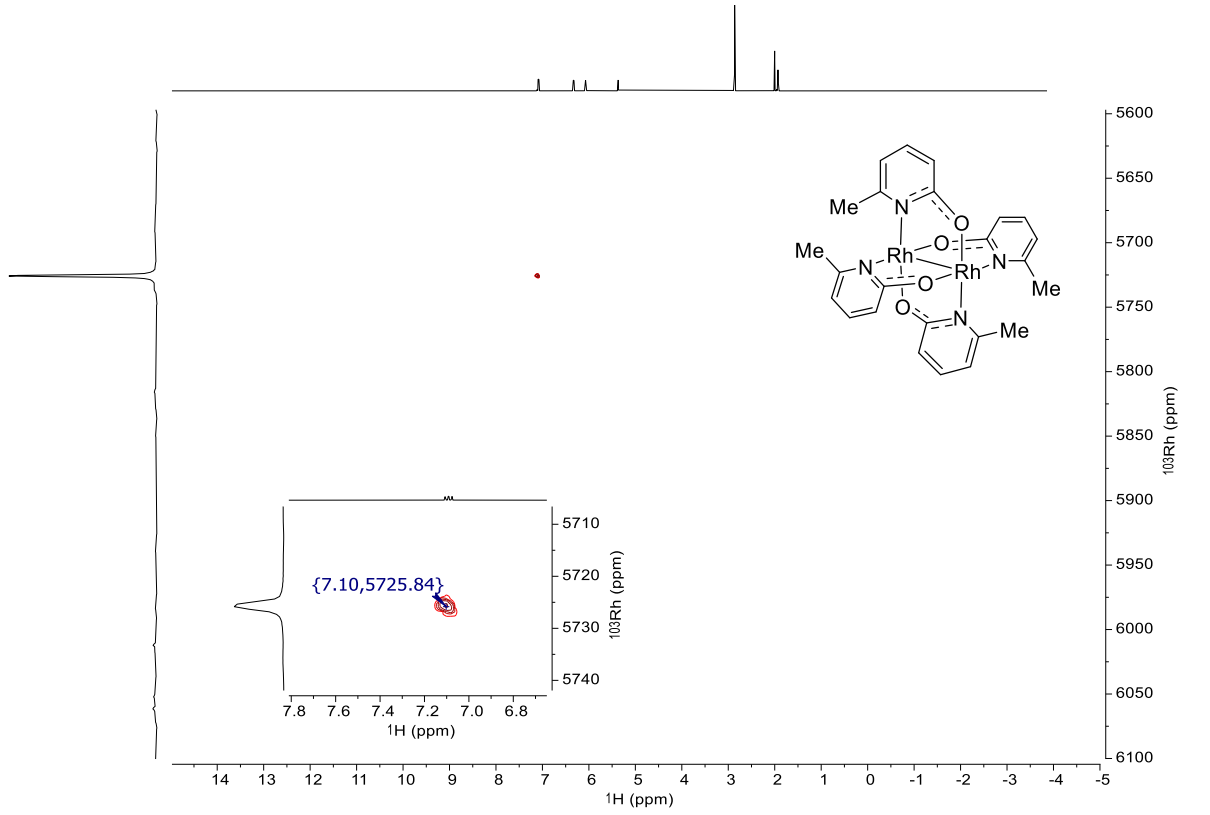

Rh_2(*S*-BNAZ)$_4$ (18): ^{1}H-NMR (400 MHz, CD_3CN)

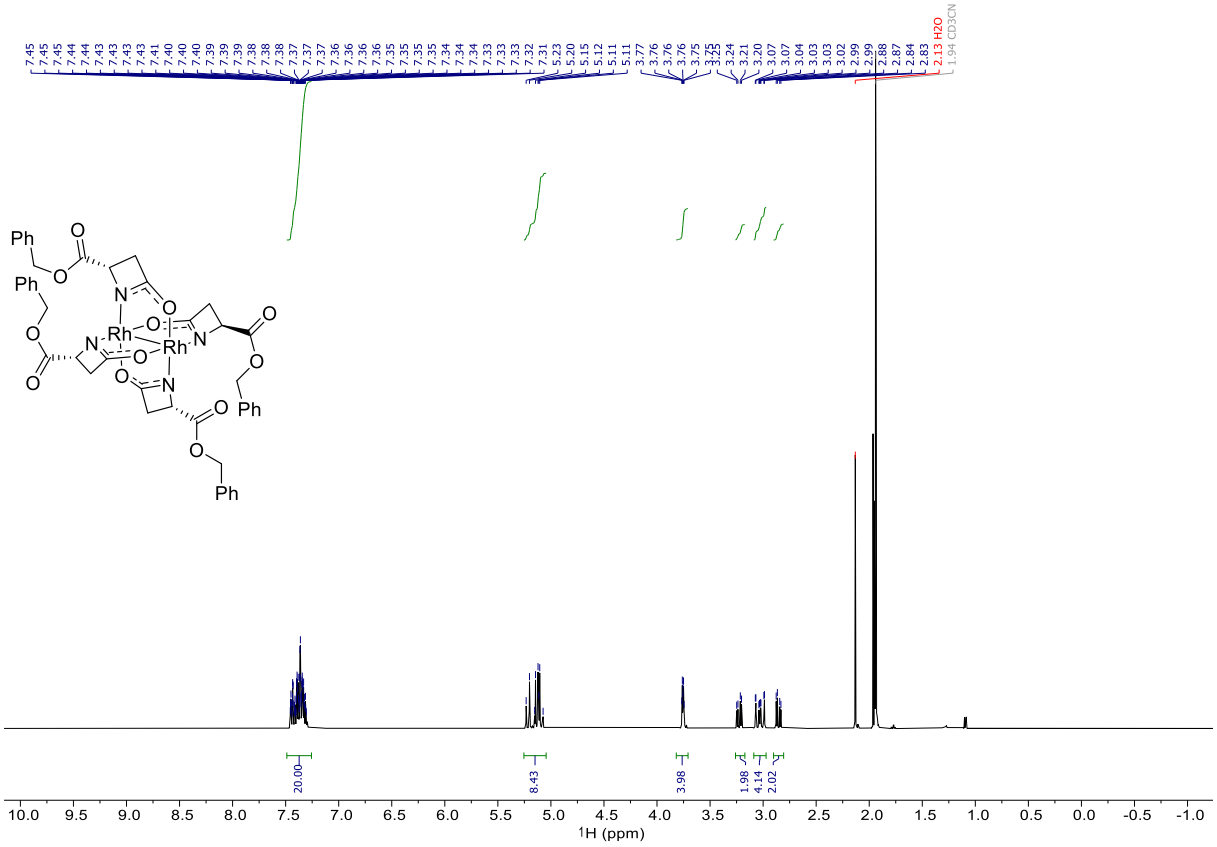

Rh_2(*S*-BNAZ)$_4$ (18): ^{13}C{^{1}H}-NMR (101 MHz, CD_3CN)

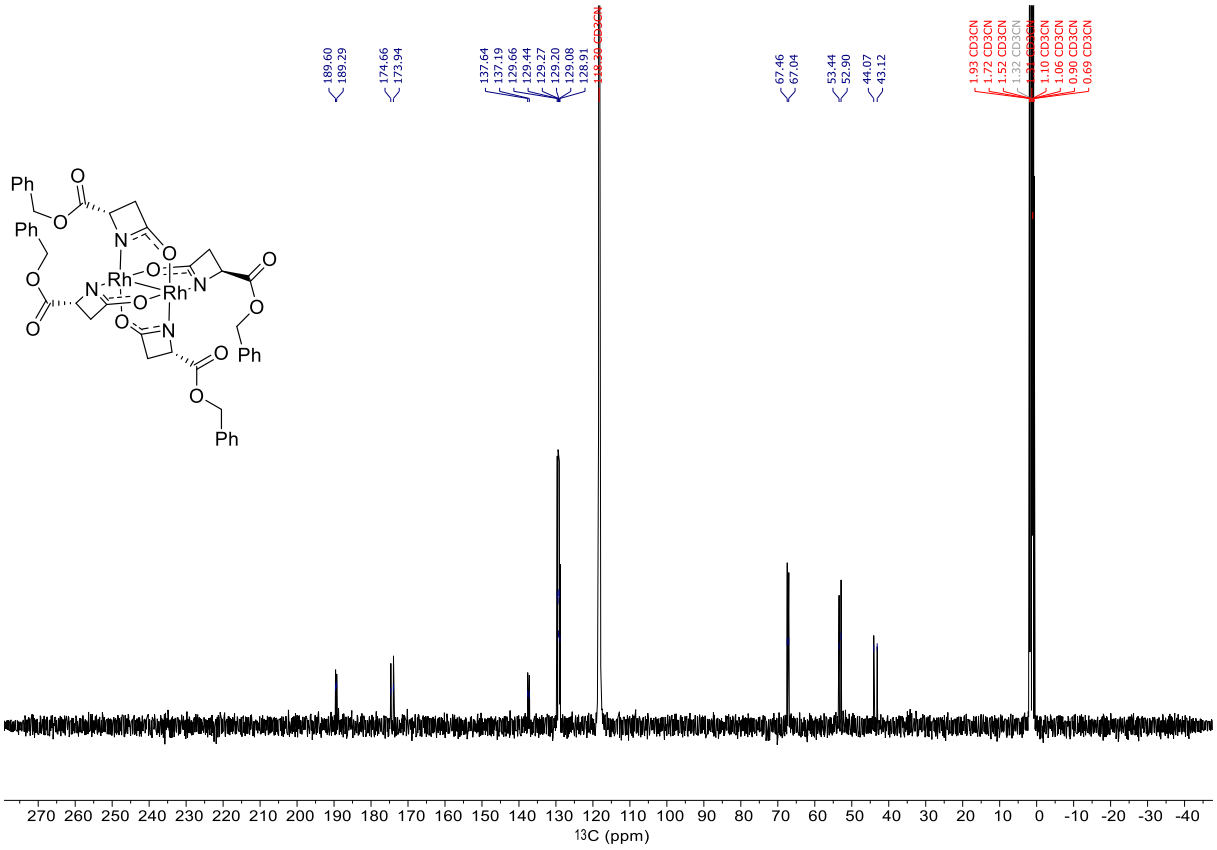

Rh_2(*S*-BNAZ)$_4$ (18): ^{1}H-^{103}Rh-HMBC (CD_3CN)

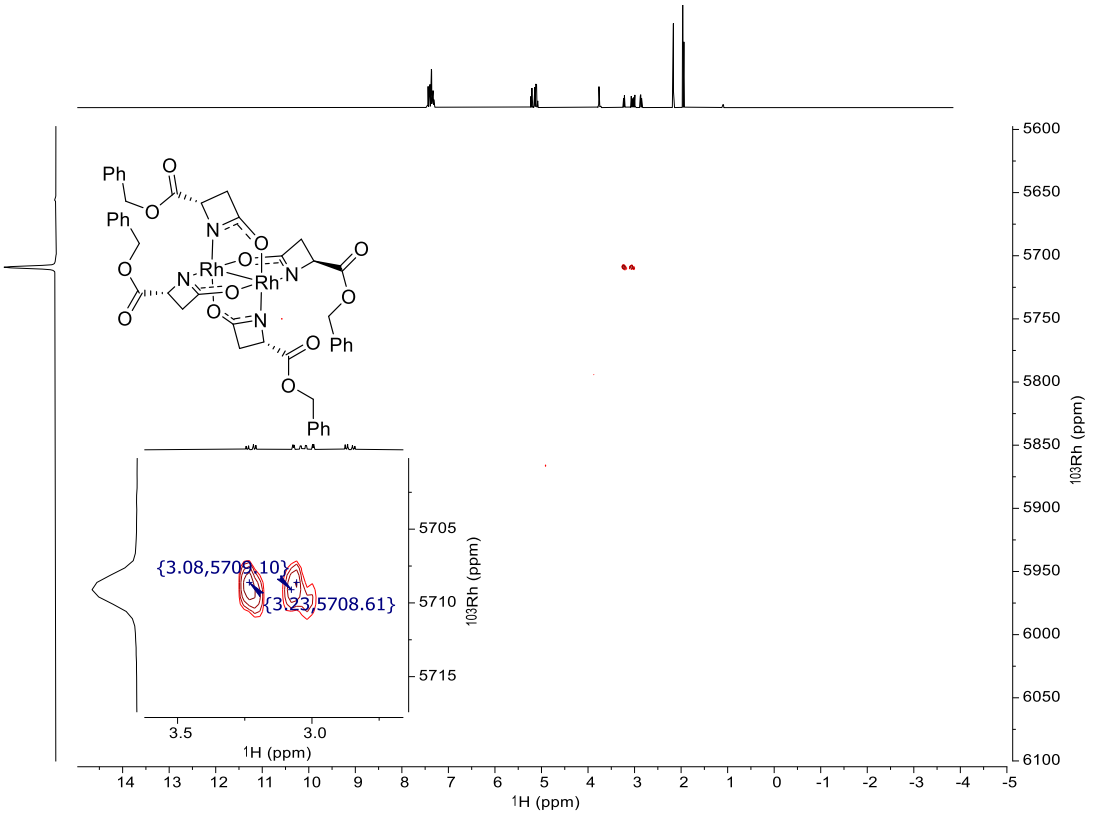

[BiRh(OTfa)$_4$]·EtOAc (19): ^{1}H-NMR (500 MHz, CD_3CN)

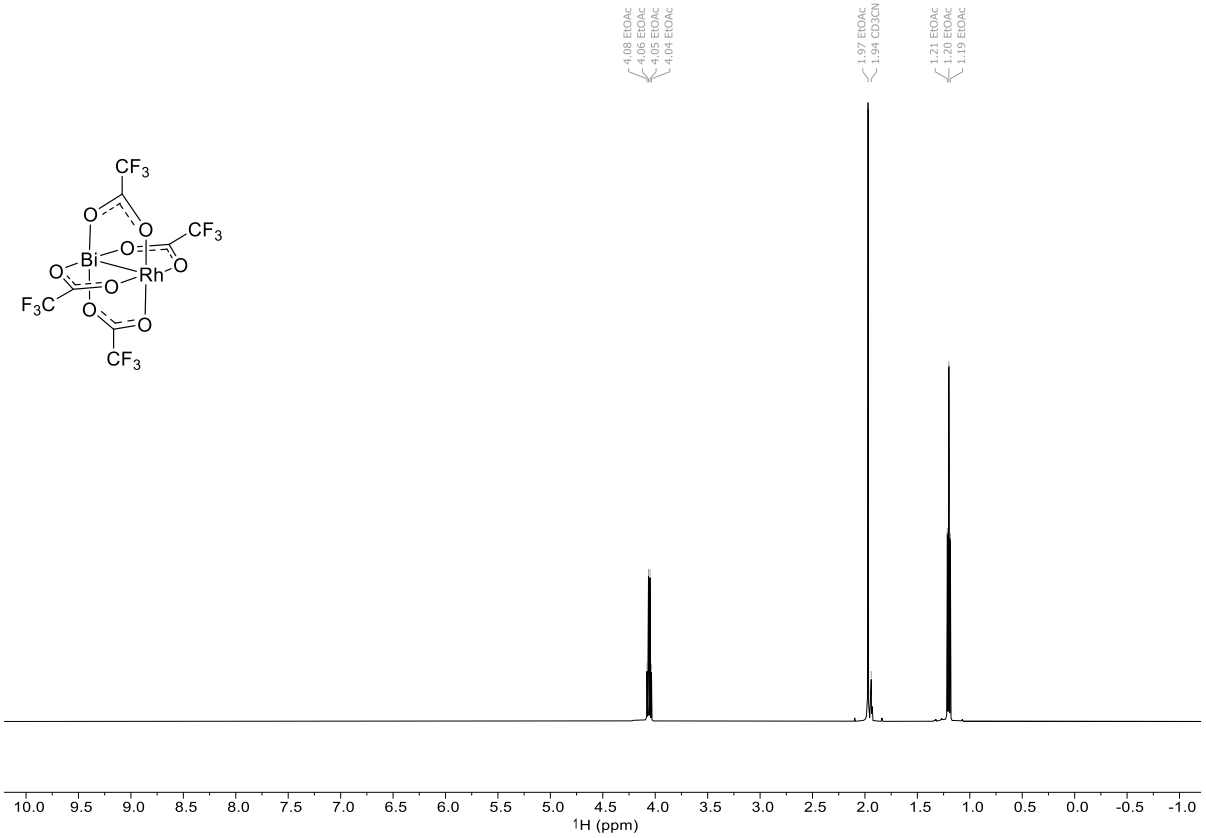

[BiRh(OTfa)$_4$]·EtOAc (19): ^{19}F-NMR (470 MHz, CD_3CN)

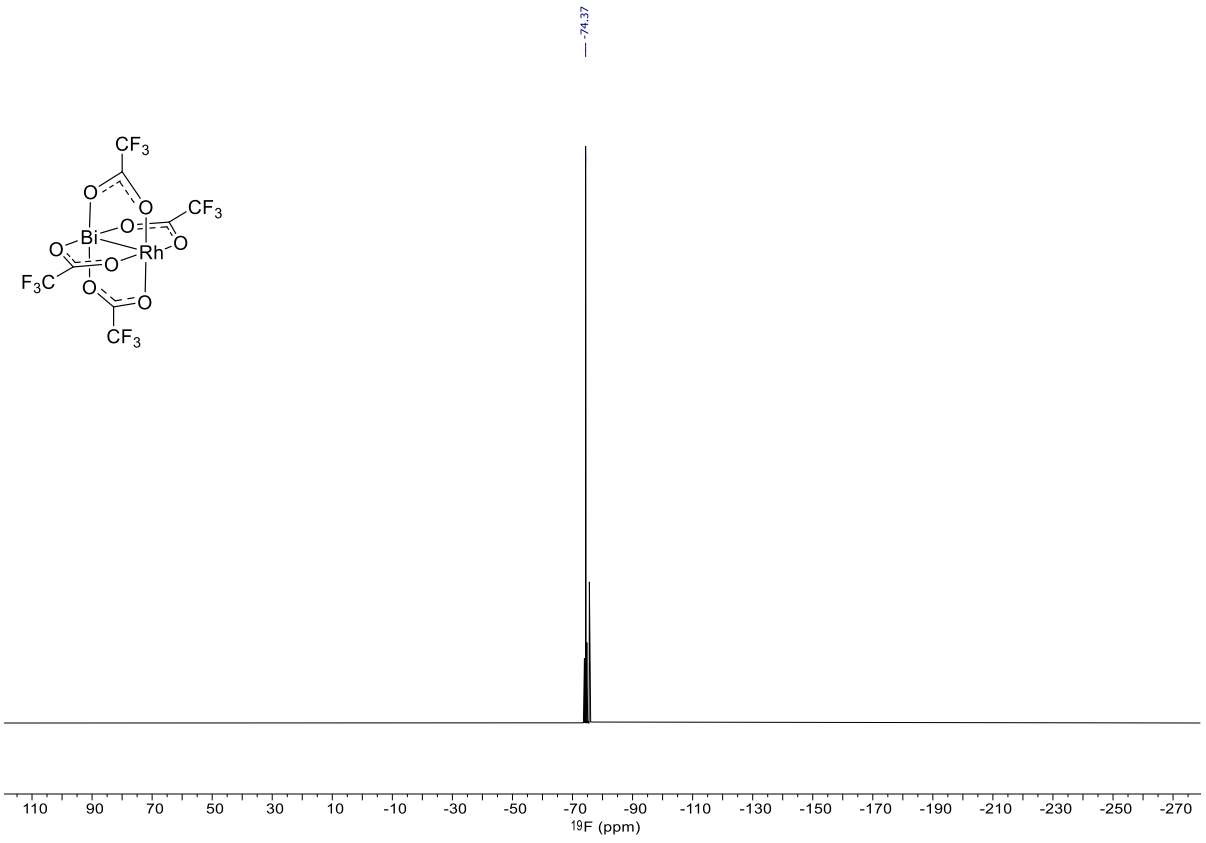

[BiRh(OTfa)$_4$]·EtOAc (19): ^{103}Rh-NMR (15.9 MHz, CD_3CN)

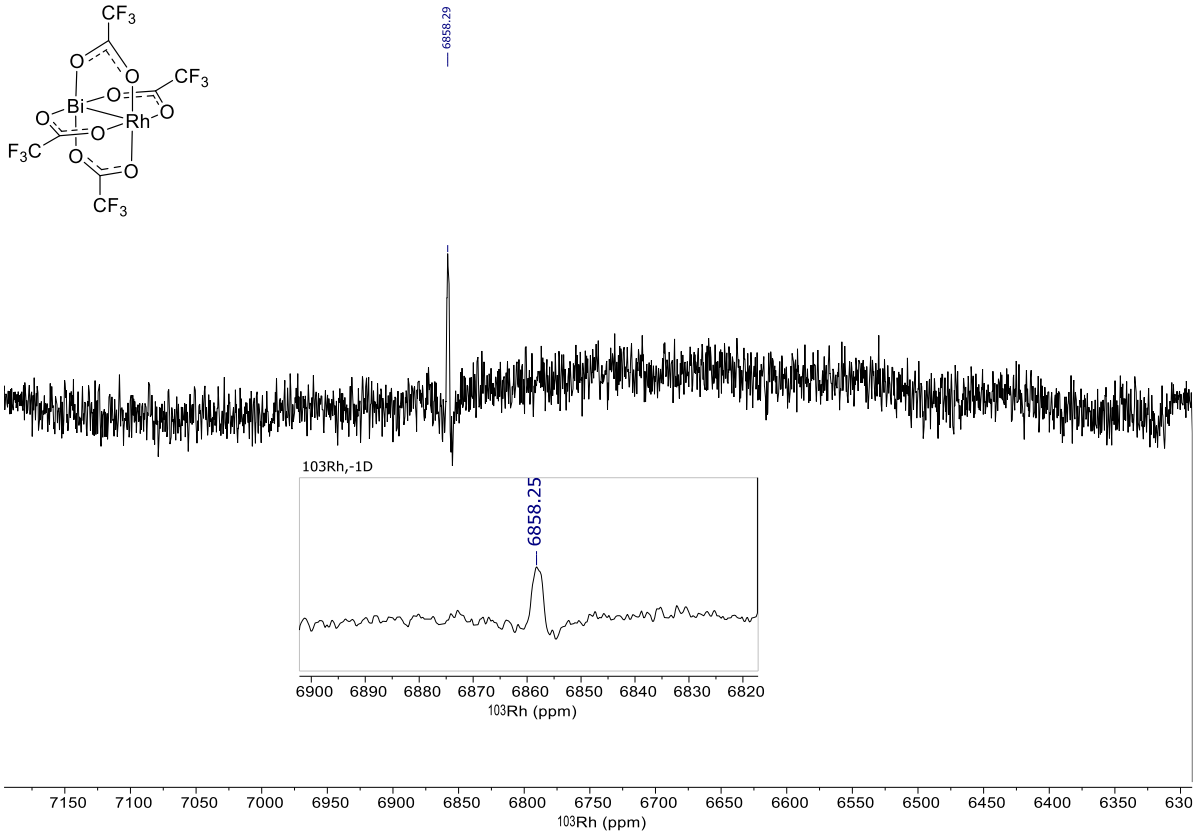

BiRh(OAc)$_4$ (20): ^{1}H-NMR (400 MHz, CD$_3$CN)

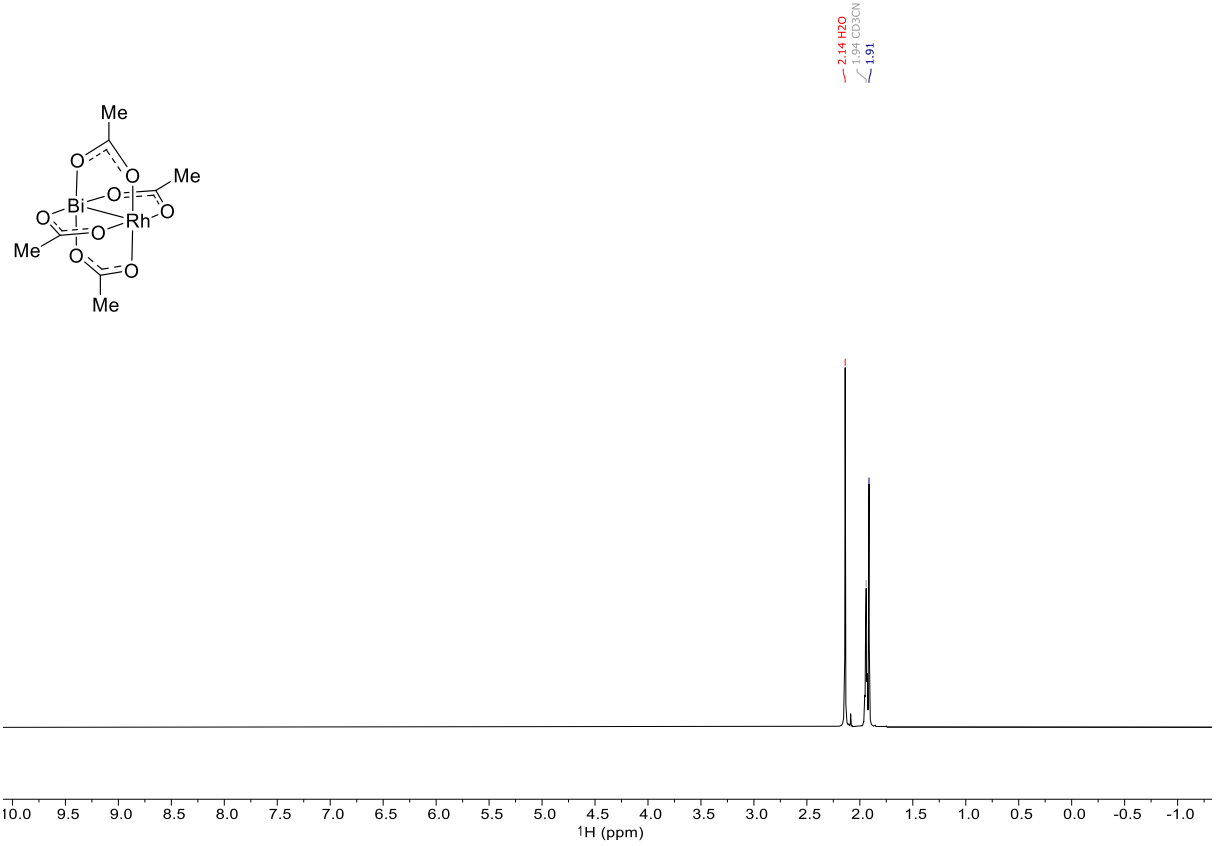

BiRh(OAc)$_4$ (20): ^{13}C{^{1}H}-NMR (151 MHz, CD$_3$CN)

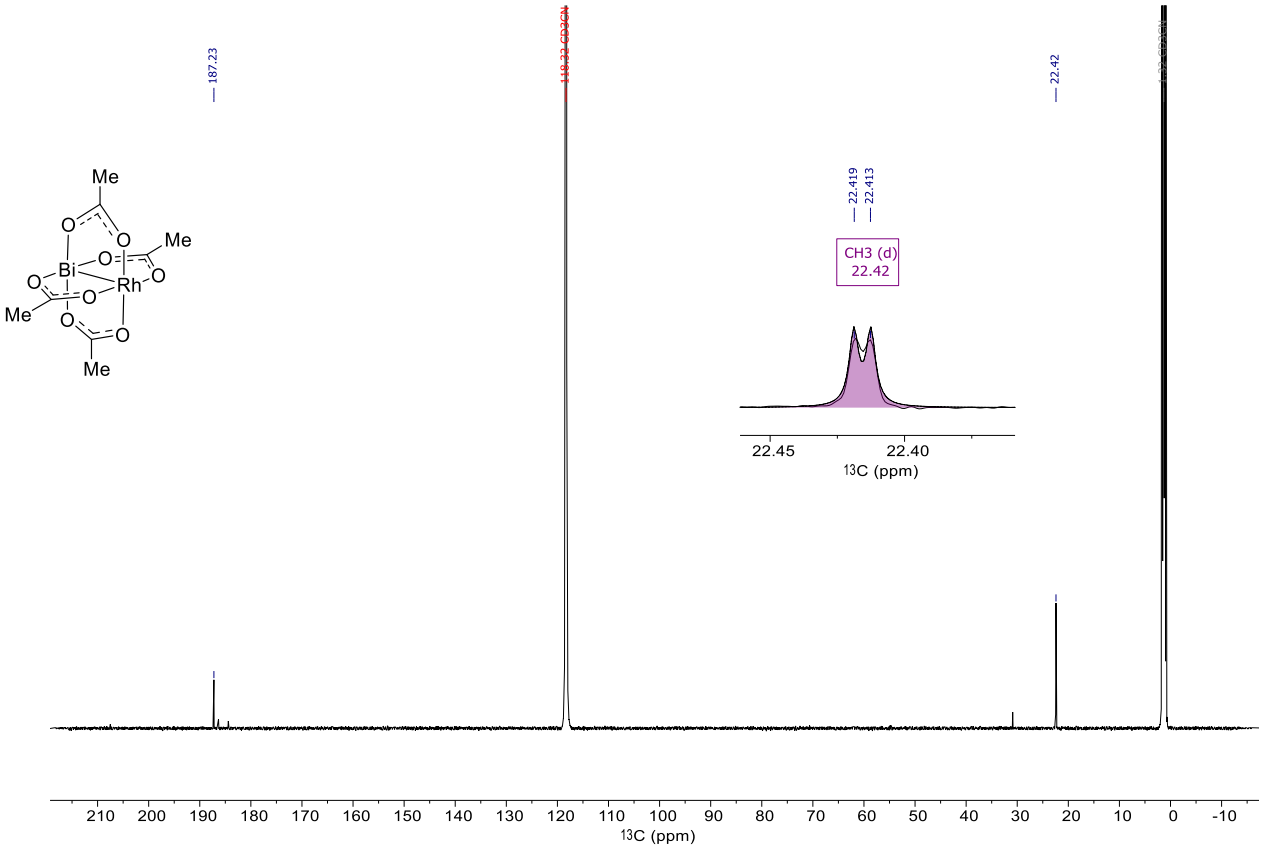

BiRh(OAc)$_4$ (20): H(C)Rh (CD_3CN)

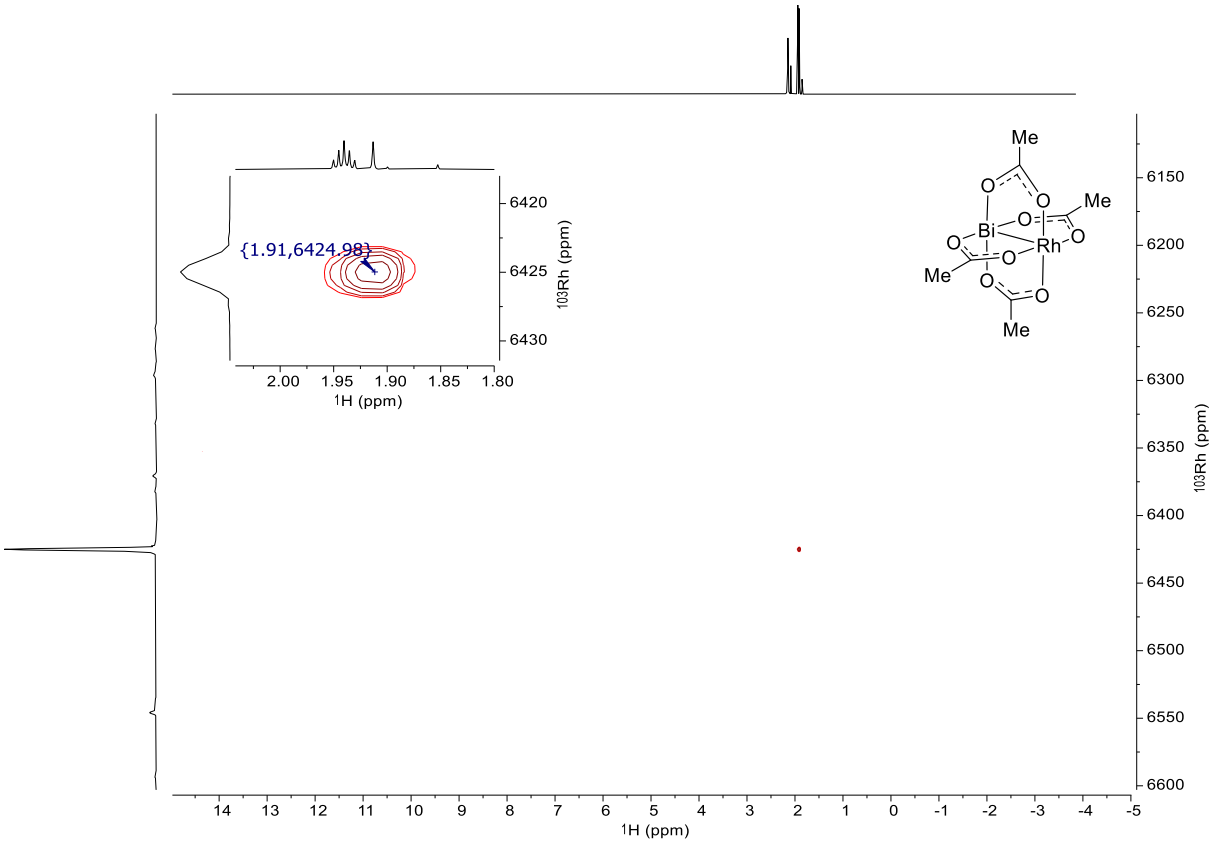

BiRh(OAc-2-^{13}C) (21-2-^{13}C): ^{1}H-NMR (500 MHz, CD_3CN)

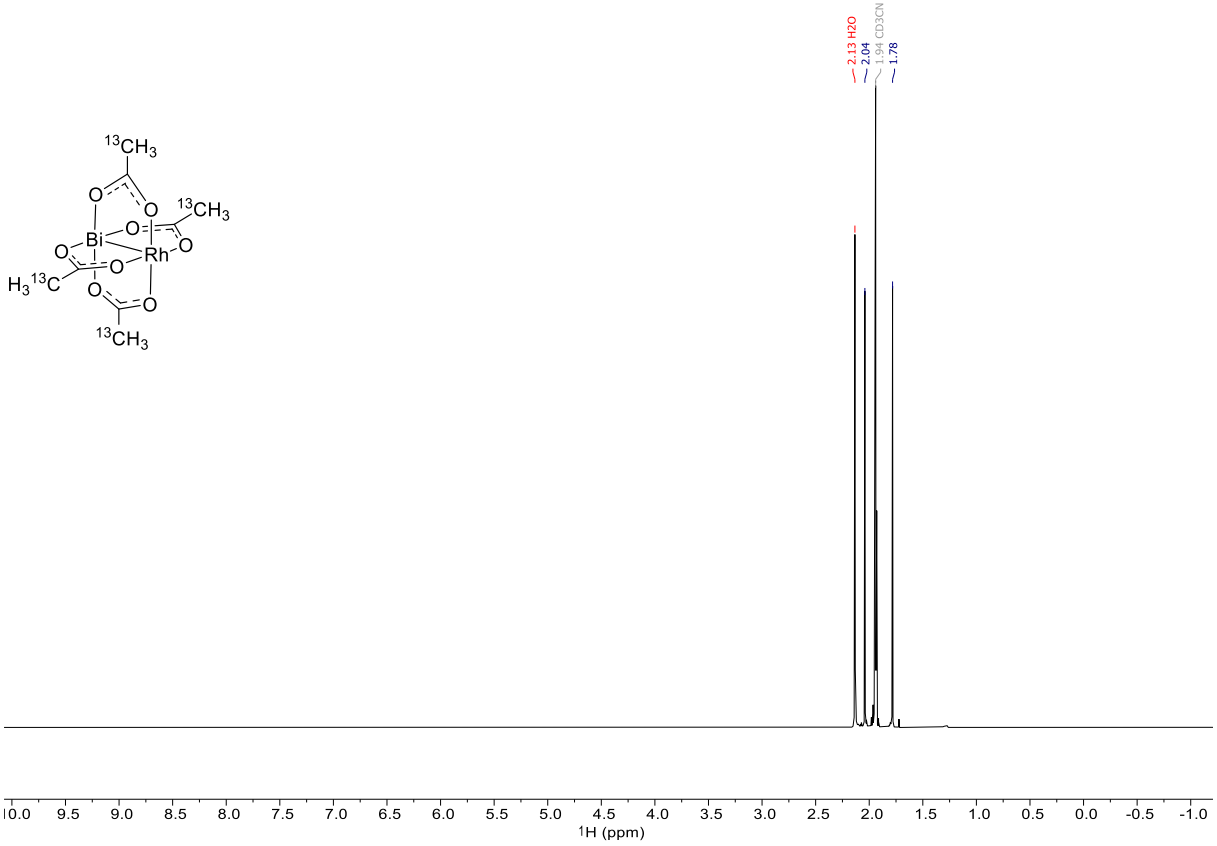

BiRh(OAc-2-^{13}C) (21-2-^{13}C): ^{13}C{^{1}H}-NMR (101 MHz, CD_3CN)

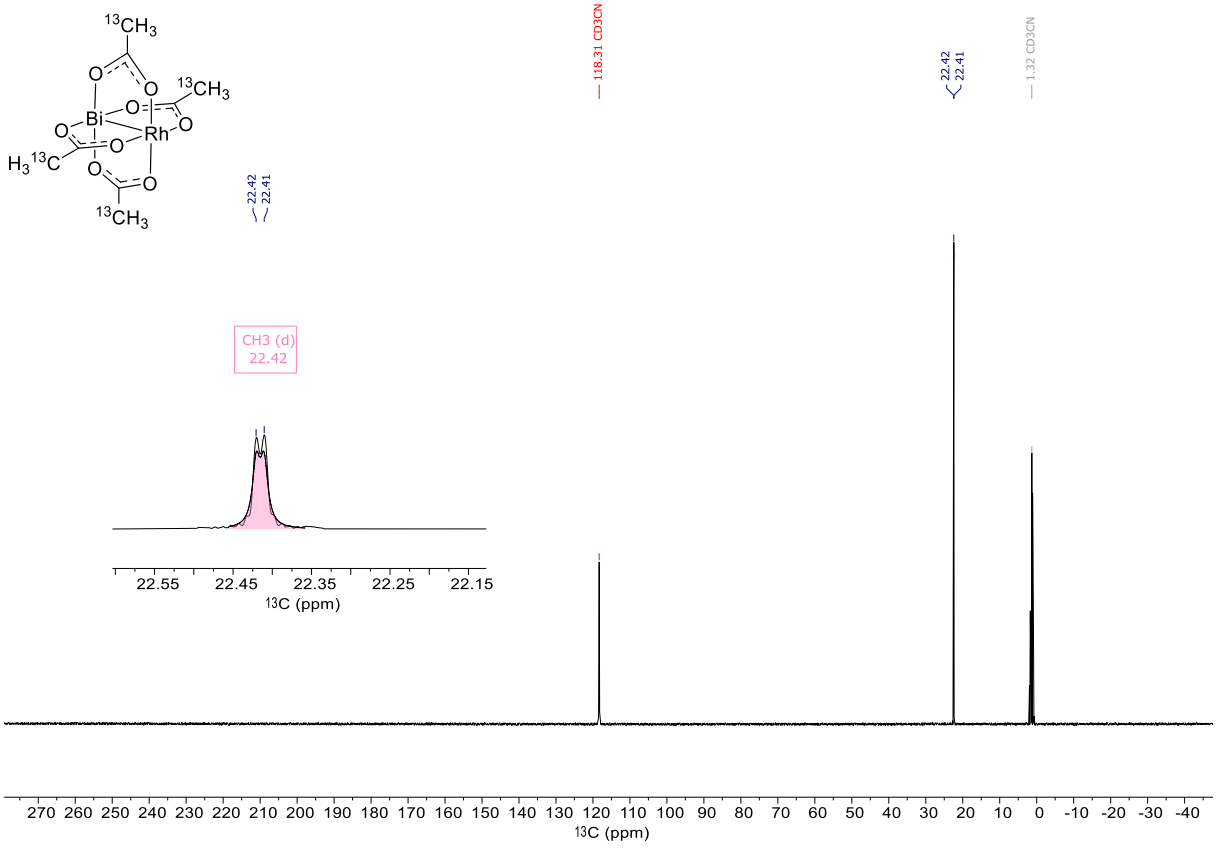

$BiRh(HCO_2)_4$ (21):^{1}H-NMR (400 MHz, CD_3CN)

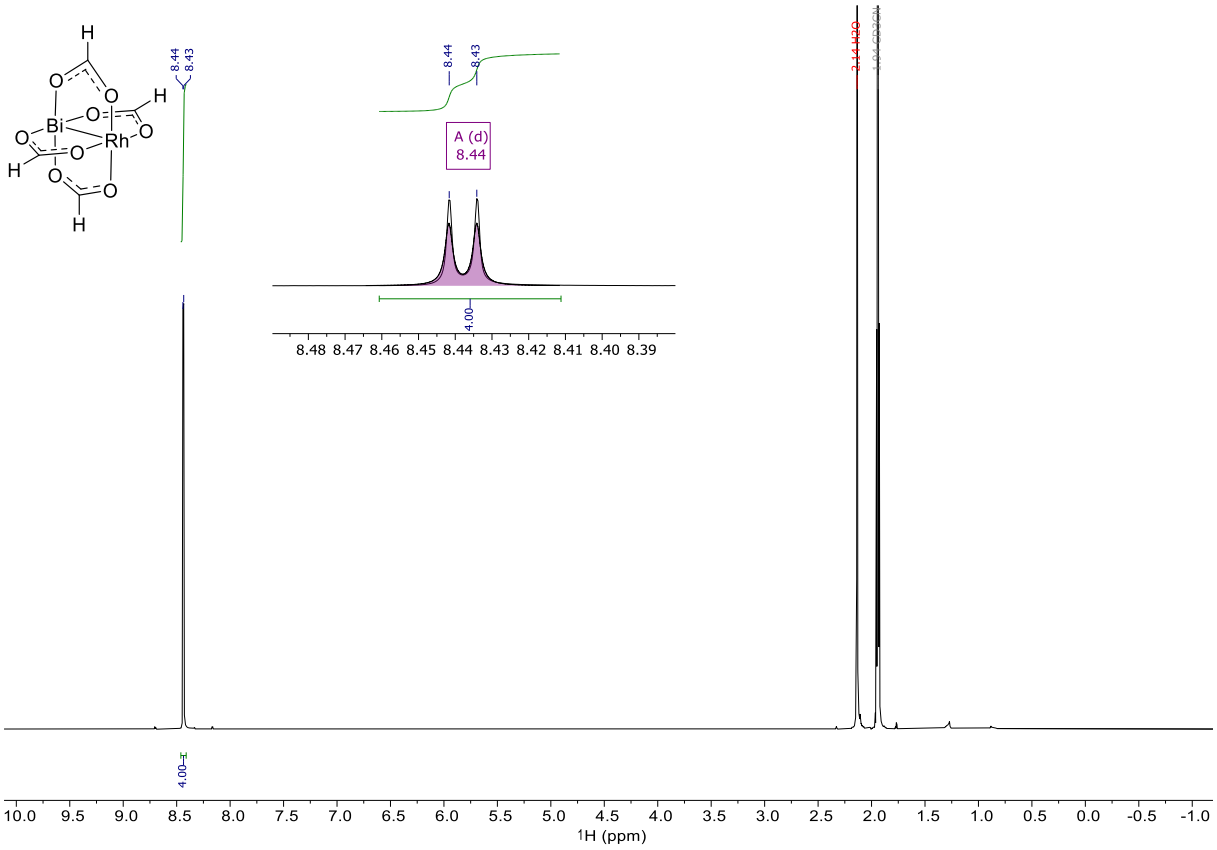

$BiRh(HCO_2)_4$ (21): $^{13}C\{^1H\}$-NMR (101 MHz, CD_3CN)

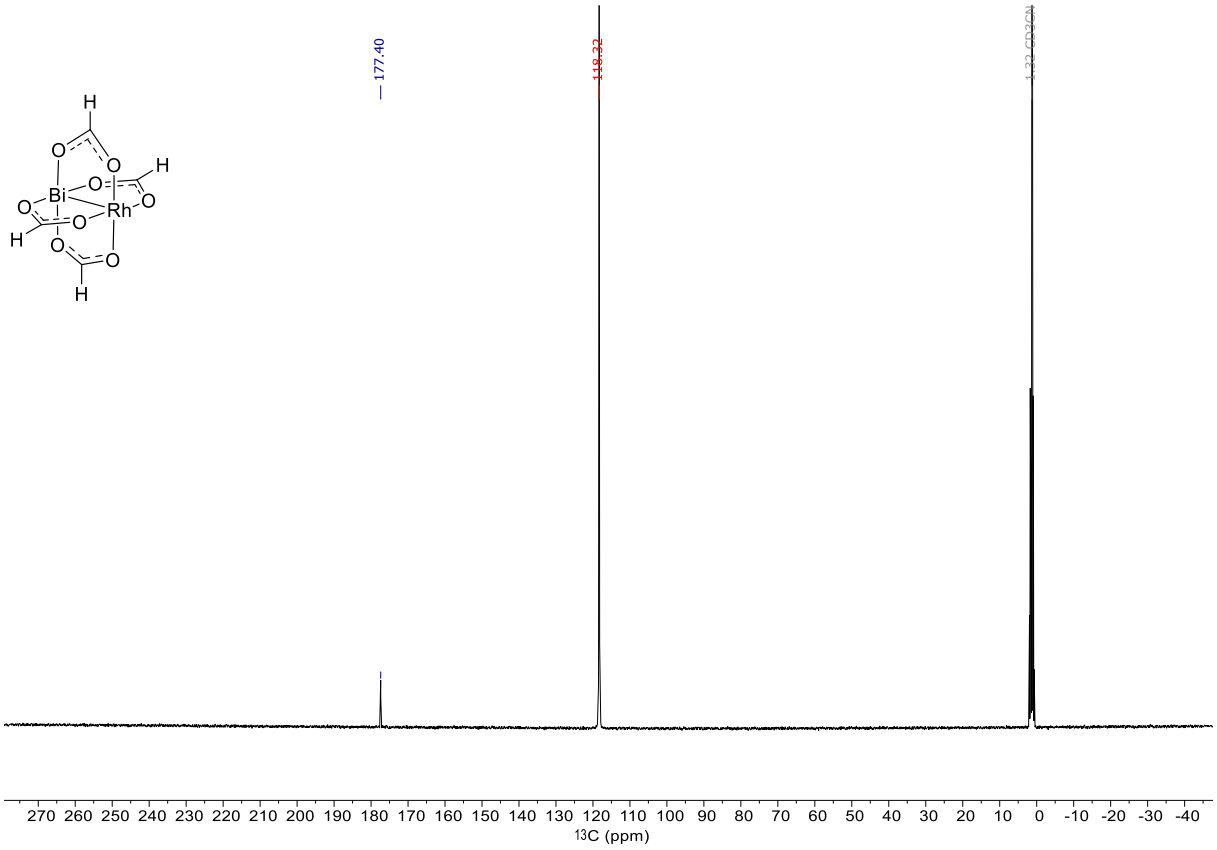

$BiRh(HCO_2)_4$ (21): ^1H-^{13}C-*edited*-HSQC (CD_3CN)

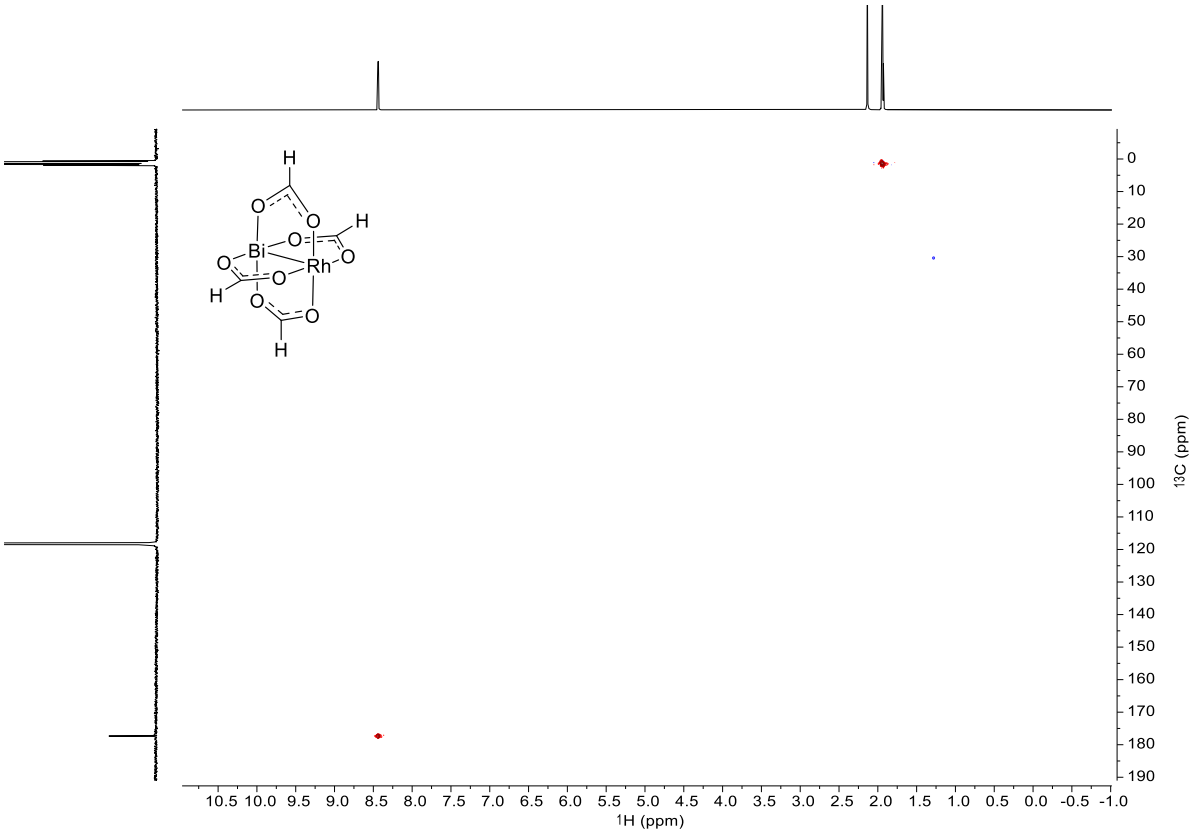

$BiRh(HCO_2)_4$ (21): ^1H-^{103}Rh-HMBC (CD_3CN)

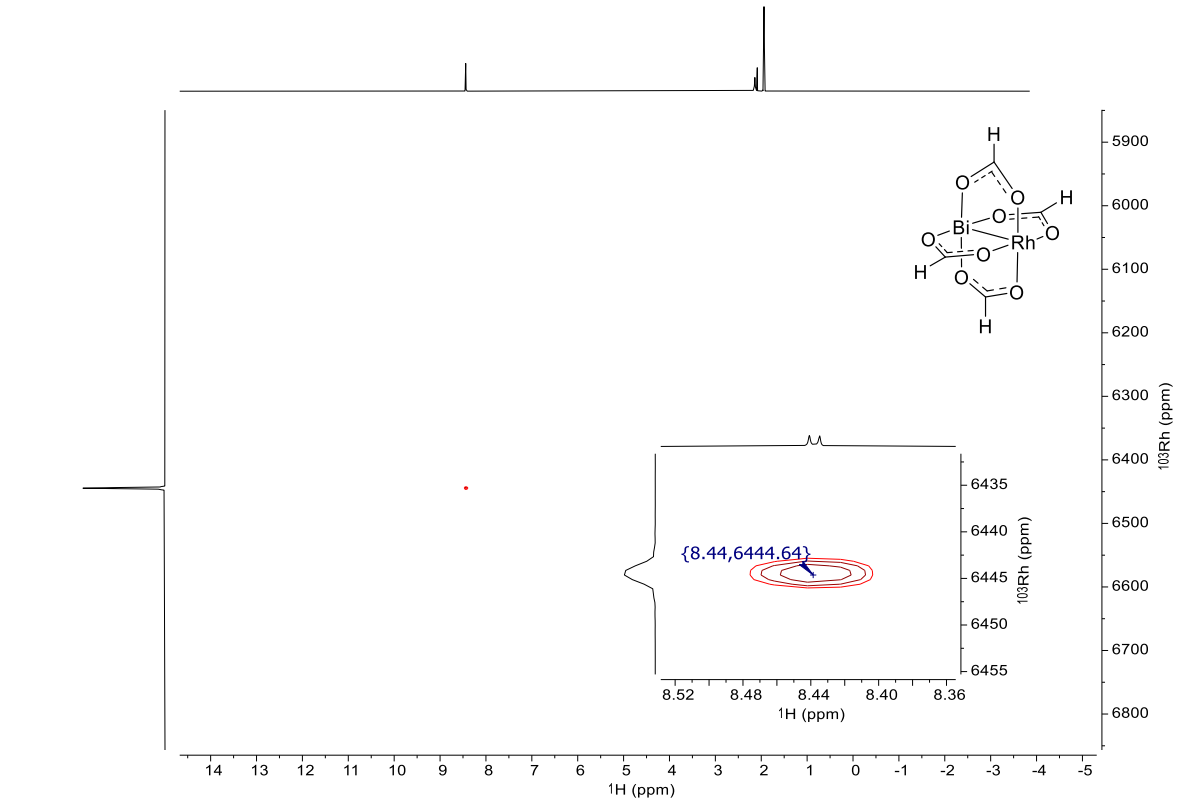

$BiRh(esp)_2$ (22): ^{1}H-NMR (400 MHz, CD_3CN)

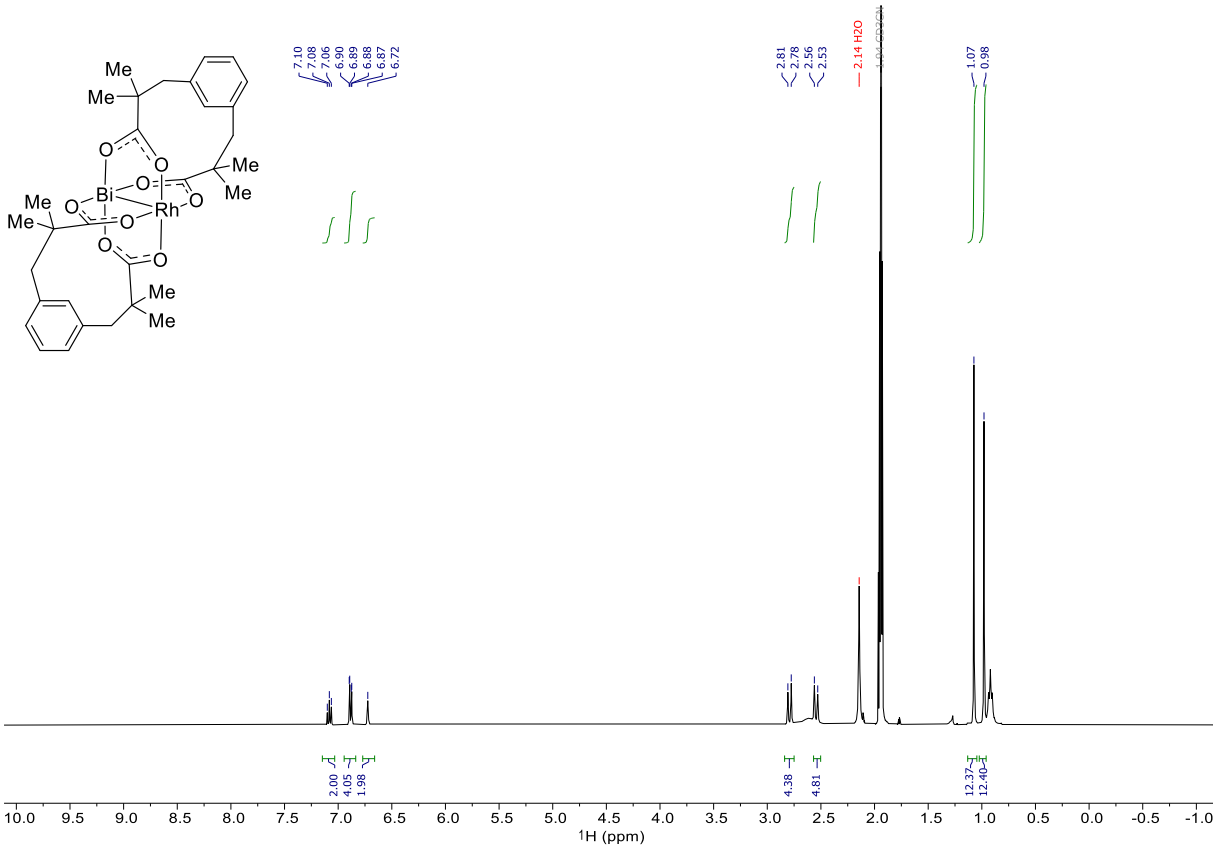

$BiRh(esp)_2$ (22): ^{1}H-NMR (500 MHz, $[D_8]$-THF)

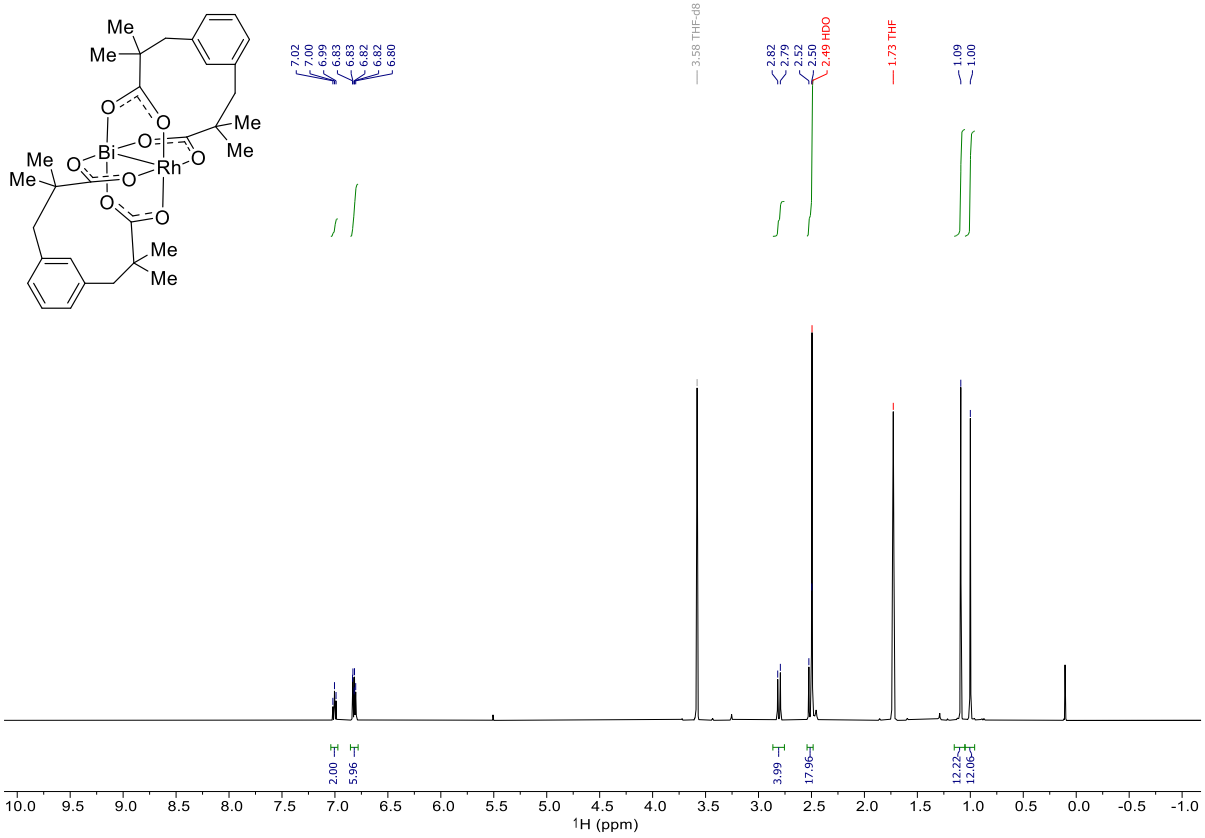

BiRh(esp)$_2$ (22): H(C)Rh ([D$_8$]-THF)

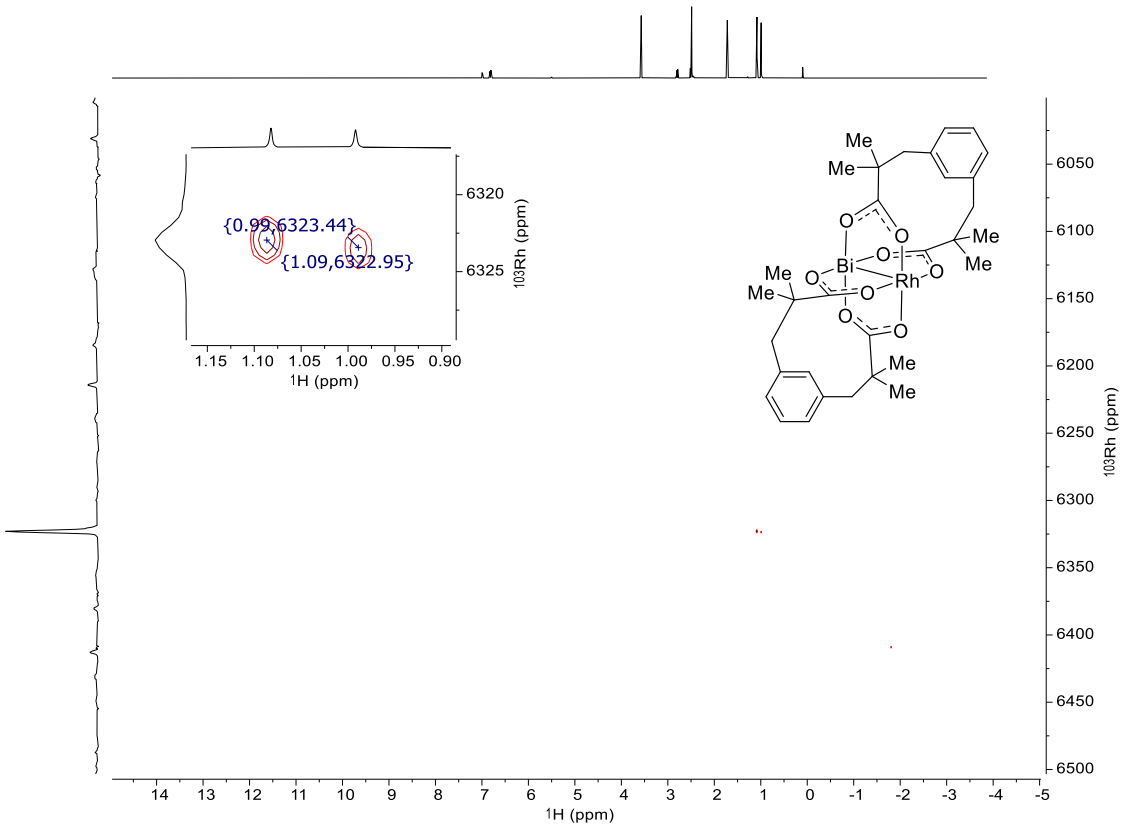

7. References

1. Fulmer, G. R.; Miller, A. J. M.; Sherden, N. H.; Gottlieb, H. E.; Nudelman, A.; Stoltz, B. M.; Bercaw, J. E.; Goldberg, K. I., NMR Chemical Shifts of Trace Impurities: Common Laboratory Solvents, Organics, and Gases in Deuterated Solvents Relevant to the Organometallic Chemist. *Organometallics* **2010,** *29* (9), 2176-2179.
2. Harris, R. K.; Becker, E. D.; Menezes, S. M. C. d.; Granger, P.; Hoffman, R. E.; Zilm, K. W., Further conventions for NMR shielding and chemical shifts (IUPAC Recommendations 2008). *Pure Appl. Chem*. **2008,** *80* (1), 59-84.
3. Collins, L. R.; van Gastel, M.; Neese, F.; Fürstner, A., Enhanced Electrophilicity of Heterobimetallic Bi–Rh Paddlewheel Carbene Complexes: A Combined Experimental, Spectroscopic, and Computational Study. *J. Am. Chem. Soc.* **2018,** *140* (40), 13042-13055.
4. Berry, M.; Garner, C. D.; Hillier, I. H.; Macdowell, A. A.; Clegg, W., Crystal structure and u.v. photoelectron spectra of tetrakis-(6-methyl-2-oxopyridinato)dirhodium. *J. Chem. Soc., Chem. Commun.* **1980,** (11), 494-495.
5. Singha, S.; Buchsteiner, M.; Bistoni, G.; Goddard, R.; Fürstner, A., A New Ligand Design Based on London Dispersion Empowers Chiral Bismuth–Rhodium Paddlewheel Catalysts. *J. Am. Chem. Soc.* **2021**.
6. Lou, Y.; Remarchuk, T. P.; Corey, E. J., Catalysis of enantioselective [2+1]-cycloaddition reactions of ethyl diazoacetate and terminal acetylenes using mixed-ligand complexes of the series $Rh_2(RCO_2)_n(L^*_{4-n})$. Stereochemical heuristics for ligand exchange and catalyst synthesis. *J. Am. Chem. Soc.* **2005,** *127* (41), 14223-30.
7. Doyle, M. P.; Bagheri, V.; Wandless, T. J.; Harn, N. K.; Brinker, D. A.; Eagle, C. T.; Loh, K. L., Exceptionally high trans (anti) stereoselectivity in catalytic cyclopropanation reactions. *J. Am. Chem. Soc.* **1990,** *112* (5), 1906-1912.
8. Alvariño, C.; Simond, D.; Lorente, P. M.; Besnard, C.; Williams, A. F., Chains, Necklaces and Weaving Chain-link Grids from Self-Assembly Reactions. *Chem. Eur. J.* **2015,** *21* (24), 8851-8858.
9. Rempel, G. A.; Legzdins, P.; Smith, H.; Wilkinson, G.; Ucko, D. A., Tetrakis(acetato)dirhodium(II) and Similar Carboxylato Compounds. *Inorg. Synth.*, **1972**, 90-91.
10. Pirrung, M. C.; Morehead, A. T., Electronic Effects in Dirhodium(II) Carboxylates. Linear Free Energy Relationships in Catalyzed Decompositions of Diazo Compounds and CO and Isonitrile Complexation. *J. Am. Chem. Soc.* **1994,** *116* (20), 8991-9000.
11. Doyle, M. P.; Zhou, Q.-L.; Simonsen, S. H.; Lynch, V., Dirhodium(II) Tetrakis[alkyl 2-oxaazetidine-4(*S*)-carboxylates]. A New Set of Effective Chiral Catalysts for Asymmetric Intermolecular Cyclopropanation Reactions with Diazoacetates. *Synlett* **1996,** *1996* (07), 697-698.

12. Sunderland, T. L.; Berry, J. F., Expanding the family of heterobimetallic Bi–Rh paddlewheel carboxylate complexes via equatorial carboxylate exchange. *Dalton Trans.* **2016,** *45* (1), 50-55.
13. Smith, M. B., *March's Advanced Organic Chemistry : Reactions, Mechanisms, and Structure 7th Edition*. Wiley: New York, 2001.
14. Mobley, T. A.; Tennyson, E. G.; Hisao, G. S., Indirect detection of the ^{183}W and ^{57}Fe nuclei using 119Sn-relayed 1H,X correlation spectroscopy. *Magn. Res. Chem.* **2010,** *48* (10), 787-792.
15. Xiang, B.; Winemiller, M. D.; Briggs, T. F.; Fuller, D. J.; Collum, D. B., Optimizing HMQC for IS_n spin systems. *Magn. Res. Chem.* **2001,** *39* (3), 137-140.
16. Helgaker, T.; Jaszuński, M.; Ruud, K., Ab Initio Methods for the Calculation of NMR Shielding and Indirect Spin−Spin Coupling Constants. *Chem. Rev.* **1999,** *99* (1), 293-352.
17. Lenthe, E. v.; Baerends, E. J.; Snijders, J. G., Relativistic regular two-component Hamiltonians. *The Journal of Chemical Physics* **1993,** *99* (6), 4597-4610.
18. van Lenthe, E.; Baerends, E. J.; Snijders, J. G., Relativistic total energy using regular approximations. *The Journal of Chemical Physics* **1994,** *101* (11), 9783-9792.
19. Sadlej, A. J.; Snijders, J. G.; van Lenthe, E.; Baerends, E. J., Four component regular relativistic Hamiltonians and the perturbational treatment of Dirac's equation. *The Journal of Chemical Physics* **1995,** *102* (4), 1758-1766.
20. Wolff, S. K.; Ziegler, T.; van Lenthe, E.; Baerends, E. J., Density functional calculations of nuclear magnetic shieldings using the zeroth-order regular approximation (ZORA) for relativistic effects: ZORA nuclear magnetic resonance. *The Journal of Chemical Physics* **1999,** *110* (16), 7689-7698.
21. Bouten, R.; Baerends, E. J.; van Lenthe, E.; Visscher, L.; Schreckenbach, G.; Ziegler, T., Relativistic Effects for NMR Shielding Constants in Transition Metal Oxides Using the Zeroth-Order Regular Approximation. *J. Phys. Chem. A* **2000,** *104* (23), 5600-5611.
22. Schreckenbach, G.; Ziegler, T., Calculation of NMR Shielding Tensors Using Gauge-Including Atomic Orbitals and Modern Density Functional Theory. *The Journal of Physical Chemistry* **1995,** *99* (2), 606-611.
23. Wolff, S. K.; Ziegler, T., Calculation of DFT-GIAO NMR shifts with the inclusion of spin-orbit coupling. *The Journal of Chemical Physics* **1998,** *109* (3), 895-905.
24. Hagemann, H. "Computational studies of relativistic effects on NMR shieldings using perturbative approaches for spin-orbit coupling", Master Thesis, HHU Düsseldorf, 2020.
25. Stoychev, G. L.; Auer, A. A.; Izsák, R.; Neese, F., Self-Consistent Field Calculation of Nuclear Magnetic Resonance Chemical Shielding Constants Using Gauge-Including Atomic Orbitals and Approximate Two-Electron Integrals. *J. Chem. Theory Comput.* **2018,** *14* (2), 619-637.

26. Perdew, J. P.; Ruzsinszky, A.; Tao, J.; Staroverov, V. N.; Scuseria, G. E.; Csonka, G. I., Prescription for the design and selection of density functional approximations: More constraint satisfaction with fewer fits. *The Journal of Chemical Physics* **2005,** *123* (6), 062201.
27. Ramsey, N. F., Magnetic Shielding of Nuclei in Molecules. *Physical Review* **1950,** *78* (6), 699-703.
28. Widdifield, C. M.; Schurko, R., Understanding Chemical Shielding Tensors using Group Theory, MO Analysis, and Modern Density-Functional Theory. *Concepts Magn. Reson., Part A* **2009,** *34A*, 91.
29. Becke, A. D., Density-Functional Exchange-Energy Approximation with Correct Asymptotic-Behaviour, *Phys. Rev. A* **1998**, *38*, 3098−3100.
30. Lee, C.; Yang, W.; Parr, R. G., Development of the Colle-Salvetti correlation-energy formula into a functional of the electron density, *Phys. Rev. B* **1998**, *37*, No. 785.
31. Becke, A. D., Density-functional thermochemistry. III. The role of exact exchange. *The Journal of Chemical Physics* **1993,** *98* (7), 5648-5652.
32. Weigend, F.; Ahlrichs, R., Balanced Basis Sets of Split Valence, Triple Zeta Valence and Quadruple Zeta Valence Quality for H to Rn: Design and Assessment of Accuracy. *Phys. Chem. Chem. Phys.* **2005,** *7*, 3297.
33. Weigend, F., Accurate Coulomb-fitting basis sets for H to Rn. *Physical Chemistry Chemical Physics* **2006,** *8* (9), 1057-1065.
34. Barone, V.; Cossi, M., Quantum Calculation of Molecular Energies and Energy Gradients in Solution by a Conductor Solvent Model. *J. Phys. Chem. A* **1998,** *102*, 1995.
35. Wolinski, K.; Hinton, J. F.; Pulay, P., Efficient implementation of the gauge-independent atomic orbital method for NMR chemical shift calculations. *J. Am. Chem. Soc.* **1990,** *112* (23), 8251-8260.
36. London; F., Théorie quantique des courants interatomiques dans les combinaisons aromatiques, *J. Phys. Radium*, **1937**, *8*, 397-409.
37. Hameka; H. F., Gauge-invariant calculation of nuclear magnetic shielding constants at the coupled–cluster singles and doubles level , Mol. Phys., 1958, 1, 203-215.
38. Ditchfield, R., Molecular Orbital Theory of Magnetic Shielding and Magnetic Susceptibility. *The Journal of Chemical Physics* **1972,** *56* (11), 5688-5691.
39. Helgaker, T.; Jørgensen, P., An electronic Hamiltonian for origin independent calculations of magnetic properties. *The Journal of Chemical Physics* **1991,** *95* (4), 2595-2601.
40. Perdew J.P.; Ruzsinszky, A.; Csonka, G. I.; Constantin, L. A.; Sun; J., Workhorse Semilocal Density Functional for Condensed Matter Physics and Quantum Chemistry, *Phys. Rev. Lett.*, **2009**, *103*, 026403.

41. Tao, J.; Perdew, J. P.; Staroverov, V.N.; Scuseria, G. E., Climbing the Density Functional Ladder: Nonempirical MetaGeneralized Gradient Approximation Designed for Molecules and Solids, *Phys. Rev. Lett*. **2003**, *91*, 146401.
42. Staroverov, V. N.; Scuseria, G. E.; Tao, J.; Perdew, J. P., Comparative assessment of a new nonempirical density functional: Molecules and hydrogen-bonded complexes. *The Journal of Chemical Physics* **2003,** *119* (23), 12129-12137.
43. Pantazis, D. A.; Chen, X.-Y.; Landis, C. R.; Neese, F., All-Electron Scalar Relativistic Basis Sets for Third-Row Transition Metal Atoms. *J. Chem. Theory Comput.* **2008,** *4* (6), 908-919.
44. Stoychev, G. L.; Auer, A. A.; Neese, F., Automatic Generation of Auxiliary Basis Sets. *J. Chem. Theory Comput.* **2017,** *13* (2), 554-562.
45. Bouten, R.; Baerends, E. J.; van Lenthe, E.; Visscher, L.; Schreckenbach, G.; Ziegler, T., Relativistic Effects for NMR Shielding Constants in Transition Metal Oxides Using the Zeroth-Order Regular Approximation. *The Journal of Physical Chemistry A* **2000,** *104* (23), 5600-5611.